Gateway exchange, climatic forcing and circulation of the Mediterranean Sea during the late Miocene:

A model perspective

Dirk Simon

2017

Utrecht Studies in Earth Sciences

No. 129

Members of the evaluation committee:

Prof. dr. Angelo Camerlenghi
OGS, National Institute of Oceanography and Experimental Geophysics
Trieste, Italy

Prof. dr. Gert de Lange
Department of Earth Sciences, Utrecht University
Utrecht, The Netherlands

Dr. Mike Rogerson
School of Environmental Sciences, University of Hull
Hull, United Kingdom

Prof. dr. Francisco Javier Sierro Sánchez
Department of Geology, Salamanca University
Salamanca, Spain

Prof. dr. Anna Wåhlin
Department of Marine Sciences, Univeristy of Gothenburg
Gothenburg, Schweden

This research was carried out at:
Tectonophysics group, Department of Earth Sciences
Faculty of Geosciences, Utrecht University
Utrecht, The Netherlands

Author's contact:
Dirk Simon, Nei Stich 37, 25946, Norddorf auf Amrum, Germany

ISBN: 978-90-6266-469-6
Printed in the Netherlands by Ipskamp Printing (Enschede).

Gateway exchange, climatic forcing and circulation of the Mediterranean Sea during the late Miocene:

A model perspective

Zeestraat-transport, klimaat-forcering en circulatie van de Middellandse Zee tijdens het laat Mioceen:

Een modelperspectief

(met een samenvatting in het Nederlands)

PROEFSCHRIFT

ter verkrijging van de graad van doctor aan de Universiteit Utrecht op gezag van de rector magnificus, prof. dr. G.J. van der Zwaan, ingevolge het besluit van het college voor promoties in het openbaar te verdedigen

op

vrijdag 9 juni 2017 des middags te 2.30 uur

door

Dirk Simon

geboren op 13 oktober 1989 te Neurenberg, Duitsland

Promotor
Prof. dr. M.J.R. Wortel

Copromotor
Dr. P.Th. Meijer

The research documented in this thesis has received funding from the People Programme (Marie Curie Actions) of the European Union's Seventh Framework Programme FP7/2007-2013/ under REA Grant Agreement No. 290201 MEDGATE.

to my parents,
Karin and Ralf-Sigmar

&

to my brothers,
Martin and Thorsten

Contents

Samenvatting (Summary in Dutch) **x**

1 Introduction **1**
1.1 The role of semi-enclosed seas . . . 2
1.2 The Mediterranean Sea . . . 3
1.3 The Messinian Salinity Crisis (MSC) . . . 6
1.4 Thesis objective and outline . . . 10
1.5 The model perspective . . . 11

2 Dimensions of the Atlantic-Mediterranean connection that caused the Messinian Salinity Crisis **13**
2.1 Introduction . . . 14
2.2 Budget Considerations . . . 15
2.3 Theoretical Basis . . . 18
2.4 Model Results . . . 22
2.5 Discussion . . . 27
2.6 Conclusions . . . 33

3 Quantifying the Mediterranean freshwater budget throughout the late Miocene: New implications for sapropel formation and the Messinian Salinity Crisis. **37**
3.1 Introduction . . . 38
3.2 Model hierarchy . . . 40
3.3 Results . . . 45
3.4 Relevance for astronomical tuning and sapropel formation . . . 52
3.5 How much extra monsoonal runoff drains into the Mediterranean? . . . 52
3.6 The precession-obliquity interference pattern . . . 54
3.7 The onset of the MSC and the PLG stage . . . 55
3.8 Conclusions . . . 57

4 Salinity stratification of the Mediterranean Sea during the Messinian crisis: A first model analysis **59**
4.1 Introduction . . . 60
4.2 Model description . . . 62
4.3 Model analysis and results . . . 64
4.4 Discussion . . . 76
4.5 Conclusions . . . 78

References **86**

Acknowledgments **95**

Publication list **99**

Curriculum Vitae **100**

"*For every action there is an equal and opposite reaction.*"

Newton's Third Law

Samenvatting

Oceanen transporteren — en fungeren als opslag van — grote hoeveelheden warmte, zout, en andere chemische verbindingen, waaronder CO_2. Ze zijn daarom een belangrijk onderdeel van het aardse klimaatsysteem. Gezien de huidige bezorgdheid over het veranderende klimaat, is het cruciaal om een goed begrip te hebben van het functioneren van oceaancirculatie. Veranderingen in de circulatie en chemische samenstelling van de oceaan zijn veelal terug te zien in de sedimenten die afgezet worden op de oceaanbodem. Niet alleen het type sediment wordt bepaald door zulke veranderingen; de chemische samenstelling en fossielinhoud van het sediment worden er ook door beïnvloed. Op deze wijze vormen de afgezette sedimenten "het geologische archief" van genoemde veranderingen. Het bestuderen van dit archief is een manier om inzicht te verkrijgen in de processen die de oceaancirculatie aandrijven.

De circulatie en sedimentatie in door land ingesloten bekkens zijn bijzonder gevoelig voor veranderingen in het klimaat; dit maakt deze bekkens uitermate geschikt om klimaatverandering te bestuderen. De gevoeligheid voor veranderingen in het klimaat is een gevolg van de beperkte grootte van de bekkens en de gelimiteerde interactie met de open oceaan. Het bekendste voorbeeld van een door land ingesloten bekken is de Middellandse Zee, met zijn ligging tussen het Europese en het Afrikaanse continent. Circulatie in de Middellandse Zee wordt aangedreven door de uitwisseling van water met de Atlantische Oceaan en door de atmosferische condities in het Mediterrane gebied en zijn omgeving, zoals winden, verdamping, neerslag en resulterende zoetwater-instroom van rivieren. Op dit moment is de Straat van Gibraltar de enige zeestraat die de Middellandse Zee en de Atlantische Oceaan met elkaar verbindt; in het verleden is deze verbinding gecompliceerder geweest. De wateruitwisseling door een zeestraat wordt sterk beïnvloed door de zeestraat-bathymetrie; hierdoor was het mogelijk dat tektonische veranderingen in het gebied rond Gibraltar gevolgen hadden voor de grootte van de wateruitwisseling. Genoemde atmosferische condities worden sterk beïnvloed door de intensiteit van de inkomende zonnestraling, die op haar beurt afhangt van de baan van de Aarde en positie van de rotatieas van de Aarde ten opzichte van de zon. Het is het samenspel van klimaat en tektoniek dat leidt tot veranderingen in de circulatie in de Middellandse Zee en dat zijn weerslag vindt in het marien-geologische archief. Het herkennen en onderscheiden van de individuele invloed van de twee drijfveren is lastig maar belangrijk voor het verbeteren van ons begrip van oceaancirculatie.

De sedimenten die zijn afgezet in de Middellandse Zee in het laatste (d.w.z. jongste) deel van het Mioceen (het Messinien, van 7,25 tot 5,33 miljoen jaar geleden) vertonen een grote variabiliteit in hun samenstelling. Sedimenten kenmerkend voor afzetting in een open oceaan worden afgewisseld door lagen met een hoge organische inhoud. 5.97 miljoen jaar geleden werd deze afwisseling onderbroken door de afzetting van evaporieten (vooral gips en steenzout). Rondom de gehele Middellandse Zee zijn gipsafzettingen uit deze tijd gevonden en kilometers dikke lagen steenzout zijn verbor-

gen onder de huidige zeebodem. Het uitzonderlijke geologische gebeuren dat geleid heeft tot de afzetting van deze evaporieten staat bekend als de Messinien Zoutcrisis en vond plaats tussen 5,97 en 5,33 miljoen jaar geleden. Deze relatief korte periode van evaporiet-afzetting is, ondanks het onderzoek van generaties van wetenschappers, nog steeds n van de grootste mysteries in de geologische geschiedenis.

Voortbouwend op een groot aantal waarnemingen en een uitgebreid kwalitatief inzicht in het laat-Mioceen, heeft mijn promotieonderzoek als doel het verbeteren van het kwantitatieve begrip van de invloed van de grootte van de verbindende zeestraat tussen de Middellandse Zee en de Atlantische oceaan en van het klimaat op circulatie en zoutgehalte in de Middellandse Zee. Dit wordt bereikt door bestaande geologische/geochemische waarnemingen te combineren met een theoretische en modelgedreven aanpak van fysische aard. In dit proefschrift ontwikkel ik (1) een theoretische benadering van de relatie tussen zeestraatgrootte en bekkensaliniteit, (2) een vernieuwende aanpak, gebruik makend van meerdere modellen, om een schatting te maken van het zoetwaterbudget (relatie tussen neerslag, rivier-input en verdamping) van de Middellandse Zee in het Mioceen, (3) een gesimplificeerd model van de oceaancirculatie van de Middellandse Zee, dat de ruimtelijke verdeling van saliniteit in het bekken in eerste orde verklaart.

De verkregen resultaten kunnen als volgt kort worden samengevat: Om een zoutgehalte in de Middellandse Zee in stand te kunnen houden dat groter is dan het huidige, moet de verbinding via de zeestraat beperkter (ondieper of smaller, of langer, of een combinatie hiervan) geweest zijn dan de huidige Straat van Gibraltar. Hoewel tijdens het laat-Mioceen de zoetwateraanvoer door de Afrikaanse rivieren mogelijk veel groter was (waarschijnlijk door afwatering in de Middellandse Zee van het destijds zeer grote Chad Meer), was het netto zoetwaterbudget van de Middellandse Zee vergelijkbaar met het huidige. Deze resultaten leiden tot de conclusie dat de Messinien Zoutcrisis voornamelijk op gang gebracht is doordat tektonische processen de verbinding van de Middellandse Zee met de Atlantische Oceaan drastisch verkleind hebben. Mijn onderzoek toont aan dat onder deze omstandigheden betreffende wateruitwisseling en zoetwaterbudget de Mediterrane waterkolom sterk gelaagd geweest kan zijn. Dit resultaat werpt nieuw licht op algemeen aanvaarde percepties van de Messinien Zoutcrisis en levert een nieuwe kwantitatieve basis voor toekomstige studies.

De behaalde proces-gerelateerde resultaten zijn niet alleen zinvol voor de Middellandse Zee als case study gebied; tezamen met de geïntegreerde onderzoeksstrategie ontwikkeld in dit proefschrift zullen zij naar verwachting bijdragen tot verdieping van inzicht in oceaancirculatie en sedimentatie in andere vergelijkbare gebieden (tegenwoordige of in het geologische verleden) en in oceaancirculatie, in het algemeen.

Hartelijk dank aan Robin, Paul en Rinus voor hun bijdrage aan het schrijven van deze samenvatting.

1

Introduction

The Mediterranean Sea is a remnant of the ancient Tethys Ocean and acquired its landlocked setting due to the convergence of the African and Eurasian plates. The semi-enclosed setting, together with the climatic forcing, gives rise to a thermohaline circulation which may be thought of as a small-scale analog of the Atlantic Meridional Overturning Circulation (AMOC). Although evaporation dominates overall, seasonal and orbital alternations in the position of the Intertropical Convergence Zone (ITCZ) entail a variable freshwater input which impacts on basin salinity (e.g., Rohling et al., 2015). The presence of the confined marine gateway of the Strait of Gibraltar allows the Mediterranean Sea to act as a marginal basin of the Atlantic Ocean. Tectonics and sea level variations affect the exchange of water, salt and heat through the gateway and can therefore trigger changes in circulation and water properties in both the Atlantic Ocean and the Mediterranean Sea. In the Atlantic Ocean, Mediterranean overflow water (MOW) leads to increased water densities in the Nordic Seas, which may affect the AMOC and therefore potentially global climate (e.g., Bryden et al., 1994; Price and Baringer, 1994; Hecht et al., 1997; Li, 2006; Rogerson et al., 2012). In the Mediterranean Sea, the limited connectivity is reflected in atypical marine sedimentation such as the regularly occurring deposition of organic-rich sapropels. The most extreme expression of changes in connectivity is the kilometer-thick salt giant formed during the so-called Messinian Salinity Crisis (MSC, 5.97-5.33 Ma, Roveri et al., 2014a, and references therein). The MSC has been associated with approximately ten times greater salt concentrations than the global average. Although the MSC has been studied for nearly half a century, its causes and consequences are still debated. This intriguing case led Rachel Flecker and co-workers to initiate the European Union Initial Training Network named MEDGATE. Ten early-stage researchers were trained in multi-disciplinary scientific and soft skills with a focus on investigation of the late Miocene gateways. Two different approaches were adopted. The direct approach gathered observations from the field in southern Spain and northern Morocco. The indirect one investigated the Mediterranean and Atlantic sedimentary record. Together, they improved our understanding of Atlantic-Mediterranean exchange and of how this impacted on the climate of the late Miocene. Within this framework, the research reported in this thesis contributes through numerical modelling. More specifically, physics-based insights are gained into gateway exchange (Chapter 2), climatic forcing (Chapter 3) and ocean circulation (Chapter 4) of the Mediterranean during the late Miocene. Our findings are evaluated against, and used to further interpret, the sedimentary record of the Mediterranean basin and its gateways, allowing quantitative inferences to be made regarding the past environment.

1.1 The role of semi-enclosed seas

A generalised depiction of a semi-enclosed sea is given in Figure 1.1. The essential feature is the limited connection with an adjacent sea or ocean (Nihoul, 1982). In comparison to larger oceans the boundary conditions (e.g., climatic forcings) and budgets (e.g., of salt or water) of semi-enclosed seas are usually better constrained. Due to their relatively small basin size investigations of the system as a whole are often possible. Examination of semi-enclosed seas is thus an elegant way to improve our understanding of gateway behaviour as well as of regional and large-scale water circulation (Nihoul, 1982). In the case of the Mediterranean Sea this is particularly relevant because this basin exemplifies the process of thermohaline circulation. The dense outflow at depth through the Strait of Gibraltar (the MOW already mentioned) triggers an inflow of Atlantic surface water into the western Mediterranean. While flowing towards the east its salinity increases due to evaporation. On its subsequent path this salinity-preconditioned water passes through marginal basins — for example, the Adriatic Sea or the Aegean Sea, which on their own are small-scale semi-enclosed seas. There, cooling during winter can rapidly decrease water buoyancy leading to the production of deep-water which ventilates the deep basin and feeds the Mediterranean thermohaline circulation (e.g., Tsimplis et al., 2006). The process resembles that in the Atlantic Ocean where spatial extent and magnitude are obviously much larger. Also in the Atlantic case marginal basins of the main ocean play an important role. Warm and salty surface waters, formed at low latitudes, are transported to higher latitudes, where their temperatures decrease rapidly in marginal basins, like the Arctic Ocean, giving rise to deep-water formation and feeding the AMOC (Figure 1.2). The global thermohaline circulation transports vast amounts of heat and salt, making it an important component in our climate system (e.g., Kuhlbrodt et al., 2007). The study of the Mediterranean basin holds the promise to contribute to understanding this process.

Apart from resembling each other in terms of circulation, the Mediterranean Sea can also be considered as a marginal basin of the Atlantic Ocean and the two are thus linked dynamically. The dense MOW (Figure 1.3) can be traced to the central North Atlantic basin (Curry et al., 2003). This overflow has been active since the early Pliocene (van der Schee et al., 2016), although older MOW imprints have been identified from upper Miocene sediments in northern Morocco (Capella, 2017; Capella et al., 2017a). An impact of MOW on AMOC has been suggested but is subject to debate (e.g., Rogerson et al., 2012). Today, MOW has a small but recognizable effect on the circulation of the Atlantic (e.g., Rahmstorf, 1998). During times when AMOC was relatively weak, for example during the last glacial maximum, MOW may have been more important in that it played a role in forming northern Atlantic deep waters (e.g., Rogerson et al., 2012). Similarly, during the MSC (i.e., late Miocene) it was more likely that MOW influenced global climate than today (e.g., Ivanovic et al., 2014). Past MOW paths are uncertain and fluctuating regional and global climate makes a correlation between outflow strength and sedimentary bedforms difficult (Flecker et al., 2015); therefore the debate is bound to continue.

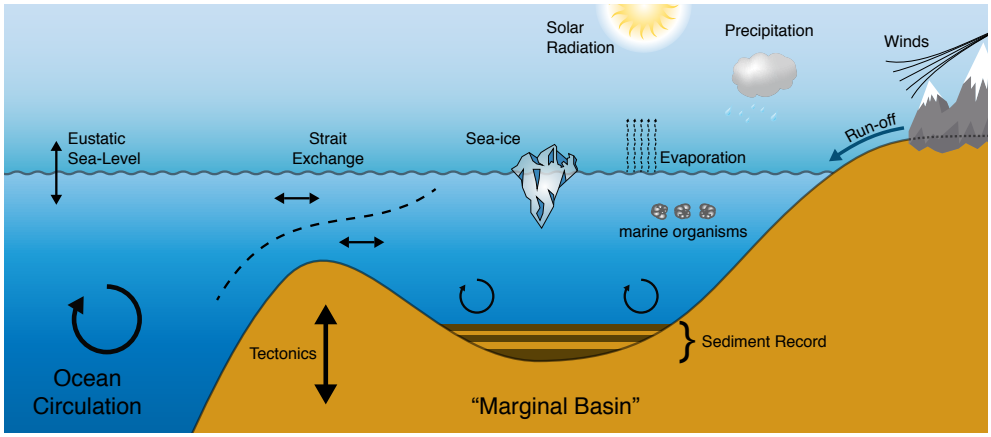

Figure 1.1 Cartoon of an idealised semi-enclosed sea. It is connected to a larger ocean via a small gateway. In such a setting the interplay between gateway connectivity and regional climate will determine its circulation and water properties. Accordingly, salinity and temperature are highly sensitive to sea level, tectonics or erosion and sedimentation in the strait region, influencing exchange efficiency, and atmospheric forcings and rivers, impacting on the sea surface (latitude dependent). Fluctuations in such alter the budget of marine and terrestrial organic matter, nutrients and isotopes, which leaves a signature in the sedimentary record.

1.2 The Mediterranean Sea

Tectonic context

The formation of the Mediterranean Sea began with the onset of convergence between the African/Arabian plate and the Eurasian plate during the late Mesozoic (e.g., Jolivet and Faccenna, 2000). The resulting gradual enclosure of mid-latitude Tethys remnants, together with the processes of subduction roll-back and extension of the overriding plate (Jolivet and Faccenna, 2000; Wortel and Spakman, 2000), shaped the region into the present system of connected sub-basins. As part of the process, around the early to middle Miocene, the Arabian Plate was pulled towards the north (Jolivet and Faccenna, 2000), closing the eastern connection of the Mediterranean Sea to the Indian Ocean (Rögl, 1999). This terminated the Tethys circumequatorial current (von der Heydt and Dijkstra, 2006) — a westward global equatorial ocean current (e.g., Bush, 1997) — causing a global climate shift and potentially playing a role in the development of the East Antartic Ice Sheet (e.g., Flower and Kennett, 1994). The formation of this eastern boundary of the Mediterranean Sea was the start of the transition towards the present-day Mediterranean circulation (e.g. Harzhauser and Piller, 2007; de la Vara and Meijer, 2016). At the same time, the ancestor of today's Black and Caspian Seas, the Paratethys, was cut off from the Mediterranean proper due to the formation of the Alpine mountain chains (e.g., Rögl, 1999).

Subduction retreat in the western Mediterranean during the Miocene caused the small Alboran plate to collide with the Iberian and the African plates (e.g., Hinsbergen et al., 2014). In the restricted space thrusts created an arc that is recognizable today as the Betic and Rifian mountains in southern Spain and northern Morocco, respectively (Platt et al., 2013). The load of these mountain chains formed foreland basins, which hosted a network of Atlantic-Mediterranean seaways (Betic and Rifian corridors). Several corridors existed at various locations and different points in time (summarised in Flecker et al., 2015). These gateways gradually closed due a combination of sediment infill (e.g., van den Berg et al., 2015, 2017; Martín et al., 2009, 2014), eustatic sea level variations (e.g., Ohneiser et al., 2015; Pérez-Asensio et al., 2012) and further tectonic restriction (recently documented by Capella, 2017). Uplift of the gateways may have been driven by lithospheric flexure (Govers, 2009), asthenospheric upwelling (Duggen et al., 2003), or rejuvenated Africa-Iberia convergence (Jolivet et al., 2006). This restriction triggered the MSC (Section 1.3; see Flecker et al., 2015; Roveri et al., 2014a, for recent in-depth summaries). A total disconnection of the Mediterranean from the Atlantic is often used as a justification for the Messinian "desiccated deep basin" model (Hsü et al., 1973). After the MSC, the Strait of Gibraltar opened and the Mediterranean as we know it today formed. As an interesting side note, there is no direct evidence that the Strait of Gibraltar only opened at the beginning of the Pliocene.

Climatic context

Conceptually, the large scale motions of Earth's atmosphere can be represented by three circulation cells, which differ in latitudinal position (low latitude, Hadley; medium latitude, Ferrel; high latitude, Polar, Figure 1.2). The low-pressure region between the southern and northern Hadley cell is called the Intertropical Convergence Zone (ITCZ, see Figures 1.2 and 1.3) and appears as a band of clouds on satellite images. The exact positioning of the three circulation cells depends on the distribution of solar radiation and will therefore change throughout the year (Figure 1.3). Due to the mid-latitudinal position of the Mediterranean, its climate is mainly driven by the interaction of the northern hemisphere Hadley Cell and westerlies, arriving from the Atlantic (Lolis et al., 2002). During summer the ITCZ moves northwards, causing Atlantic storms to have less impact on the Mediterranean. This leads to dry and warm conditions. During winter the ITCZ migrates further south, which allows the westerlies to supply the Mediterranean with mild but moist air. Additionally, during winter, cold air masses (e.g., Mistral or Bora) are channelled through gaps in the Alpine ranges or cascade down mountain valleys towards the Mediterranean (e.g., Maheras et al., 1999; Casford et al., 2003). The resulting cooling of the sea surface is important for Mediterranean deep-water formation (Rohling et al., 2015). Due to the seasonal shift of the ITCZ, the precipitation patterns across Africa vary (e.g., Marzocchi et al., 2015). River drainage catchments are subject to variable amounts of rainfall during the year (Figure 1.3), which leads to fluctuating runoff into the Mediterranean basin. For the present day, this is best examplified by the Nile catchment. In the past other drainage networks may have existed (e.g., Chad-Eosahabi, Griffin, 2006). De-

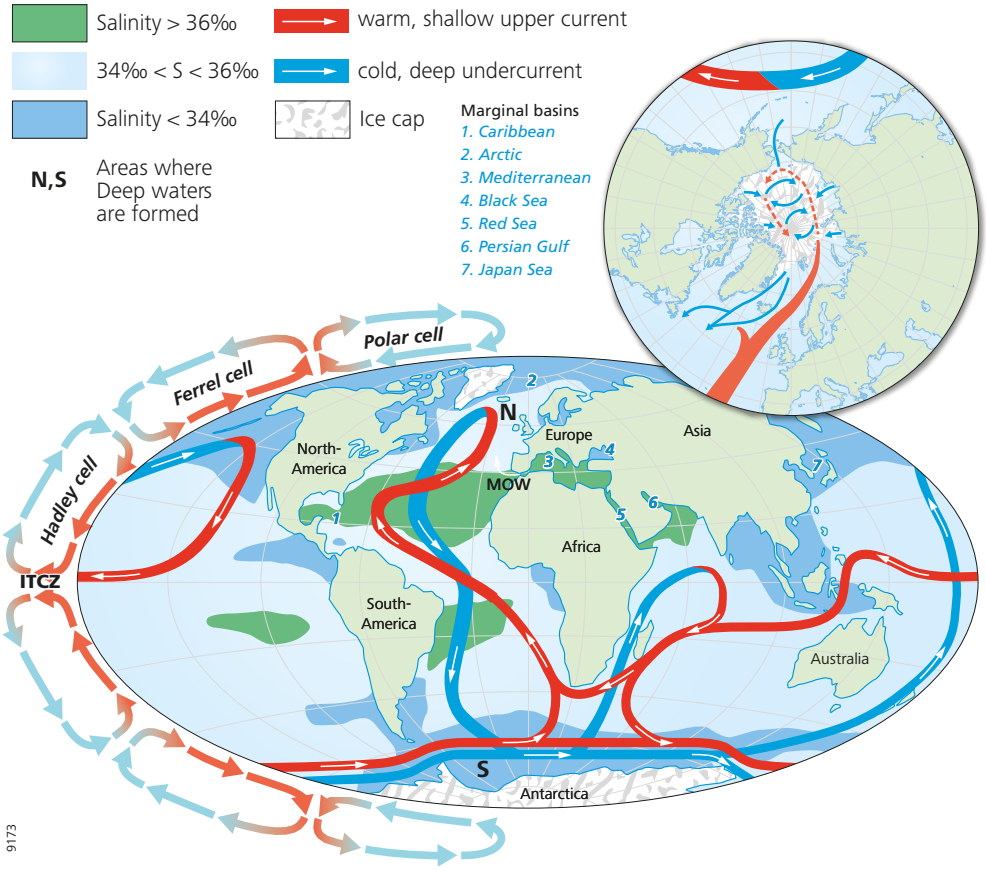

Figure 1.2 Simplified sketch of the global overturning circulation. Deep-water is formed due to temperature decrease at high latitudes (northern Atlantic, **N**) and by wind-driven upwelling occurring along the Antarctic Circumpolar Current (**S**). Indicated are saltier (green) and fresher (dark blue) ocean waters. The numbers indicate some of the marginal seas around the Earth. Atmospheric circulation cells are drawn on the left hand side. After Kuhlbrodt et al. (2007), Rahmstorf (2002) and Rohling et al. (2015).

spite these strong river fluctuations, it is evaporative loss that dominates the sum of evaporation, precipitation and runoff in the Mediterranean Sea (e.g., Mariotti et al., 2002).

Not only seasons affect the distribution of solar radiation across the Earth's surface, also changes in Earth's orbit play a role. Insolation (solar radiation received at the top of the atmosphere) is determined by the orbital path and position of Earth relative to the Sun. The three most important orbital effects are (1) axial precession of the Earth, (2) the tilt of the Earth's rotational axis relative to its orbit (obliquity)

and (3) the eccentricity of the elliptical Earth orbit around the Sun, with the Sun at one of the focal points. Several studies suggest or show that during a precession minimum the ITCZ shifts northward, causing increased river fluxes into the Mediterranean (e.g., Rossignol-Strick, 1983; Bosmans et al., 2015a; Marzocchi et al., 2015). Other studies propose that also an obliquity maximum will trigger a northward shift of the ITCZ (e.g., Bosmans et al., 2015a; Tuenter et al., 2005). Laskar et al. (2004) calculated how these orbital parameters changed throughout the Neogene period. By correlating them with sedimentary successions, sediment layers are dated to high accuracy (astronomical tuning, e.g., Hilgen and Krijgsman, 1999; Hilgen et al., 2007; Krijgsman et al., 1999a; Sierro et al., 1999).

The sedimentary record

Investigating Neogene sediments (i) outside the Mediterranean Sea, (ii) in relatively small sedimentary basins in southern Spain and northern Morocco, and (iii) inside the Mediterranean basin, improves our understanding of the Atlantic-Mediterranean exchange. If this approach is applied prior, during and after the MSC, correlations provide insight into the evolving climatic and tectonic environment during the late Miocene. As MOW exits the Strait of Gibraltar at depth, it causes erosion and leads to deposition of sandy bedforms known as contourites along the Iberian margin (Hernández-Molina et al., 2014). These sediments were investigated by IODP expedition 339 (e.g., Hernández-Molina et al., 2014; Bahr et al., 2015; van der Schee et al., 2016). Dating and stratigraphic correlation of upper Miocene sediments in the Betic and Rif basins have been used to reconstruct the evolution of the Atlantic-Mediterranean corridors (e.g., Martín et al., 2009). Uplift rates during the phase of closure of the Rifian Corridor have been derived from main offsets detected in seismic stratigraphy. These offsets were created by syn-depositional high-angle faults cross-cutting the gateway axis (Capella et al., 2017b). During the late Miocene, Mediterranean basin sediments show a clear transition from normal open marine conditions to restricted marine conditions and finally to evaporitic environments associated with the Messinian Salinity Crisis.

1.3 The Messinian Salinity Crisis (MSC)

Although documented much earlier (e.g., Mayer-Eymar in 1967 described by Selli, 1960; Ruggieri, 1967) the Messinian salt was recognized broadly by the scientific community only after the discovery of evaporites in the deep basin during the Mediterranean cruise DSDP Leg 13, whose goal was "to explore the origin and development of a small ocean basin — The Mediterranean" (Ryan et al., 1973). The MSC is now one of the greatest mysteries in geological history, leading to a vast number of scientific papers published on the topic. MSC observations relevant as a background for this thesis are summarized in the following.

The Messinian sedimentary record is complex, due to its spatial and compositional variations. Figure 1.3 illustrates the distribution of the evaporites within the Mediterranean basin. Gypsum is found mainly around the Mediterranean margins and is well

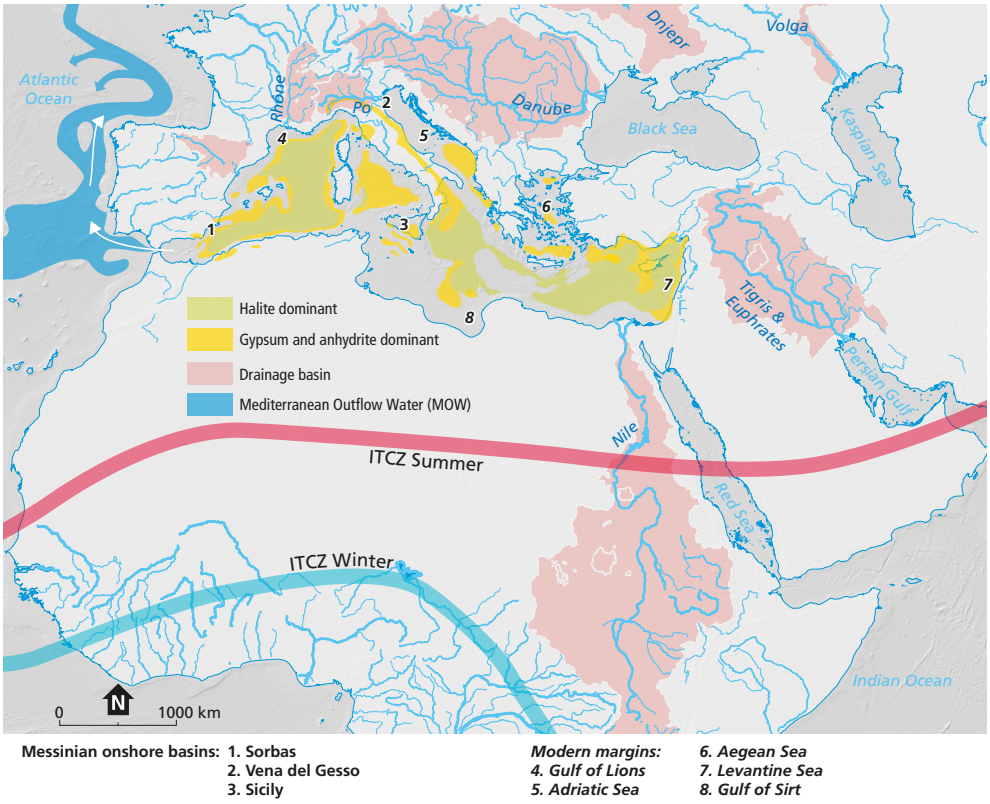

Figure 1.3 Present-day shaded topography map of the wider Mediterranean region. Indicated are the Messinian evaporite deposits, the major rivers and drainage basins and the Mediterranean outflow water (MOW). Numbers refer to Messinian and modern basins. After Roveri et al. (2014a), Flecker et al. (2015), Marzocchi et al. (2015) and Farr et al. (2007).

exposed on land. Halite lies beneath the deep basin (up to 3 km in thickness, Ryan, 2008) and is exposed in several mines on Sicily. Lofi et al. (2011) summarize and describe the Mediterranean-wide evaporitic units. For instance, halite can be identified as a transparent layer on seismics. Also an erosion surface is revealed (the M-reflector or MES, Messininan erosional surface, Ryan et al., 1973), which has been traced to river valleys (e.g., Rhone: Clauzon, 1973; Nile: Chumakov, 1973). Pre-evaporite marls have been correlated and tuned throughout the entire Mediterranean basin (Hilgen and Krijgsman, 1999; Hilgen et al., 2007; Krijgsman et al., 1999a; Sierro et al., 1999). Krijgsman et al. (1999a) used this integrated high-resolution stratigraphy to date the MSC onset to an age of 5.96 Ma. This age was redefined later to an age of 5.971 Ma by Manzi et al. (2013), based on a reinterpretation of the first gypsum bed in the Sorbas basin. In 2007 several MSC experts gathered at a CIESM (Mediterranean

Science Commission) meeting to define a stratigraphic consensus model (Figure 1.4) consisting of three stages:

Stage 1 ($\sim$ 5.97–5.61 Ma) — *Primary Lower Gypsum*
The Primary Lower Gypsum (PLG) consists of marl-gypsum alternations. 17 and 16 gypsum cycles in Italy and Spain, respectively, correspond well and imply a total duration of approximately 350-370 kyrs for the PLG (Roveri et al., 2014a). It has been suggested that these variation are precession-controlled (Krijgsman et al., 2001). Originally, the gypsum beds were defined to correspond to precession maxima (insolation minima), which relate to relatively dry (circum-)Mediterranean climates (Krijgsman et al., 2001). However, based on the application of new laboratory techniques it has recently been suggested that the details are not straightforward. Low salinity was measured in gypsum fluid inclusions (Natalicchio et al., 2014) and contradicting water origins implied by strontium isotopes, sulfur and oxygen isotopes compared to gypsum hydration were discovered (Evans et al., 2015). It is suggested that the Mediterranean sea level was approximately equal to the Atlantic one. This is in agreement with the quantitative analysis of Krijgsman and Meijer (2008).

Stage 2 ($\sim$ 5.61–5.55 Ma) — *resedimented gypsum and halite*
The consensus model places the halite deposition and the MES in a short time interval ($\sim 50 - 60$ $kyrs$) between the PLG and the Lago Mare phase. This follows from downward tuning from the base of the Pliocene. Some gypsum found, has been identified as resedimented. This extreme stage is often linked to a desiccated Mediterranean (Hsü et al., 1973).

Stage 3 ($\sim$ 5.55–5.33 Ma) — *Upper Evaporites and Lago Mare*
The final stage of the MSC consists of gypsum, which may be resedimented, and brackish facies. These are correlated basin-wide and demonstrate Paratethian fauna (Stoica et al., 2016), which again indicates a water-filled Mediterranean basin.

Although this consensus model can explain most (currently available) data, a continuous Messinian record of the deep Mediterranean is needed to prove it. Biological and geochemical constraints help to link this stratigraphic model to the Atlantic-Mediterranean exchange. Shells of marine fauna (e.g., foraminifera) record the isotopic composition of the seawater during the time of growth. Prior to and after the MSC the Mediterranean $^{87}Sr/^{86}Sr$ ratio was comparable to the global oceanic value. During the MSC it dropped significantly towards Nile values (Flecker et al., 2002; Topper et al., 2011). This further emphasizes the fact that exchange with the global ocean was very limited during the MSC. The isotopes of osmium, described by the ratio $^{187}Os/^{188}Os$ behave in a similar way. A recent study (Kuroda et al., 2016) compares the osmium record with the results of a box model to gain insight into the hydrology of the Mediterranean — an approach that already demonstrated its strength when applied to the strontium record (e.g., Flecker et al., 2002; Topper et al., 2011; Modestou et al., 2017). In order to make global correlations, a Mediterranean $\delta^{18}O$ record would be valuable because it directly relates to global temperature and

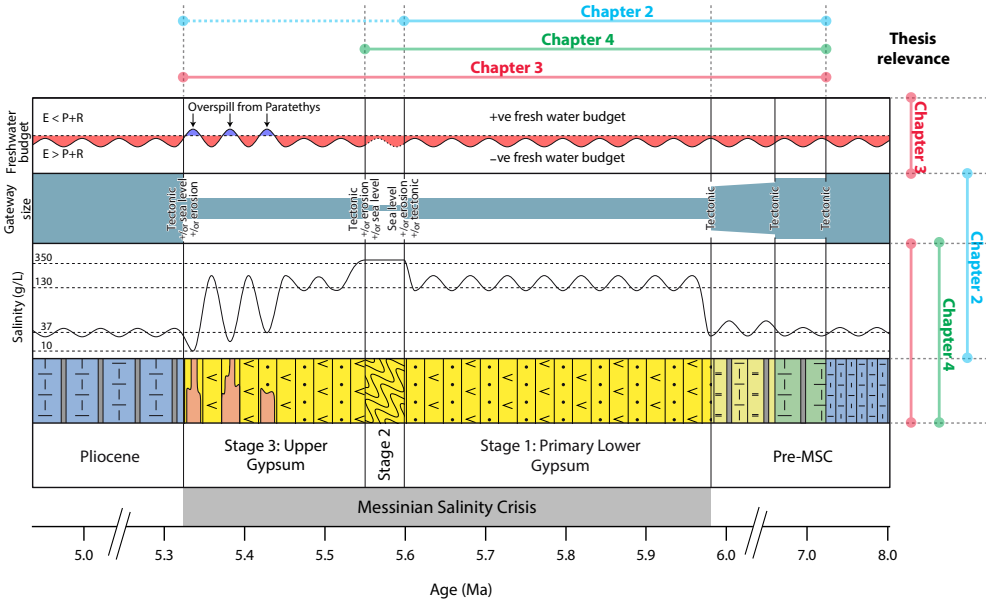

Figure 1.4 Illustration of the main features of the Mediterranean's exchange history in the late Miocene-Pliocene including lithology, Mediterranean salinity, a qualitative representation of gateway size and the probable drivers (tectonics, erosion, sea level) of changing dimensions and the Mediterranean's freshwater budget (E = evaporation and P = precipitation over the Mediterranean and R is the river discharge into the Mediterranean Sea). After Flecker et al. (2015). The subject and time span targeted by each of the three following chapters are indicated along the right and top edge of the diagram, respectively.

ice-volume. However, the extreme paleoenvironmental conditions during the MSC made it impossible for normal marine fauna to live or to be recorded in the sedimentary record. Already from 7.8 Ma onwards distinct steps in the evolution of benthic foraminiferal fauna are observed (Kouwenhoven et al., 2003). Diversity decreased and equilibrium species were replaced with increasingly stress-tolerant fauna. These biological constraints indicate that the Mediterranean already transitioned towards the MSC much before the onset of gypsum deposition (5.97 Ma, Manzi et al., 2013). Flecker et al. (2015) integrate the presented Mediterranean observations and summarize the knowledge prior to the MEDGATE project on Atlantic-Mediterranean exchange during the late Miocene. Figure 1.4 is a modified version of their conclusion figure (Flecker et al., 2015, their Figure 9). It shows the MSC stages and a schematic representation of the observational evidence in the Mediterranean record. In addition, it illustrates qualitatively how the Mediterranean salinity may have evolved in conjunction with the Mediterranean freshwater budget and the Atlantic-Mediterranean gateway size.

1.4 Thesis objective and outline

Building on the *qualitative* knowledge of the late Miocene (Figure 1.4, after Flecker et al., 2015), this thesis has the objective to improve our *quantitative* understanding of external forcings (gateway size, climatic forcing) and their impact on the Mediterranean Sea (e.g., overturning circulation and salinity distribution and evolution). This is achieved by complementing the available geological/geochemical observations with a physics-based theoretical and modelling approach (Section 1.5). The three main questions addressed in this thesis are outlined below. Figure 1.4 illustrates how these central topics complement each other and indicates their position under the MEDGATE umbrella.

To which extent do gateway dimensions control water exchange and basin salinity?
Chapter 2 builds a theoretical framework which combines the theory of hydraulic control with the effect of bottom friction. With this we relate gateway dimensions to Atlantic-Mediterranean exchange flux, as well as to Mediterranean salinity. This allows us to constrain the sizes (depth, width and length) of the seaway that must have existed during and prior to the MSC.

How did the Mediterranean freshwater forcing evolve during the late Miocene?
Chapter 3 develops a novel multi-model technique, which combines coupled climate simulations with regression and threshold/box models. This provides a means to estimate the evolution of the freshwater budget of the Mediterranean Sea during the late Miocene and allows us to predict synthetic sedimentary records and the temporal variation of basin salinity. Using our findings to analyse pre-MSC marls and the gypsum-marl alternations of the PLG, leads to discussion of the mechanism driving sapropel formation, the evolution of the north African drainage network (e.g., Chad-Eosahabi), the obliquity effect seen in Mediterranean sedimentary successions and the onset of the MSC.

Is the water column expected to be stratified during the Messinian crisis?
Chapter 4 considers vertical stratification of the water column. A box model is set up that includes a simple representation of a haline overturning circulation and mixing. The model is forced by Atlantic exchange and evaporative loss and is used to systematically explore the degree of stratification that results under a wide range of combinations of parameter values. By evaluating the model results with the constraints available for the Messinian, we can decide on the likelihood of significant stratification during the MSC.

The process-related insights are not only important for the Mediterranean Sea as a case study. The overall approach and the newly developed modeling techniques in this thesis also hold the promise to help our understanding of circulation and sedimentation of other regions (during other geological periods) and of ocean circulation in general.

1.5 The model perspective

Depending on the research question, a certain model type may have advantages over others. In this thesis we are considering box models and General Circulation Models.

Box models can be applied if a large part of a system evolves in a similar way. A common example is the carbon cycle, in which carbon is transferred between a set of carbon reservoirs (e.g., ocean, atmosphere, living organisms and sediments) by physical and biological processes (Slingerland and Kump, 2011). By design, box models isolate mechanisms, which allows an analysis on a specific aspect of a system. In the classical Mediterranean example, water and salt balance were combined to relate the exchange flux at the Strait of Gibraltar to basin salinity (Nielsen, 1912). In a seminal study, Bryden and Stommel (1984) extended this basic model with strait dynamic theory. This was applied to the MSC by Rohling et al. (2008) and Meijer (2012). Other examples are box models that investigate intra-basin connectivity (e.g., Topper and Meijer, 2013; Meijer, 2006), isotopic mass balance (e.g. Flecker et al., 2002; Topper et al., 2011) or sea-level variations (e.g., de la Vara et al., 2016). The duration of the late Miocene is on the order of millions of years. Box models are capable of calculating such time-spans with minimum computing time, which makes them the most-used tool in our research. Chapter 2 demonstrates a pure box model-based study. Spatial resolution is generally poor in box models, but can be improved by subdividing boxes (e.g., Chapter 4).

If higher spatial resolution is needed, an oceanic general circulation model is the tool of choice. The Princeton Ocean Model (POM) is a commonly used model in our group in Utrecht. Due to its orthogonal curvilinear grid, small topographic features such as gateways can be resolved with more detail than the larger basins (e.g., Topper and Meijer, 2015a; de la Vara et al., 2015; Simon et al., 2016).

Global *General Circulation Models* (GCMs) include not only the circulation of the ocean, but couple it to a model for the circulation of the atmosphere and often also to models for changes in vegetation. High resolution and regional models of this type are also used for weather forecasting. In collaboration with colleagues at Bristol University, simulations (Chapter 3) were setup with the UK Met Office General Circulation Model (HadCM3L version 4.5, see Valdes et al., 2017, and references therein for a full description). The model has a horizontal resolution of 3.75^o longitude by 2.5^o latitude and has 19 vertical levels in the atmosphere and 20 in the ocean. The oceanic and atmospheric components are coupled once per model day and they are, in turn, coupled with the TRIFFID vegetation model (Hughes et al., 2004, and references therein). HadCM3L has previously been used to simulate late Miocene climate (e.g., Bradshaw et al., 2012) and Eocene climate (e.g., Tindall et al., 2010). A recent assessment shows that the HadCM3 family of models simulates large-scale features of the modern climate system (both over land and ocean) with accuracy comparable to many of the latest CMIP5 models (5^{th} Climate Modelling Intercomparison Project; Valdes et al., 2017). Unfortunately, long time spans such as the entire late Miocene (7.25 - 5.33 Ma), cannot be transiently simulated. Therefore, we performed snapshot experiments, adding to the set of simulations of Marzocchi et al. (2015). The entire series of GCM experiments was extended with a regression model (Chapter 3).

2

Dimensions of the Atlantic-Mediterranean connection that caused the Messinian Salinity Crisis

What KIND OF GATEWAY IS NEEDED TO CAUSE A SALINITY CRISIS? Although several reconstructions of possible Atlantic-Mediterranean gateways are proposed for the late Miocene, so far the gateway that must have existed before the desiccation of the Mediterranean during the Messinian is unknown. This study uses the theory of hydraulic control combined with the effect of bottom friction in order to find out, to first order, the geometrical dimensions of the connection that existed during the Primary Lower Gypsum stage ($5.97 - 5.61\ Ma$) of the Messinian Salinity Crisis ($5.97 - 5.33\ Ma$). The connecting strait is assumed to behave in a similar way as existing straits, such as the Strait of Gibraltar or the Bosphorus. A salinity crisis in an enclosed basin results, when its connection to the open ocean is highly restricted. A strait needs to be relatively shallow, narrow and/or long in order to result in exchange fluxes that are of around 25% or less of the exchange at the Strait of Gibraltar today. Considering the evaporite deposits together with global sea level variations we estimate the cross section of a strait responsible of the MSC to have a minimum depth of $\sim 30 - 45\ m$ and a maximum width of $\sim 0.7 - 2\ km$ for lengths in the range up to $\sim 500\ km$. These dimensions are consistent with only a few of the Miocene corridors identified. The calculations are extended to explore the implications for sedimentary structures on the corridor floor.

2.1 Introduction

Thick sequences dominated by evaporites (up to $\sim 2\ km$) are present in the Mediterranean Neogene record. Famous gypsum outcrops are located all around the Mediterranean, for example in Spain (Sorbas Basin, Krijgsman et al., 2001) or Italy (Vena del Gesso Basin Lugli et al., 2010). Halite is evident in the deep basin record (Lofi et al., 2011) and in mines on Sicily. This Messinian Salinity Crisis (MSC, Hsü et al., 1973; Roveri et al., 2014a) has been dated, using cyclostratigraphy, to a late Messinian age (5.97-5.33 Ma, Krijgsman et al., 1999a; Manzi et al., 2013). It has been the focus of geologists for about half a century, but the cause of the crisis is still a topic of great debate.

In order to precipitate such evaporites the water salinity of the Mediterranean Sea must have been higher than $130 - 160\ g/kg$ for gypsum and greater than $350\ g/kg$ for halite. Such extreme salinities in a basin like the Mediterranean are triggered by the interplay between the climate and the connection to the global ocean (Atlantic). This connecting strait is under the influence of tectonics and global sea level changes. The climate parameter that is most important in this context is the water budget (evaporation, precipitation and river input). If the drainage of the Chad basin is excluded, the water budget during the late Miocene is predicted to be of a similar dimension as today (Gladstone et al., 2007). This leads to the argument that the Atlantic-Mediterranean connection is of great importance in seeking answers about the MSC (Flecker et al., 2015).

Several studies suggest that the Atlantic connection was completely closed during later stages of the MSC in order to desiccate the basin (Roveri et al., 2014a). Although alternative interpretations exist (Braga et al., 2006), it is broadly accepted that in the first stage of the crisis, the Primary Lower Gypsum (PLG, 5.97–5.61 Ma, Roveri et al., 2014a; Manzi et al., 2013), gypsum was deposited all around the margins of the Mediterranean in about 400 $kyrs$. For this PLG stage, previous model studies (e.g., Topper et al., 2011) show that a connection between the Atlantic and the Mediterranean must have existed in order to supply the Mediterranean with enough evaporites. Figure 2.1 summarises some Atlantic–Mediterranean connections that have been reconstructed for the late Miocene (Santisteban and Taberner, 1983). These did not all coexist at the same time, but opened and closed at various times, related to tectonic movements. Notably, Martín et al. (2014) provide paleogeographical maps for specific moments in the evolution of the region. Seaways existed through today's southern Spain (Martín et al., 2014, 2009) and northern Morocco (Krijgsman et al., 1999b). All of these reconstructed corridors are dated to have, probably, closed before the start of the MSC (5.97 Ma). This brings up the question: Where was the gateway that caused the MSC and what did it look like?

In this study the geometry of the gateway is addressed. Strait dynamic theory is implemented in a box model in order to predict the water exchange fluxes through the Atlantic–Mediterranean gateway. Previous model studies (e.g., Meijer, 2012; Rohling et al., 2008) considered this connection as a short strait, comparable to Gibraltar, and therefore assume that effects of length of the gateway can be ignored. Considering the reconstruction of late Miocene gateways (Figure 2.1), however, it is clear that the

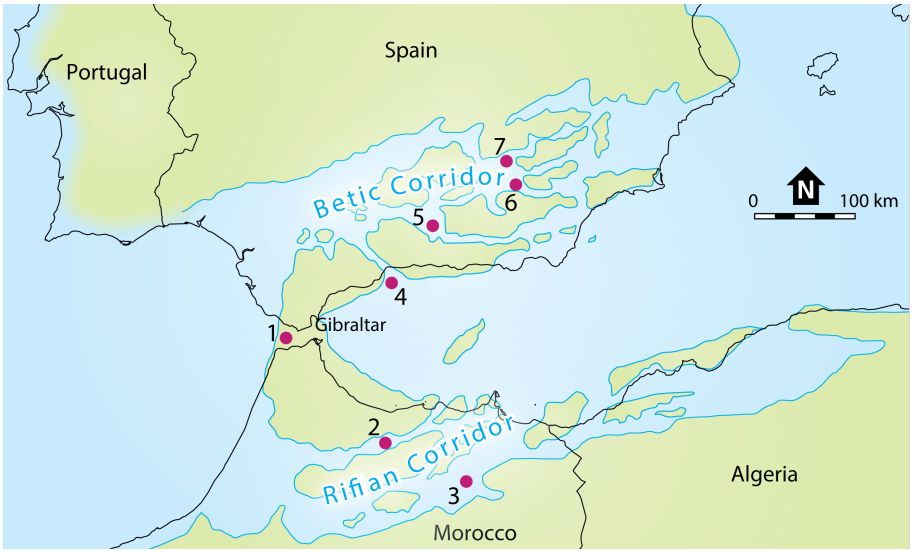

Figure 2.1 Map of the gateway region between the Atlantic and the Mediterranean. Today's coastline is shown by black lines, which indicate the Strait of Gibraltar. The reconstruction of the late Miocene of the region is shown in green (based on Santisteban and Taberner, 1983). Gateways at that time are thought to have cut through the south of Spain (Betic Corridor) and the north of Morocco (Rifian Corridor). The positions of seven corridors are indicated with red dots. For more details about each of these, please consider Table 2.1 in the Discussion Section 2.5.

effects of length have played a crucial role (Anati et al., 1977; Pratt, 1986; Garrett, 2004). In order to include the effects of length the effect of friction is implemented which allows us to give predictions about all three gateway dimensions (depth, width and length).

2.2 Budget Considerations

For the PLG stage the sea level of the Mediterranean is thought to be equal to the global level, based on two facts: (1) Facies analyses of the lower gypsum in several basin in the western Mediterranean show strong correlation, which excludes a substantial sea level fall (Lugli et al., 2008; Roveri et al., 2014a). (2) Moreover, a lowered Mediterranean sea level would not allow for a Mediterranean outflux. Consequently, all the salt flowing in from the Atlantic would be captured within the basin and would raise the salinity beyond gypsum saturation (Meijer and Krijgsman, 2005), for which no evidence is seen in the record. Therefore all the inflowing and outflowing water of the Mediterranean needs to be balanced, as indicated in Figure 2.2A. We will sometimes use the term "flux" and sometimes "flow". The physical meaning of "flux" is volume transported per unit time. "Flow" refers to water motion in general and is

commonly used to describe the velocity of a certain water mass (e.g., Section 2.5).

The water budget of the Mediterranean is regulated by the balance of evaporation (E), precipitation (P) and river input (R). In order to sustain a basin of enhanced salinity compared to its connected ocean, evaporation must exceed precipitation and river input, leading to a negative water budget. Today's examples of such basins are the Mediterranean, the Red Sea or the Persian Gulf. On the other hand, today's Black Sea, due to a positive water budget, features a lower salinity compared to its connected "ocean".

The Atlantic influx causes the Mediterranean salinity to increase, leading to a density difference between basin and ocean. This density difference establishes an exchange flow, so that Mediterranean waters start outflowing into the Atlantic. Given that we consider Mediterranean sea level equal to the global one, the five sources and sinks of water of the Mediterranean (Figure 2.2) result in the water volume conservation equation:

$$Q_{in} \;=\; Q_{out} \;+\; e \tag{2.1}$$

where Q_{in} is the Atlantic influx, Q_{out} the Mediterranean outflux and $e = E - P - R$ the effective evaporation (Figure 2.2A). The salt budget depends only on the Atlantic exchange, as evaporation, precipitation and river input are assumed to be fresh water sources and sinks:

$$V\frac{d(S_M)}{dt} \;=\; S_A Q_{in} \;-\; S_M Q_{out} \tag{2.2}$$

where the left hand side represents the change of salinity of the Mediterranean basin. V is the volume of the Mediterranean basin and S_M and S_A are the salinities of the Mediterranean and the Atlantic, respectively. The salinity unit (g/kg) we are using in the study is the amount of salt mass (g) dissolved in a certain water mass (kg). Although we are dealing with a high salinity in the Mediterranean, leading to an enhanced density, the difference between its density and that of the Atlantic is still small enough in order to make the Boussinesq approximation. This allows us to set all densities, which are not multiplied by the acceleration of gravity, to an average reference value (Pratt and Whitehead, 2007). Each factor in Equations 2.1 and 2.2 would be multiplied by this reference and therefore it cancels, which simplifies the mathematics by far, but only has a negligible effect on the final results (Pratt and Whitehead, 2007).

If we consider the steady state case, meaning that the basin salinity reached a certain value at which it stays constant, the left hand side of Equation 2.2 will be zero. Meijer (2012) showed that the basin response time to reach steady state after changes in sill depth is of the order of 10 $kyrs$ (Figure 6 in Meijer, 2012). This in itself does not conflict with our study, as our aim is to estimate the basin salinity for certain gateway dimensions and boundary conditions for a much longer time scale. As we consider the time span of the PLG stage (~ 400 $kyrs$), phase lags of the order of thousands of years are negligible. A second insight from Meijer (2012) is that due to this lag in the time, depending on the situation, the salinity reached might be slightly lower than the estimated steady state salinity. As our study focuses on first order variations similar to Rohling et al. (2008), such a slight overestimation needs to be

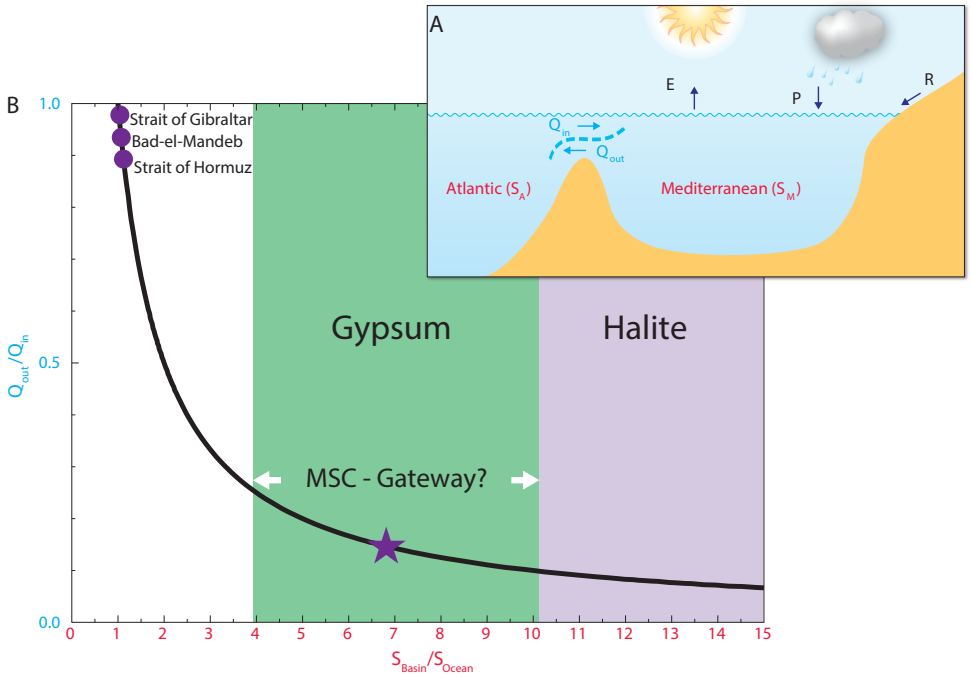

Figure 2.2 A) Main water sources and sinks of the Mediterranean basin: Evaporation (E), precipitation (P), river input (R), influx of water from the Atlantic (Q_{in}) and Mediterranean outflux (Q_{out}). B) Equation 2.3 leads to this inverse relation between outflux/influx and salinity ratio (S_{basin}/S_{ocean}) (black curve). A great salinity difference can only be sustained with a very low outflux relative to the influx. Three of today's gateways are indicated on the plot (Tsimplis et al., 2006; Johns et al., 2003; Sofianos et al., 2002) . Furthermore the regions in which the Mediterranean basin would be at gypsum (green) or halite (purple) saturation are indicated, showing how different a gateway during the PLG (indicated by star and white arrows) must have been compared to today's gateways.

kept in mind, but should not greatly affect the conclusions of the study. Therefore we rewrite formula 2.2 to its rearranged steady state form:

$$\frac{Q_{out}}{Q_{in}} = 1/(\frac{S_M}{S_A}) \tag{2.3}$$

Already this simple relationship indicates that the Atlantic–Mediterranean connection during the PLG stage must have looked different from the gateway today, as illustrated in Figure 2.2B. The curve shows an inverse relationship. To sustain an enhanced salinity (right of the plot) the outflux has to be much smaller than the influx. The outflux needs to be less than 25% of the influx of water to reach gypsum saturation and less than 10% to reach halite. This is extremely small compared to

today's gateways, where the outflux is close to equalling in influx.

During the PLG stage the Mediterranean must have been of the order of gypsum saturation. Consequently, the outflux must have been of the order of 5-10 times smaller than the influx due to a gateway of quite different dimensions. But, how can basin salinity be related to gateway dimensions instead of to fluxes? In the next section we will consider this question by considering strait dynamic theory following the example in previous hydraulic control papers (Meijer, 2012; Rohling et al., 2008; Bryden and Stommel, 1984; Assaf and Hecht, 1974).

2.3 Theoretical Basis

We will consider a gateway between the Atlantic and the Mediterranean with a rectangular cross-section (depth h and width w) and constant length l (Figure 2.3). This simplified geometry allows us to study the importance of each strait dimension in isolation.

The Momentum Equation

In order to relate the strait dimensions to the flow rates we consider the momentum equations for each layer (see Appendix for details). As there are many different forces that affect the water flow, it is necessary to weigh their importance.

In ocean straits the horizontal length scale is much greater than the vertical one, which enables us to use the shallow-water equations. These are derived by applying the long-wave approximation to the Navier Stokes equations by integrating along the depth of the fluid, which allows for a simplified mathematical formulation (Pratt and Whitehead, 2007). Following Assaf and Hecht (1974) and Pratt and Whitehead (2007) the conservation of momentum between the bottom and top layer in our gateway can be written as:

$$u_{out}\frac{du_{out}}{dx} - u_{in}\frac{du_{in}}{dx} = g'\frac{dh_{in}}{dx} + C_D\frac{u_{out}^2}{h_{out}} \tag{2.4}$$

where u_{out}, u_{in} and h_{out}, h_{in} are the outflow and inflow velocities and layer depths, respectively. x stands for the direction along the corridor, while C_D is the bottom friction coefficient and g' the reduced gravity. This momentum equation is for the case of steady flow, as it is common practise in these kind of problems (e.g., Meijer, 2012; Pratt, 1986; Assaf and Hecht, 1974).

The left hand side of Equation 2.4 represents the difference in inertia of the two water layers. If $Q_{in} \approx Q_{out}$, this difference can be approximated to be very small, which led Anati et al. (1977) to ignore it. In the MSC case, the influx must have been quite different from the outflux, making it important to retain the term.

The first term on the right hand side represents the pressure gradient between the Atlantic and the Mediterranean. This gradient is due to the density difference of the two basins/layers. It is hidden within the reduced gravity term:

$$g' = g\frac{\Delta\rho}{\rho_M} = g\frac{\rho_M - \rho_A}{\rho_M} \tag{2.5}$$

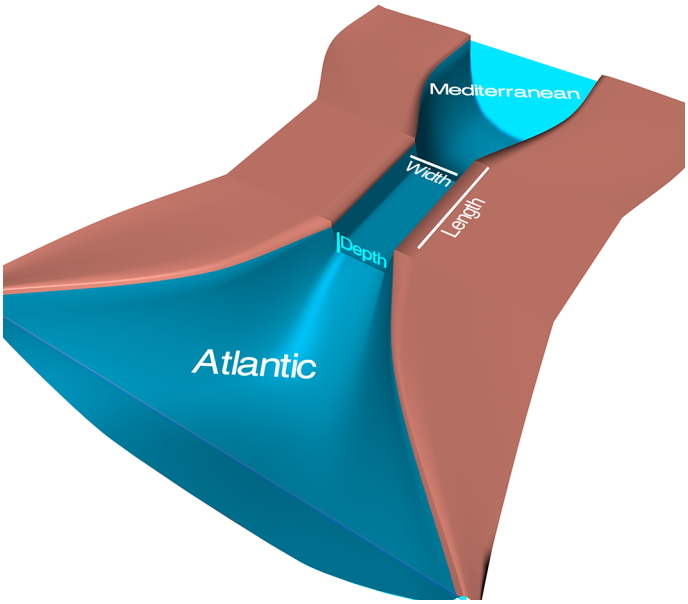

Figure 2.3 The simplified gateway between the Atlantic and the Mediterranean, we consider it rectangular in shape and of constant width w, depth h and length l.

In order to connect this relation to the salinity difference between basin and the ocean, an equation of state is needed. Following Bryden and Stommel (1984) we use:

$$\rho_M = \rho_A + \beta(S_M - S_A) \tag{2.6}$$

where $\beta = 0.77\ (kg/m^3)/(g/kg)$ is the haline contraction coefficient. In view of our emphasis on elevated salinity the effect on the density of temperature and pressure is ignored (see Topper et al., 2011, for a discussion). Both Warren (2006) and Feistel (2008) reported density of seawater to increase essentially linearly with salinity up to conditions close to gypsum saturation (starting at 130 g/kg) which justifies our use of a constant coefficient (Meijer, 2012).

The second term on the right hand side of Equation 2.4 is the friction term. It concerns the bottom friction, meaning the retardation force on the bottom layer due to the shear between water flowing in the bottom layer and the gateway floor. It is crucial to consider this term here, as it will allow us to account for the length of the gateway, rather than just the cross section (Meijer, 2012; Rohling et al., 2008). The bottom friction coefficient depends on parameters like the channel bottom topography and the sediments present (Te Chow, 1959). As we have no control on what these might have been in the last corridor before the MSC desiccation, we will use a range of values of today's gateways 0.005 to 0.012 (Zaremba et al., 2003; Gu and Lawrence, 2001; Pratt, 1984). The friction along the other surfaces or interfaces of the gateway

are not taken into consideration. Side wall friction can generally be ignored if the hydraulic radius ($w * h/(w + 2h)$) is about equal to h, as it is valid for this study (Officer et al., 1976). Surface friction is assumed to have an effect on the asymmetry of the interface between the layers, but a negligible effect on the exchange flux (Gu and Lawrence, 2005) and will therefore not be considered in this study. Assaf and Hecht (1974), Gu and Lawrence (2005) or Zaremba et al. (2003) include the effect of interfacial friction between the two layers. This would also be an option in this study. We decided, though, not to include the effect of interfacial friction in our theory for two reasons: (1) Due to interfacial friction another friction factor needs to be considered. Not many measurements from today's gateways exist regarding this friction factor and it seems generally hard to predict (Zhu and Lawrence, 2000). (2) Already by including the bottom friction the importance of the length and friction can be analysed (Pratt and Whitehead, 2007). A further effect linked to the interface, that we ignore, is the interfacial mixing. This mixing between the counterflowing layers is known to occur, but it is not well understood how it affects the exchange flow (Ivey, 2002). Özsoy et al. (2001) studies interfacial mixing for the case of the Bosphorus. In general mixing between the two layers might decrease the density difference between them, this would lead to a lower reduced gravity in Equation 2.5 and thus correspond to a weaker exchange between the Atlantic and the Mediterranean.

The Coriolis effect will have a greater effect on the momentum balance with increasing width of the gateway. Generally, the Coriolis force can be neglected if the width of the gateway is smaller than the Rossby radius $R = \sqrt{g'h}/f$, where h is the total gateway depth and f ($= 8.5 * 10^{-5} s^{-1}$) is the Coriolis parameter for the appropriate latitude (Whitehead, 1998). As our focus is on gateways of width of $\sim 10\ km$ or less, the simplification is justified.

In order to relate Equation 2.4 to the water and salt conservation equation in Section 2.2, the velocities need to be changed to water fluxes, using $Q_{out} = u_{out} * h_{out} * w$ for the bottom layer and likewise for the top layer. After rearrangement the resulting relation (see Appendix) is:

$$\frac{Q_{in}^2}{h_{in}^3} + \frac{Q_{out}^2}{h_{out}^3}(1 + F) = w^2 g' \tag{2.7}$$

where w is the corridor width and $F = C_D / \frac{dh_{out}}{dx}$ the factor that brings in the effect of friction. If F is set to zero, which effectively equals a "frictionless" or "lengthless" gateway, Equation 2.7 becomes the well known hydraulic control equation (e.g., Bryden and Stommel, 1984).

Computing the interface position and basin salinity

Equation 2.7 relates the water fluxes to the strait dimensions. By combining it with the conservation of salt and water (see Appendix), this turns into Equation 2.8, that can be used to predict the expected average basin salinity for specific gateway dimensions and effective evaporation across the basin. For depth, width and length we will explore a range of values in the next section. Evaporation will be set according to previous climate studies (e.g., Gladstone et al., 2007, which is also close to today's

value, Mariotti et al., 2002) and will be further discussed in Section 2.5.

$$\frac{1}{(1-\frac{S_A}{S_M})^2(1-f)^3}+\frac{(1+F)}{(\frac{S_M}{S_A}-1)^2 f^3}=BC\frac{S_M-S_A}{\rho_A+\beta(S_M-S_A)} \tag{2.8}$$

where

$$f=h_{out}/h \quad BC=\frac{h^3w^2g\beta}{e^2} \tag{2.9}$$

There are two further variables that need to be set: (1) the average interface gradient ($\frac{dh_{out}}{dx}$ in F) of the interface of the two water layers and (2) the interface height $f=h_{out}/h$.

We let the interface along the channel vary linearly, so that $\frac{dh_{out}}{dx}\approx\frac{h}{l}$. This is a simplification, but based on the following reasoning we concluded that it is a valid approximation given the first order nature of our analysis. Anati et al. (1977) compared laboratory experiments to theory that is also based on Equation 2.4, but by ignoring the inertia term on the left hand side. They found that the results came to reasonable agreement. Nevertheless, Gu and Lawrence (2005) showed that the interface along the channel can be approximated to being linear in the middle of the channel (part in our focus), but is curved towards the ends. Gu and Lawrence (2005) compared their results to those of Anati et al. (1977) indicating that the flux is slightly overestimated for short channels and slightly underestimated for long channels in the Anati study, but in a range that is acceptable in our first order model set-up, which focuses on the average exchange flux through the corridor instead of on the interface. One major improvement of our model, compared to that of Anati et al. (1977) is the inclusion of the inertia of the two layers flowing which will further decrease the uncertainty and give a realistic result (see Pratt and Whitehead, 2007, for further discussion). Moreover, the interface gradient always occurs in combination with the bottom friction coefficient C_D in the term F. The variation of C_D will already give a range of answers, which will make effect of variation in interface gradient relatively small.

Another important variable to be considered is the interface depth $f=h_{out}/h$. Whereas Meijer (2012) considered many different interface depths in order to study how it affects the exchange, in this study we will focus on a single one: that of the maximal exchange solution (Farmer and Armi, 1988, 1986; Armi and Farmer, 1987; Dalziel, 1992). The maximal exchange solution provides, for a given gateway geometry, the lowest possible basin salinity. If the interface lies below or above of where the maximal exchange requirement places it, the exchange is less than maximal and basin salinity higher. The same holds true if we were to include interface friction or the Coriolis force: these also reduce strait efficiency and would yield higher salinity for a given strait geometry. Thus, if our question is which strait geometry is needed to reach a specific elevated basin salinity (for instance, the gypsum saturation value), our analysis provides us with the minimum cross section and the maximum length of the responsible gateway. The actual gateway may have been deeper, wider or shorter, but only if there were other factors at play reducing its efficiency.

The method to find the interface depth for maximal exchange is described in

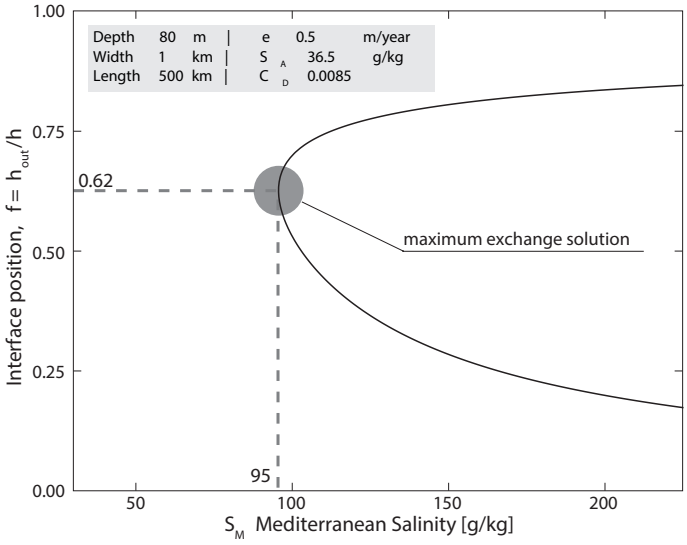

Figure 2.4 Plot of interface depth $f = h_{out}/h$ and Mediterranean salinity S_M, using Equation 2.8. There is only one salinity that has a single solution for the interface. This salinity is the solution for maximum exchange, as indicated by the grey circle and the dashed lines. The parameters used for this example are indicated in the box.

Stommel and Farmer (1953) and Bryden and Stommel (1984). Although we follow the same reasoning, our Equation 2.8 looks slightly different from Equation 5 in Bryden and Stommel (1984) because friction is included. Equation 2.8 is plotted in Figure 2.4 for a specific case. The y-axis indicates the depth of the non-dimensionalised channel depth at the centre of the channel and the x-axis is the expected salinity of the lower layer, which in our case equals Mediterranean salinity. The graph shows that in this case for salinities lower than about 95 g/kg there is no solution to Equation 2.8 while above this value there are always 2 possible interface positions that would lead to the same basin salinity. Here we basically present the same idea as Figure 2 in Bryden and Stommel (1984), but in a way that allows us to compare directly the interface position with basin salinity. The turning point on the graph is the only point where a unique solution exists, which equates to the maximal exchange solution. Using differential techniques it is possible to find the exact value at the turning point for any kind of channel dimensions, Atlantic salinity and effective evaporation.

2.4 Model Results

Equations 2.3 and 2.8 allow us to calculate Mediterranean salinity and the exchange fluxes in the gateway for given gateway dimensions. The overall result is that in order to restrict a basin strong enough to cause highly saline waters, the gateway

connecting it to the global ocean needs to be relatively long, shallow and/or narrow. This intuitive result is quantified below.

Cross Section Variations

The effect of variations in gateway cross section on basin salinity and exchange flux is illustrated in Figure 2.5. Depth and width are considered separately, although their general behaviour is similar, as already studied in Meijer (2012) for short gateways.

For depth approaching 150 m and beyond and for width exceeding 5 km the curves show minor variations in the exchange flux ratio and basin salinity. Such "large" gateway dimensions apply to straits like the present Strait of Gibraltar (depth ~ 300 m and width ~ 14 km). As seen in Figure 2.2, the salinity difference between the Atlantic and the Mediterranean is indeed very low today (about 2 g/kg) and the outflux almost matches the influx.

Shallower (less than 150 m) and narrower (less than 5 km) gateways show much stronger variations in response to changes in depth or width. Whereas the exchange flux strongly decreases towards a state in which the outflux is much smaller than the influx, the basin salinity increases in large steps with small decrease in depth or width. This highly nonlinear trend will have a major impact on the basin salinity when the gateway is already narrow or shallow. If such a shallow gateway is influenced by global sea level variations the salinity of the basin may change dramatically. This has already been considered by Rohling et al. (2008) and will be reconsidered in section 2.4.

The effect of length and friction can also be seen in Figure 2.5, as the variation of these two factors determines the thickness of each coloured band. Minimum salinity and maximum exchange ratio refer to the frictionless case and maximum salinity and minimum flux corresponds to a bottom friction coefficient of $C_D = 0.012$ and a length of $l = 1000$ km.

Length Variations

The effect of gateway length is further demonstrated in Figure 2.6. The general trend indicates that the longer the gateway, the greater the restriction and therefore the higher the basin salinity. The reason for this is that the bottom friction slows down the bottom current, which allows less water to flow out. Because of the conservation of water (Equation 2.1), if less water flows out, less water flows into the Mediterranean. The resulting steady state has a lower exchange flux ratio (more restriction) and results in a higher basin salinity.

In general it can be seen that for shorter gateways (less than 400 km) the salinity increases and flux decreases in a more rapid and nonlinear way with increasing length. This levels out into a roughly linear increasing salinity and decreasing flux for longer gateways. The deeper or wider a gateway is, the less important the effect of length, as seen in Figure 2.6 (top right). With width equal to $5km$ the salinity only varies by about 10 g/kg for the 100 m deep corridor and about 30 g/kg for the 50 m deep corridor. Although these variations are large in a normal oceanographic sense, they are minor against the background of a basin leading into gypsum and, even, halite

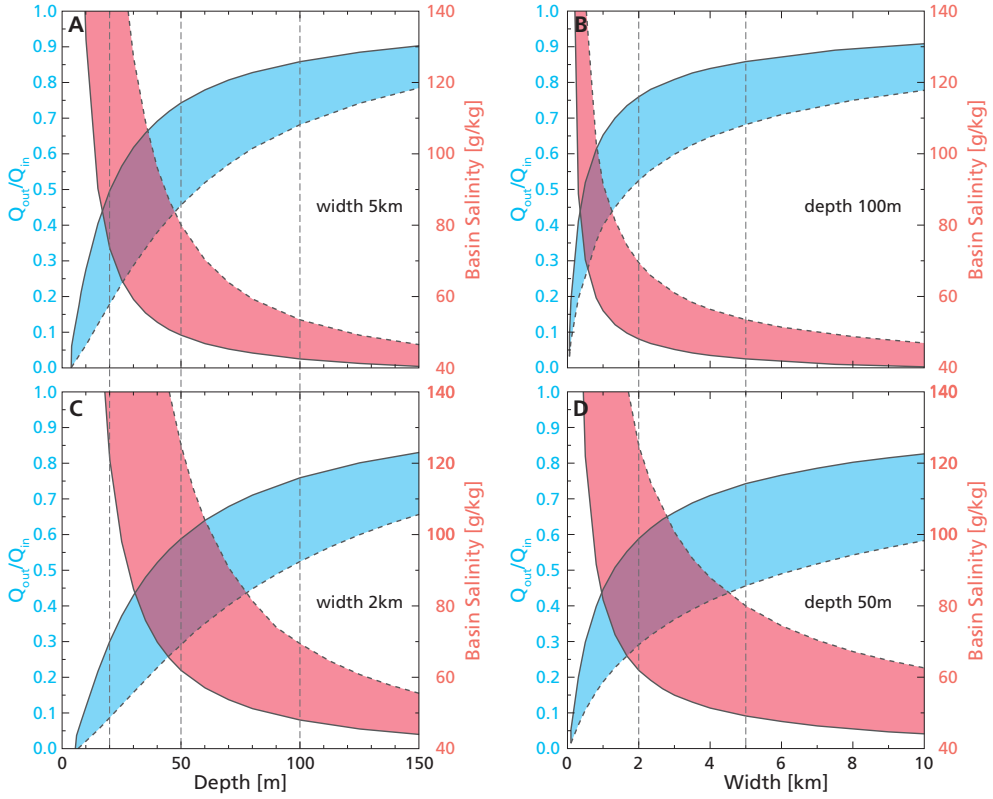

Figure 2.5 Panels show basin salinity (red) and exchange flux ratio (blue) and how they vary for different gateway depth (left hand side) and different width (right hand side). Each variation is presented by a range (coloured area) due to the change in length and friction factors used. The minimum salinity or maximum flux ratio always refers to the case of no friction or effectively no length ($F = 0$). This is indicated by the solid black line at the bottom of the red region and top of the blue region. The maximum salinity or minimum flux ratio always refers to $F = C_D * l/h$, where the maximum C_D is 0.012 and we let the length l vary up to 1000 km at first. This is indicated by the dashed black line at the top of the red region and bottom of the blue region. The role of length in setting the range is demonstrated in Figure 2.6 for the cases (depth 20 m, 50 m and 100 m and width 2 km and 5 km) indicated with the vertical dashed black lines.

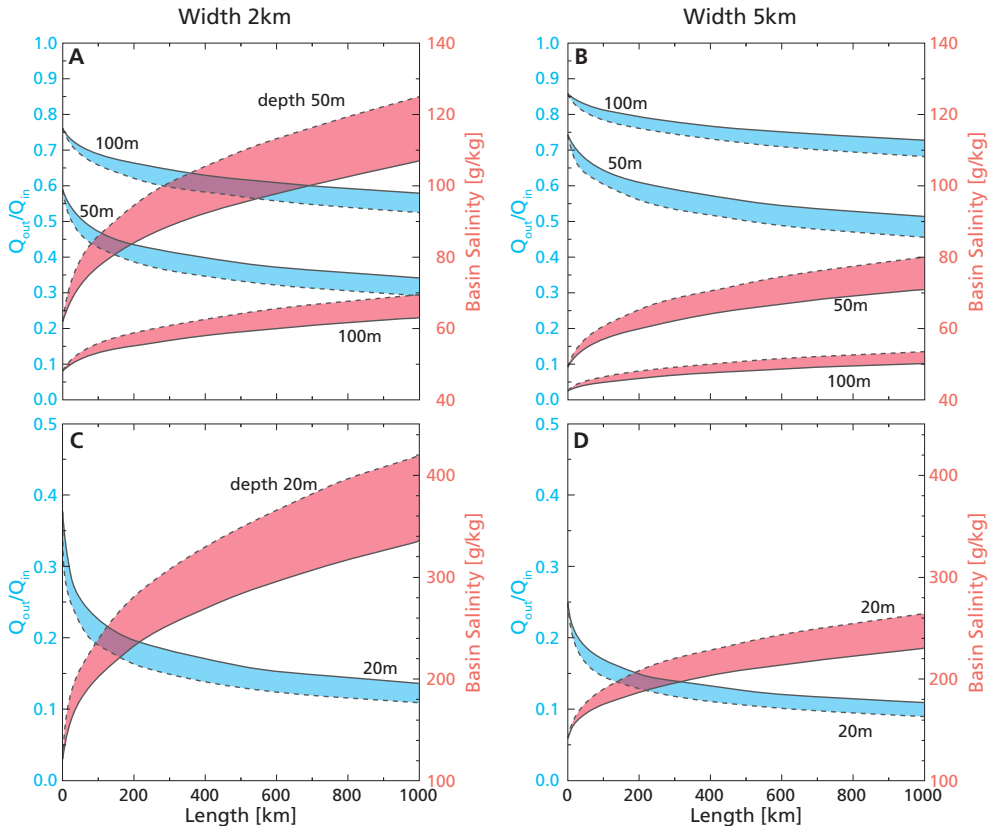

Figure 2.6 Plots of variations in water flux ratio and basin salinity with gateway length. The variations shown are the ones indicated by the vertical dashed lines in Figure 2.5. Bottom friction coefficients are set to the range of $0.005 - 0.012$. The minimum salinity or maximum flux ratio always refers to the case of $C_D = 0.005$, which is indicated by the solid black line at the bottom of the red region and top of the blue region. The maximum salinity or minimum flux ratio always refers to $C_D = 0.012$, which is indicated by the dashed black line at the top of the red region and bottom of the blue region. Top: Gateway depths are 50 m and 100 m for gateway width of 2 km (left side) and 5 km (right side). Bottom: Gateway depth of 20 m, due to this very shallow depth different salinity and flux ratio scales had to be chosen.

saturation. Therefore for these deep and wide corridors the effect of length and friction is minor in the context of the MSC. On the other hand, for shallower or narrower gateways as shown in Figure 2.6 (left and bottom) the salinity variation due to length can be much more severe and may actually control whether the basin reaches, for example, gypsum saturation.

Gateway dimensions that lead to gypsum saturation in the Mediterranean

The maximum possible length a gateway connecting the Atlantic to the Mediterranean can have had is around 500 km, because this is the maximum distance through Spain or Morocco. If we set the gateway to this length, it is possible to reorganise the above results in order to show what kind of cross section is needed to reach gypsum saturation in the basin. The result is shown in Figure 2.7. It shows, again, that greater cross section will lead to a less saline basin and a smaller cross section to a more saline basin. Any cross section picked in the green region will lead to a basin of gypsum saturation. This might, for example, be a gateway of 10 km width and 10 m depth or a gateway of 800 m width and 70 m depth.

This still allows for many different cross sections for a certain gateway length, therefore here we need a method for limiting these results in order to get a first order estimate of the gateway dimensions that led to the MSC. Our approach is similar to Rohling et al. (2008), but in reverse.

The PLG phase of the MSC lasted from 5.97 Ma to 5.61 Ma (Manzi et al., 2013). During this ~ 400 $kyrs$ period, layers of gypsum were deposited in various locations around the margins of the Mediterranean (Krijgsman et al., 1999a). The gypsum occurs in regular alternations that have been tuned to be caused by climate cycles due to precession of the Earth (Krijgsman et al., 2001). What is not seen is an expression of obliquity-controlled sea level variations (Krijgsman et al., 1999a; Hilgen et al., 2007). Apparently, the gateway dimensions were such that changing global sea level did not cause basin salinity to either pass below, or reach beyond, the gypsum saturation field.

The global sea level is thought to have varied by around 10 m before the start of the MSC (6.14 Ma) and up to an amplitude of around 30 m at 5.26 Ma (Aharon et al., 1993; timescale of Hilgen, 1991). Further evidence for these fluctuations were given by Braga and Martín (1996), estimating sea level changes of the order of tens of meters in the Sorbas basin. These estimates of $10 - 30$ meter sea-level variations are consistent with the amplitude of the benthic $\delta^{18}O$ changes in Site 982 (Hodell et al., 2001). Therefore we assume that a sea level variation of an amplitude of around 20 m need to be able to sustain a Mediterranean basin at gypsum saturation.

We can now return to Figure 2.7 and pick the gateway that will allow for these sea level changes, but still satisfies the gypsum saturation. For a gateway of 500 km length the minimum depth is around 30 m and the maximum width is around 1.5km. By repeating this thought process for various length up to 500 km it is possible to find a range of the gateway cross sections that existed during the PLG stage of the MSC. From this we can conclude that the cross section during that time had a minimum depth of about $30 - 45$ m and a maximum width of about $0.7 - 2$ km.

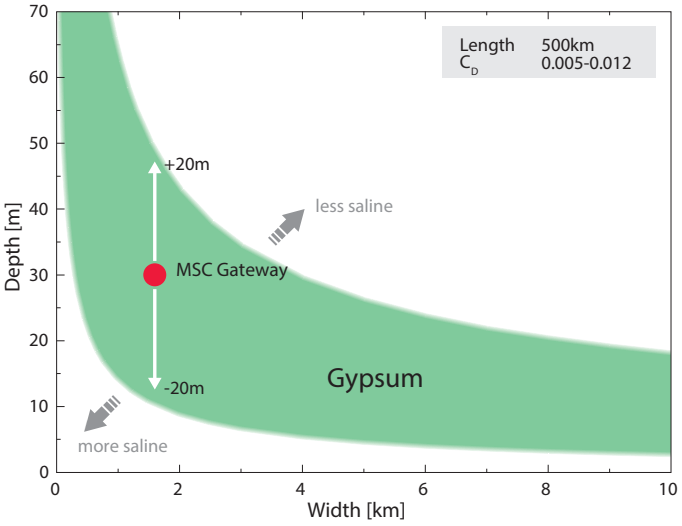

Figure 2.7 The range of combinations of depth and width of a 500 km long gateway, that will cause gypsum saturation in the Mediterranean. The bottom friction coefficient is in the range $C_D = 0.005 - 0.012$. Moreover the sea level variation of an amplitude of 20 m are indicated with the gateway at its minimum depth.

2.5 Discussion

In this study, the theory of hydraulic control with the inclusion of bottom friction is used in order to relate the exchange flux and basin salinity to the strait dimensions. Here we evaluate some of the assumptions and the effect on the model results of specific variables. We also consider our results in the light of previous work and explore their implications.

Model Evaluation

Response to Climate Change

"Climate" in our model is represented by the effective evaporation $e = E - P - R$. It is set to a value that lets 0.5 m of Mediterranean water at the surface disappear within a year, which is based on Gladstone et al. (2007). Gladstone et al. (2007) exclude the drainage of the Chad basin, which could lead to increase in river input and therefore to a less negative, or even positive water budget.

Already by considering the water and salt conservation (Equations 2.1 and 2.3) it is clear that an increase in e will lower the flux ratio and a decrease in e will increase the flux ratio. Figure 2.8 shows how our model responds to different values of e for a given gateway. Basin salinity basically changes linearly. Meijer (2012) considered some variation of effective evaporation in his model. Figure 4c in Meijer (2012) illustrates that an effective evaporation variation of 0.50 ± 0.25 $m/year$ will

lead to a salinity variation of about $\pm 30\ g/kg$. This is consistent with what we predict for the frictionless case, keeping in mind that the interface position in Meijer (2012) is constant for each case, but ours is always the maximal exchange solution. When friction is included the linear trend stays, but the salinity change is more extreme for a given e variation. For an effective evaporation variation of $0.50 \pm 0.25\ m/year$ the salinity variation is about $\pm 60\ g/kg$. Such a linear trend makes it straightforward to extrapolate Figures 2.5 and 2.6 for different effective evaporation values.

Response to interface position

For our model we choose to stay within the overmixing limit (Stommel and Farmer, 1953; Bryden and Stommel, 1984), which sets the interface to its lowest energetic state. This is the state that will ensure the maximal exchange between the two water masses. To note is that the bottom friction slows down the bottom current and therefore causes the interface to sit higher than it is expected without friction. Different points on the curve of Figure 2.4 indicate how the interface changes if the system would not be at maximal exchange. Meijer (2012) considers different interface positions for the frictionless hydraulic control case. With friction we notice that for less restricted gateways small changes in the interface position will hardly effect the basin salinity. The greater the restriction, however, the more sensitive will the predicted salinity change with interface position. Therefore it is also important to consider the factors that control, whether the system can be considered to be in maximal exchange. Armi and Farmer (1987) summarise the main features that need to hold in order to consider an exchange to be maximal. This comes down to the requirement that the flow through the strait is bounded by supercritical flows at each side. Whether a flow is defined to be supercritical depends on the combined Froude number, if that is larger than unity, the flow is said to be supercritical. On the Atlantic side of our channel the bottom layer becomes very shallow and the flow velocities high, therefore the combined Froude number will easily reach a supercritical stage. On the Mediterranean side, the depth of the top layer start tending towards zero, as the flow enters the basin, which also set the flow in a supercritical stage. This indicates to us that it is a reasonable assumption to take the flow to be maximal. This requirement always holds, even for unsteady cases or when friction is considered (Armi and Farmer, 1987).

Further restricting effects

Our study focuses on gateways of constant depth, width and length. Figure 2.1 shows reconstructed gateways that seem more complex. The more complex the geometry of these gateways is, the more additional effects on the exchange flux and therefore on the basin salinity will come into play. Potential complexities are channels with many bends and curves, that could resemble a meandering river, islands sitting within a channel, multiple channels, or varying cross section (depth and width). We speculate that these effects could lead to: (1) An increased effective length of the channel, leading to further restriction, as indicated in Figure 2.6. (2) An effectively smaller cross section, due to changing depth and width, which would also lead to more restriction,

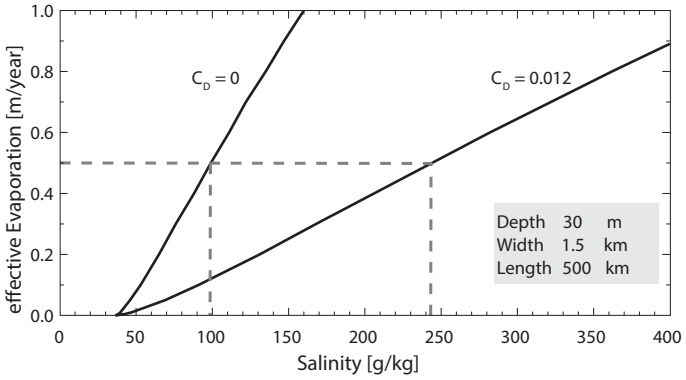

Figure 2.8 The effect of the change in effective evaporation on the basin salinity for a gateway of depth of 30 m, width of 1.5 km and length of 500 km for the zero friction case and the maximal friction case. The dashed line indicates the salinity values for this gateway example.

as demonstrated in Figure 2.5. (3) More turbulence at side or bottom, which would add an extra retardation effect. Once more control is available about the connection that existed during the PLG stage from field and proxy studies, it becomes meaningful to study these effects in more detail. For example with a regional ocean general circulation model (see de la Vara et al., 2015).

Interfacial friction will also further restrict the exchange, in a way that is expected to be similar to the role of bottom friction. That is, less important for deeper and shorter gateways and potentially more important for shallower and longer ones. Zhu and Lawrence (2000) conclude that the friction factor associated with interfacial friction in not easy to measure or predict accurately, because of its dependence on turbulence between the flows. Although it is thus hard to say to which extent interfacial friction will affect the exchange, it is clear that it will allow for gateway dimensions that can be slightly deeper, wider or shorter in order the reach the same salinity in the basin. Mixing across the interface between the two flowing layers would have a similar effect (see Theory Section 2.3). Therefore, the greater the interfacial mixing, the lower the exchange of water between the ocean and the basin. This would lead to higher basin salinities, just as decreasing gateway depth or width or increasing its length.

A final factor of which the effect is likely to always remain highly uncertain, is the occurrence of tides. Our velocities may be thought of as representing the mean state, averaged over multiple tidal cycles, only to the extent that tides impose a linear oscillation on the exchange flows. For specific channel geometries resonance may occur (Officer et al., 1976) and the effect may be nonlinear. To tackle this uncertainty in a meaningful way would seem to require knowledge regarding channel geometry much more precise than we have available.

Relevance of the results

Implications for sedimentary bed forms within the gateway

Although, so far, we focused on water transports, our results can also be expressed in terms of the mean velocities of flow in each of the two layers (using $Q = u * h * w$, where u is the layer velocity). The rate of flow in the bottom layer is of particular interest because it is related to the sedimentation, transport and/or erosion that occurs on the gateway floor. This potentially provides another link between the model and geological observations.

Here we focus on a gateway of channel dimensions depth 30 m, width of 1.5 km and length 500 km. For an effective evaporation, that would remove 0.5 m of water from the whole surface of the Mediterranean per year, this gateway would cause an exchange flux that would lead to gypsum saturation in the basin, as shown in the results (Section 2.4). Figure 2.9 illustrates this gateway with the two water layers indicated. The mean outflow velocity along the channel is calculated from modelled outflux. The depth of the bottom layer varies along the channel. The interface is taken to be linearly varying along the channel, leading to a relative high flow velocity close to the Atlantic and a much lower one on the Mediterranean side, with a gradual variation in between. This does not give the exact interface depth at a certain channel position, but provides values for mean velocity that are of the right order. Figure 2.9 also shows how the mean flow velocity varies for a certain position along the corridor. Because the velocities are plotted with a log-scale it is straightforward to link the velocities to the bed form diagram on the right. This diagram is simplified from experimental/laboratory studies of steady unidirectional water flows of rivers, by Boguchwal and Southard (1990) and Ashley et al. (1990). Although there are several different bed form diagrams in use with various velocities or shear stresses studied, we decided to use this one, as according to Leeder (1999) it is the most simple representation, which is in accordance with the our aim to gain first order insights. It has been used in numerous of studies, although it is important to keep in mind that the scaling from laboratory experiments to natural environments and the use of a mean velocity can cause uncertainties (Leeder, 1999; Kostaschuk and Villard, 1996).

Figure 2.9 indicates that on the Mediterranean side for finer grains we should expect ripples and no motion for coarser grains. The further away from the Mediterranean and the closer to the Atlantic, the cross section of the bottom layer decreases and the corresponding increase of the average flow velocity would lead to dunes and anti-dunes.

This first look at the problem already provides important insight. Although intuitively one might expect that a very restricted gateway would be associated with high flow rates and therefore would perhaps be dominated by erosion, here we show that the velocities would correspond to "normal", well known sedimentary structures that should be able to be recognised in the field. Betzler et al. (2006) and (Martín et al., 2001) describe cross-bedded strata within the Guadix basin and the Guadalhorce corridor. It is important to stress, though, that these two studies consider sediments of ages older than 7.8 Ma and 6.3 Ma, respectively, which relate to earlier stages of the gateway we are looking for. We are here considering the corridor that must

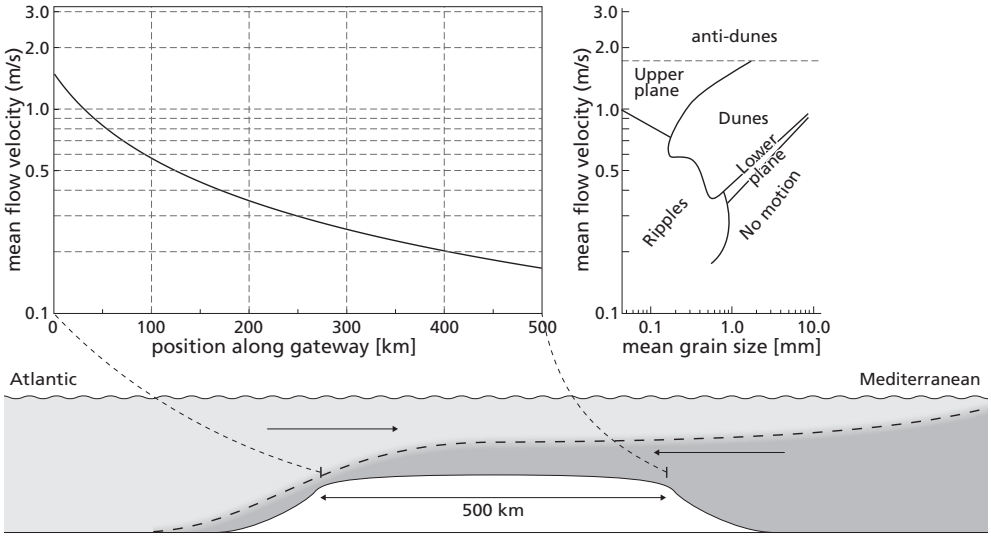

Figure 2.9 At the bottom our idealised gateway for a depth of 30 m, a width of 1.5 km and a length of 500 km is shown. The plot on the top left indicates the approximated mean flow velocity (log scale) of the bottom layer, using our model, for the positions along the gateway. This can be easily compared to the simplified bed form phase diagram on the top right, following Leeder (1999), Boguchwal and Southard (1990) and Ashley et al. (1990).

have existed during the first stage ($5.97 - 5.61\ Ma$) of the MSC (Topper et al., 2011; Roveri et al., 2014a).

Which gateway was the last existing one?
The purpose of this study is to estimate the dimensional limits of the Atlantic–Mediterranean connection during the PLG stage. We know that a connection must have existed (Topper et al., 2011), but where the connection was is still to be determined. Figure 2.1 shows several of the Atlantic–Mediterranean corridors reconstructed for late Miocene time. They did not all coexist at the same time but opened and closed through time related to tectonic movements. The reconstructions are based on connecting sediment patches of equal ages. Commonly, closing ages are determined from sedimentary successions that document a change from marine to continental conditions (e.g., Krijgsman et al., 1999b). Most of the corridors are associated with an unconformity (e.g., Hüsing et al., 2010 or Krijgsman et al., 1999). From the outcrop alone it is not possible to determine whether the unconformity is non-depositional such that the youngest marine sediments are indicative of the timing of the last marine connection, or is erosional so that exchange persisted, but the record of it has been removed. An additional source of uncertainty regarding the age of closure comes from the question whether the end of marine sedimentation in

Position on Figure 2.1	Gateway	Width [km]	Length [km]	Depth (Gypsum) [m]
1	Strait of Gibraltar	13	60	$5-11$
2	northern Rifian	10	400	$8-17$
3	southern Rifian	50	600	<8
4	Guadalhorce (Betics)	2	150	$17-35$
5	Granada (Betics)	2	50	$15-29$
6	Guadix (Betics)	2	50	$15-29$
7	North-Betic Strait	20	200	<10

Table 2.1 Many gateways have been reconstructed for the late Miocene, here is a list of the main ones. They are also indicated on the map of Figure 2.1 with the numbers given in the first column. The table shows the approximate width and length from the reconstructions. The last column shows the depths these gateways would need to have in order to cause a Mediterranean at Gypsum saturation, based on our study. The dimensions follow from the studies by Blanc (2002); Wernli (1988); Krijgsman et al. (1999b); Martín et al. (2001); Corbí et al. (2012); Hüsing et al. (2010); Betzler et al. (2006); Martín et al. (2009) and by personal communication with José M. Martín.

a basin adjacent to a corridor is indicative of the time of closure of the corridor itself (see, for example for the Granada basin, Martín et al. (1984) and García-Veigas et al. (2013, 2015) versus Corbí et al., 2012).

A new approach to constraining the timing of closure is the use of isotope water mass tracers measured in continuous Atlantic records. For the Rifian corridors (from the section Ain el Beida in northwest Morocco), Ivanovic et al. (2013) suggest that at least a component of the age gap is generated by erosion. Likewise, for the Guadalhorce Corridor (Betics) an end of the Mediterranean outflow can be dated to 6.18 Ma (Pérez-Asensio et al., 2012).

In an attempt to contribute to this discussion, we will look at the problem from a different angle, considering the dimensions only, irrespectively of the proposed closure time. The most important corridors are summarised in Table 2.1, together with their estimates of width and length. Corridor width (Table 2.1, column 3) represents a minimum, as the edges of the seaways may have been removed by erosion. Corridor length (Table 2.1, column 4) is a matter of definition. We took the length of the corridors to be the length at which the width is relative constant and minimal. Our model predicts for each of these combinations of corridor width and length a gateway depth that could sustain a Mediterranean at gypsum saturation. We do so for the whole set of corridors, to be able to study as many different cases as possible. The calculated depths are indicated in the last column of Table 2.1.

For the wider and/or shorter corridors (Strait of Gibraltar, southern Rifian, North-Betic Strait) the calculated depth would be of the order of 10 m or less. Such a very shallow depth would cause the basin salinity to move in and out of the gypsum saturation (as discussed in Section 2.4) if the global sea level varies, or might even close the strait, which would lead to falling sea level in the Mediterranean during the PLG, which is not seen in the record (see Section 2.2 for discussion). Narrower or longer gateways (northern Rifian, Guadalhorce, Guadix and Granada) yield a depth

up to around 35 m. These depths would permit such sea level variation.
Our model suggests, purely in terms of dimensions and disregarding the proposed ages, that only the northern Rifian, the Guadalhorce, the Guadix and the Granada corridor are corridors of the type that could cause the Mediterranean to reach gypsum saturation during the PLG stage. All these are suggested to have been closed before the PLG stage (last to close is the Guadalhorce corridor around 6.3 Ma (Martín et al., 2001). This brings us back to one of the initial question: Where was this gateway located and where can we find the sediments deposited within it? It could be that there existed a corridor of dimensions similar to the ones listed above, that does not appear in the records at all, because it has been removed by erosion, for example due to the opening of the Strait of Gibraltar (Garcia-Castellanos et al., 2009).

2.6 Conclusions

This study uses the theory of hydraulic control including the effect of bottom friction in order to explore the dimensions of the gateway that must have existed during the PLG phase of the MSC. The results were compared with field observations and constraints on sea level variation locally and globally. This allows us to consider what sedimentary regime is anticipated within in the gateway and which of the possible corridors may have been the conduit for exchange during PLG precipitation.

Our main findings are:

1. In order to cause a salinity crisis, the outflux through the gateway needs to be around 25% or less of the influx to reach gypsum saturation and around 10% or less to reach halite saturation.

2. A basin of enhanced salinity relative to its connected ocean needs a negative water budget and a restricted gateway. Restriction, effectively, means a reduction in exchange flux ration (Q_{out}/Q_{in}), which can be achieved by shallowing, narrowing and/or lenghtening of the gateway.

3. The idealised Atlantic-Mediterranean connection that led to the MSC has been approximated, to first order, to a minimum depth of $30-45$ m and a maximum width of about $0.7-2$ km for a gateway length up to 500 km.

4. Sedimentation is expected in the PLG gateway, with ripples on the Mediterranean side and dunes/anti-dunes on the Atlantic side.

5. The calculated gateway dimensions alone (i.e. disregarding the, as yet, limited geological constraints on the age of closure) would exclude some of the reconstructed late Miocene gateways from being the conduit for exchange during the PLG stage of the MSC. The only gateways that lie in the right dimension region are the northern Rifian, the Guadalhorce , the Guadix and the Granada corridor.

Chapter 2 — Appendix — Detailed Theory

From the conservation of momentum to hydraulic control

How to move from the shallow water equations to the hydraulic equation including bottom friction is laid out here, following Assaf and Hecht (1974) and Pratt and Whitehead (2007):

$$u_{out}\frac{du_{out}}{dx} - u_{in}\frac{du_{in}}{dx} = g'\frac{dh_{in}}{dx} + C_D\frac{u_{out}^2}{h_{out}} \tag{2.10}$$

This equation represents the difference in inertia between bottom and top layer on the left hand side and the pressure gradient and friction term on the right hand side, where u_{out}/u_{in} and h_{out}/h_{in} are the average out/inflowing velocity and the average bottom/top layer depth, respectively. g' is the reduced gravity, C_D the bottom friction coefficient and x represents the direction along corridor. Now $Q = u * h * w$ is used to transfer from velocities to fluxes, which becomes important later in order to connect to the conservation of salt and water.

$$\frac{Q_{out}^2}{w^2 h_{out}}\frac{d(1/h_{out})}{dx} - \frac{Q_{in}^2}{w^2 h_{in}}\frac{d(1/h_{in})}{dx} = g'\frac{dh_{in}}{dx} + C_D\frac{Q_{out}^2}{w^2 h_{out}^3} \tag{2.11}$$

To simplify the differentials the quotient rule $\frac{dh^{-1}}{dx} = -h^{-2}\frac{dh}{dx}$ is applied:

$$-\frac{Q_{out}^2}{h_{out}^3}\frac{dh_{out}}{dx} + \frac{Q_{in}^2}{h_{in}^3}\frac{dh_{in}}{dx} = w^2 g'\frac{dh_{in}}{dx} + C_D\frac{Q_{out}^2}{h_{out}^3} \tag{2.12}$$

Lawrence (1993) shows that the surface slope along the channel depends on the density difference of the two water layers and on the Froude numbers of the different flows, but is also directly proportional on the channel bottom slope. The channel bottom slope of our channel is zero, therefore the surface slope is also zero. This leads us to the equation $h = h_{in} + h_{out} = constant$, which allows us to simplify the equation, as it has been done often before (e.g., Assaf and Hecht, 1974; Zaremba et al., 2003), to:

$$\frac{Q_{out}^2}{h_{out}^3}\frac{dh_{in}}{dx} + \frac{Q_{in}^2}{h_{in}^3}\frac{dh_{in}}{dx} = w^2 g'\frac{dh_{in}}{dx} + C_D\frac{Q_{out}^2}{h_{out}^3} \tag{2.13}$$

This can be rearranged to:

$$\frac{dh_{in}}{dx}\left[\frac{Q_{out}^2}{h_{out}^3} + \frac{Q_{in}^2}{h_{in}^3} - w^2 g'\right] = C_D\frac{Q_{out}^2}{h_{out}^3} \tag{2.14}$$

which can be written as:

$$\frac{Q_{in}^2}{h_{in}^3} + \frac{Q_{out}^2}{h_{out}^3}[1 + F] = w^2 g' \tag{2.15}$$

where

$$F = C_D / \frac{dh_{out}}{dx} \tag{2.16}$$

Connecting the conservation of momentum, salt and water

Combining equations of the conservation of salt and water, the Knudsen relations (Knudsen, 1900; Nielsen, 1912) follow:

$$Q_{in} = \frac{e}{1 - S_A/S_M} \tag{2.17}$$

$$Q_{out} = \frac{e}{S_M/S_A - 1} \tag{2.18}$$

Inserting these into Equation 2.15, it results in:

$$\frac{e^2}{(1 - S_A/S_M)^2(1-f)^3} + \frac{e^2}{(S_M/S_A - 1)^2 f^3}(1 + F) = h^3 w^2 g' \tag{2.19}$$

where $h_{out} = fh$ and $h_{in} = (1 - f)h$.
This turns into:

$$\frac{1}{(1 - S_A/S_M)^2(1-f)^3} + \frac{1 + F}{(S_M/S_A - 1)^2 f^3} = BC * \frac{S_M - S_A}{\rho_A + \beta(S_M - S_A)} \tag{2.20}$$

where

$$BC = \frac{h^3 w^2 g \beta}{e^2} \tag{2.21}$$

Equation 2.20 is the equation used to plot Figure 2.4, which is used to compute all the results for different gateway settings.

3

Quantifying the Mediterranean freshwater budget throughout the late Miocene: New implications for sapropel formation and the Messinian Salinity Crisis

The cyclic sedimentary record of the late Miocene Mediterranean shows a clear transition from open marine to restricted conditions and finally to evaporitic environments associated with the Messinian Salinity Crisis. This evolution has been attributed to changes in Mediterranean-Atlantic connectivity and regional climate, which has a strong precessional pulse. 31 Coupled climate simulations with different orbital configurations have been combined in a regression model that estimates the evolution of the freshwater budget of the Mediterranean throughout the late Miocene. The study suggests that wetter conditions occur at precession minima and are enhanced at eccentricity maxima. We use the wetter peaks to predict synthetic sapropel records. Using these to retune two Mediterranean sediment successions indicates that the overall net freshwater budget is the most likely mechanism driving sapropel formation in the late Miocene. Our sapropel timing is offset from precession minima and boreal summer insolation maxima during low eccentricity if the present-day drainage configuration across North Africa is used. This phase offset is removed if at least 50% more water drained into the Mediterranean during the late Miocene, capturing additional North African monsoon precipitation, for example via the Chad-Eosahabi catchment in Libya. In contrast with the clear expression of precession and eccentricity in the model results, obliquity, which is visible in the sapropel record during minimum eccentricity, does not have a strong signal in our model. By exploring the freshwater evolution curve in a box model that also includes Mediterranean-Atlantic exchange, we are able, for the first time, to estimate the Mediterranean's salinity evolution, which is quantitatively consistent with precessional control. Additionally, we separate and quantify the distinct contributions regional climate and tectonic restriction make to the lithological changes associated with the Messinian Salinity Crisis. The novel methodology and results of this study have numerous potential applications to other regions and geological scenarios, as well as to astronomical tuning.

3.1 Introduction

At present, net evaporation and cooling increases the density of Mediterranean surface water, making it sink and ventilate the water column. This process of deep-water formation establishes a density gradient between the Mediterranean and the Atlantic, which drives anti-estuarine exchange at the Strait of Gibraltar (Rohling et al., 2015, and references therein). The Mediterranean sedimentary record demonstrates that this circulation pattern has not always been active. Atypical marine deposits occur in the form of organic-rich sediments (sapropels, Kidd et al., 1978), which populate the Mediterranean succession from the middle Miocene onwards (Rohling et al., 2015, and references therein), as well as by evaporites, which were precipitated during the Messinian Salinity Crisis (MSC; Roveri et al., 2014a, and references therein). The occurrence of these anomalous sediments has been linked to changes in climate and Atlantic-Mediterranean connectivity. Sapropel formation is thought to occur due to stratification of the Mediterranean water column and enhanced surface productivity (e.g., Rohling et al., 2015, and references therein). These are generally considered to be related to a northward shift of the Intertropical Convergence Zone (ITCZ, Figure 3.1) during precession minima, when more North African monsoon rainwater contributes to the Mediterranean freshwater budget (Rossignol-Strick, 1983), but sapropels may also develop during rapid global sea-level fluctuations causing changes to the Mediterranean-Atlantic connectivity (e.g., Grant et al., 2016; Hennekam, 2015). The substantial volumes of Messinian gypsum and halite are indicative of a much higher Mediterranean salinity than today. Possible triggers for brine concentration consistent with evaporite precipitation include eustatic restriction of the Mediterranean connection with the global ocean, and/or tectonic changes in the gateway region (see Flecker et al., 2015), together with strong, net evaporative loss across the basin surface.

To date, neither the gateway evolution, nor the past Mediterranean freshwater budget evolution have been quantitatively constrained. Previous studies of the freshwater budget have either (1) assumed it was constant, and used the present day value (Blanc, 2000); (2) used a budget derived from a late Miocene idealized Atmospheric General Circulation Model (AGCM) simulation by Gladstone et al. (2007) (e.g., Chapter 2, Simon and Meijer, 2015); (3) assumed that the freshwater budget is driven by fluvial discharge and changes linearly in phase with summer insolation at 65^oN (e.g., Hennekam, 2015); or (4) that fluvial discharge varies as an idealised sine function (Topper and Meijer, 2015b). All these studies assume that changes in the freshwater budget control sedimentation (Ryan, 2008) and astronomical tuning uses this concept to date sedimentary successions with an accuracy on precession scale (e.g., Hilgen and Krijgsman, 1999).

Here, by contrast, we calculate a freshwater evolution for the Messinian ($7.25-5.33$ Ma) using a novel multi-model approach, which is based on fully coupled climate model simulations rather than on summer insolation at 65^oN. This allows us to estimate the variation in precipitation (P), evaporation (E) and river discharge (R) throughout the Mediterranean region over the entire late Miocene and hence, to disentangle gateway and climate effects on the Mediterranean's environmental evolution for the first time. High temporal (~ 1 kyr) quantitative results are derived from an

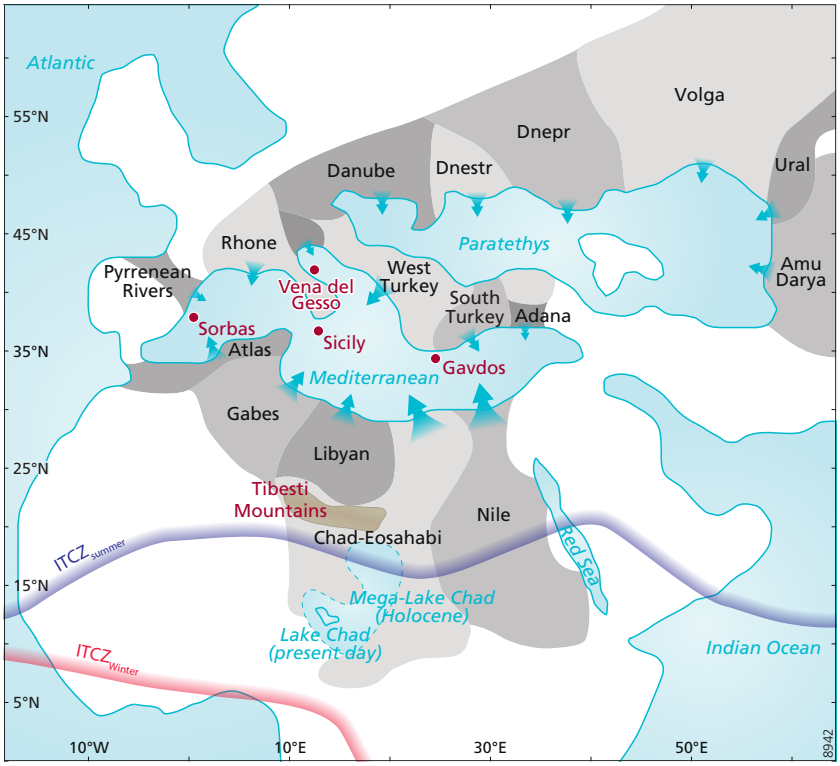

Figure 3.1 Schematic palaeogeographic map of the Mediterranean region during the late Miocene, based on Markwick (2007). Indicated are rivers that drained or might have drained into the Mediterranean during the late Miocene, their catchment areas (schematic, following Gladstone et al., 2007), the present-day northern hemisphere summer and winter Intertropical Convergence Zone (ITCZ) and relevant field sections/areas (red). On a side note, the position of the summer ITCZ plotted is approximately the position of the summer ITCZ at precession maxima and the winter ITCZ plotted is approximately the summer ITCZ at precession minima (Marzocchi et al., 2015). In the GCM the Atlantic Ocean has been disconnected to capture the restricted basin behavior of the Mediterranean Sea during the MSC.

ocean-atmosphere-vegetation General Circulation Model (GCM; HadCM3L; Marzocchi et al., 2015). These GCM results are extended through time using a regression model (RM) to estimate the freshwater budget. Assuming that a simple threshold value of the freshwater budget controls sediment type, we use the budget curve to calculate the pre-MSC sapropel pattern and compare it with late Miocene sapropel-bearing successions exposed in southern Spain (Abad composite, Sorbas, western Mediterranean) and Sicily (Falconara, central/eastern Mediterranean). We also apply the curve to an investigation of the environmental changes that occurred at the

onset of the MSC using a box model developed by Meijer (2006). Figure 3.2 illustrates how the various components of this study interconnect. Our approach provides a new way to study the relationship between insolation, the Mediterranean freshwater budget and astronomical tuning. It provides new insights into the conditions under which sapropels and evaporites form and helps to distinguish the role of the Mediterranean freshwater budget in generating the regions environmental evolution from changes in Mediterranean-Atlantic connectivity.

3.2 Model hierarchy

General Circulation Model (GCM)

All numerical simulations are carried out using the UK Met Office General Circulation Model (HadCM3L version 4.5, see Valdes et al., 2017, and references therein for a full description), which is coupled to the TRIFFID vegetation model (Hughes et al., 2004, and references therein). This model has been previously used to simulate late Miocene (e.g. Marzocchi et al., 2015; Bradshaw et al., 2012) and Eocene (e.g., Tindall et al., 2010) climate. All our model simulations start from a 2000-years spin-up (Bradshaw et al., 2012), and are run for 200 years, which allows, at least, the atmospheric variables to be close to equilibrium and exhibit no significant trends (see Supplement in Marzocchi et al., 2015). In all simulations, CO_2 concentrations and the palaeogeography are fixed to the pre-industrial value of 280 ppm and to a late Miocene reconstruction derived from Markwick (2007), respectively. Each GCM experiment differs in the seasonal and latitudinal incoming solar radiation at the top of the atmosphere (hereafter, referred to as insolation). Insolation is determined by the orbital path and position of Earth relative to the Sun. The three most important orbital effects are (1) axial precession of the Earth, (2) the tilt of the Earths rotational axis relative to its orbit (obliquity) and (3) the eccentricity of the elliptical Earth orbit around the Sun, with the Sun at one of the focal points. The orbital solutions of Laskar et al. (2004) determine how these orbital parameters changed through time for the Neogene period. The core of our GCM experiments (22 simulations) was carried out by Marzocchi et al. (2015) to study sub-precessional changes on the North African monsoon during the late Miocene. These 22 simulations (Figure 3.3C) are positioned at a relatively high eccentricity and spread not just across a whole precession cycle, but also from a maximum to a minimum obliquity (Figure 3.3). In order to sample a wider range of orbital parameters, we ran additional simulations to gain more insight into the behaviour of the freshwater budget during low eccentricities (Figure 3.3B) and during the most extreme precession values for the period of interest (Figure 3.3A).

Regression Model (RM)

Assessing the Mediterranean freshwater budget from the GCM

Precipitation, evaporation and runoff can be directly extracted from each grid box of the GCM. The annual mean runoff into the ocean is calculated following the method and river catchments defined by Gladstone et al. (2007). Each drainage basin shown

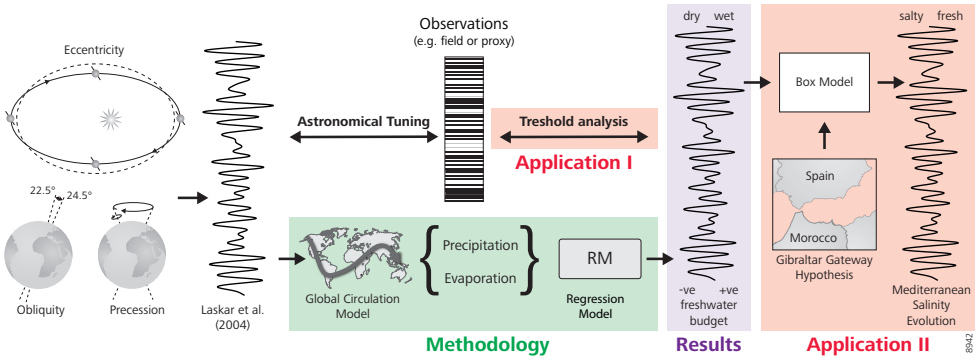

Figure 3.2 This flow chart illustrates how our multi-model approach compares with other methods and data. Oscillations in the orbit of the Earth are used during astronomical tuning to date sediment successions to high accuracy. Our method (green): we feed Earth insolation, based on orbital parameters in a GCM, from which we extract the precipitation, evaporation and river runoff across the Mediterranean region. These snap-shot results are extended in time via a RM. Results (blue): resulting is the Mediterranean freshwater budget evolution. Applications (red): we can compare our results to the sedimentary record directly (e.g. with a threshold analysis) (I) and we use them to calculate the Mediterranean salinity evolution for a certain Atlantic–Mediterranean gateway (II).

in Figure 3.1 can be considered separately, so the impact of different combinations of basins draining into the Mediterranean at any specific time can be explored. While almost all the late Miocene river catchments resemble those that exist today (Figure 3.1), the prominent exceptions are the spatially extensive North African drainage basins that are currently dry (e.g. Chad-Eosahabi, Libya and Gabes; Figure 3.1). The sedimentary record in the Gulf of Sirt (Figure 1.3) is testament to a substantial fluvial system that drained the North African catchment west of the Nile from at least the Eocene, and continued to supply both water and sediment to the Mediterranean Sea during the late Miocene (Bowman, 2012). This is consistent with a more humid climate relative to today and an associated greening of the Sahel region (Colin et al., 2014). However, the southward extent of the Chad-Eosahabi drainage basin and its route across North Africa remain a matter of considerable debate, given that the palaeodrainage networks, which have been reconstructed using a variety of remote sensing techniques, are fragmentary as a result of being partly buried beneath aeolian sands. Griffin (2002, 2006) and Ghoneim et al. (2012) propose a fluvial link between Lake Mega-Chad and the Mediterranean, while Paillou et al. (2012) suggest that the rivers flowing into the Gulf of Sirt in the Miocene are instead likely to have drained north and east off the Tibesti Mountains, with a drainage divide between Chad and the Mediterranean. As Paillou et al. (2012) point out, there currently is insufficient evidence to confirm or refute a Miocene connection between Lake Mega-Chad and the Mediterranean. This issue is critical for calculating the freshwater budget of the Mediterranean as the southward extent of these North African catchments dictates

how much monsoonal precipitation can be transferred into the Mediterranean (Marzocchi et al., 2015; Bosmans et al., 2015a). In this study we have opted to model the largest possible drainage basin (Chad-Eosahabi; Figure 3.1) while acknowledging that in reality, the catchment and its resulting freshwater contribution to the Mediterranean may well have been significantly smaller. However, compared to proxy reconstructions indicating a greening of the Sahara during the mid-Holocene, most GCM simulations tend to underestimate the northward expansion (north of 21^oN) of the summer monsoon (e.g. Pausata et al., 2016, and references therein). Consequently, we can assume that the intensified monsoonal rainfall in the late Miocene simulations of Marzocchi et al. (2015) could also be confined too far south in North Africa. Furthermore, Zhang et al. (2014) suggest that a greening of the Sahara would have occurred at every precession minimum from the late Miocene onwards.

Another important influence on the Miocene Mediterranean freshwater budget may have been the Paratethys, the lacustrine precursor of the Black and Caspian seas (Figure 3.1). New studies suggest that it was connected to the Mediterranean around 6.12 Ma (e.g., van Baak et al., 2015). Such a connection means that the Paratethys is both a potential water source (see de la Vara et al., 2016, for further discussion) and sink. The Paratethys has been implicated in hypotheses for several significant environmental phases of the MSC (Roveri et al., 2014a): the Lago Mare phase (e.g., Marzocchi et al., 2016) and the Primary Lower Gypsum (PLG) deposition Grothe (2016). In contrast to the case of the Mediterranean, these Paratethys fluctuations are not precessional, but dominantly seasonal (Marzocchi et al., 2016). As we are considering annual changes, the freshwater input from the Paratethys is omitted.

Extending the GCM results via the RM

Typically, the influence of orbital parameters is evaluated through sensitivity tests of idealised extreme scenarios (e.g., Bosmans et al., 2015a; Tuenter et al., 2005). However, to calculate a continuous orbitally-driven evolution, it is important to (1) use age-specific orbital parameters (Laskar et al., 2004); (2) constrain climatic behaviour between orbital extremes; and (3) evaluate the system response to different orbital combinations over time Laskar et al. (2004). Therefore the GCM simulations used here provide an excellent basis, as they cover a large range of orbital configurations. Visual comparison of the freshwater budget behaviour with summer insolation at 65^oN through time suggests a temporal relationship between the two (Figure 3.3), with a clear anti-phase response of the freshwater budget to insolation. However, there is a much more pronounced inflection towards higher ("wetter") values at insolation maxima (Figure 3.3C). This indicates that the evolution of the Mediterranean freshwater budget does not simply depend on summer insolation at 65^oN, but must either be influenced by other factors or depend on a non-linear combination of the orbital parameters. Therefore, instead of linking the summer insolation curve at 65^oN directly to the Mediterranean freshwater evolution (e.g., Hennekam, 2015), we calculate these freshwater values independent of the insolation target curve. To do so, we assume that the annual mean P, E and R depend on a linear combination of precession, obliquity, eccentricity, their squared terms and their cross-terms, giving a maximum

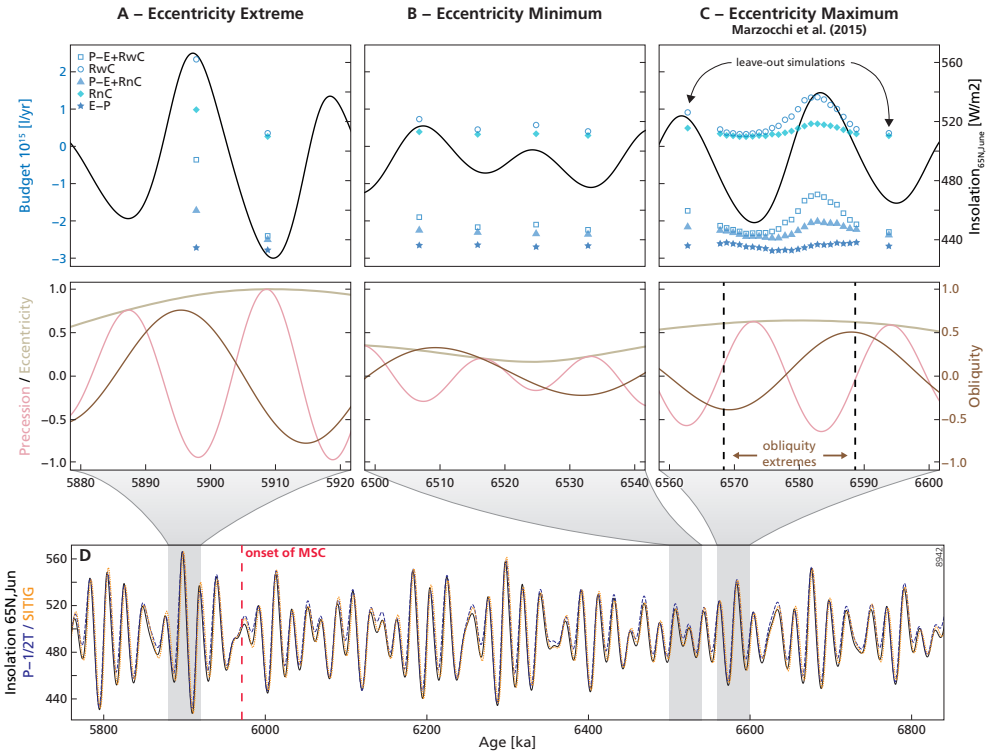

Figure 3.3 Summary of the GCM results and their position in time relative to the orbits. Figure A-C illustrate different data groups: (A) the most extreme insolation during the late Miocene, (B) the 400 *kyrs* minimum at ~ 6.52 Ma and (C) the eccentricity maximum at ~ 6.58 Ma (Marzocchi et al., 2015) and two of the leave-out experiments. The astronomical curves (precession, obliquity and eccentricity) are normalised and centered around zero. Plot D gives an overview where the orbits fed into the GCM stand in time during the late Miocene.

of nine possible orbital terms (Equation 3.1, 3 linear terms and 6 non-linear terms). We then calculate a linear regression for each combination of these nine orbital parameters (using the package R, version 2.9; http://CRAN.R-project.org/package=leaps) and use a selection framework to identify the most appropriate regression equation amongst the large number of possible combinations For each regression with equal number of subset terms (one to nine), 10 combinations with the highest coefficients of determination (R^2) values above 0.9 are selected. By means of validation, their outcome is compared to three additional GCM experiments (Figure 3.3C, 6.563 Ma, 6.594 Ma and for the present-day orbit) that were not used to generate the regression. The regression equation that predicts these simulations most closely is then used to calculate the late Miocene freshwater evolution of the Mediterranean (see Equation 3.1 in combination with Table 3.1). The difference between the freshwa-

ter budget calculated by the additional GCM simulations and for the same orbits by the RM is used to estimate an uncertainty. This operation was performed five times to calculate different (combinations of) components of the freshwater budget: (1) precipitation minus evaporation (P-E) across the Mediterranean; (2) the rivers draining into the Mediterranean excluding the Chad-Eosahabi runoff (RnC); (3) the rivers draining into the Mediterranean including the Chad-Eosahabi runoff (RwC); and the net freshwater budget (4) without the Chad-Eosahabi basin (P-E+RnC); and (5) with the Chad-Eosahabi basin (P-E+RwC).

Applications of the freshwater budget evolution

This section describes examples of supplying the freshwater budget to a Mediterranean setting in which the sea-level was equal to that of the Atlantic. To consider a MSC desiccation scenario, reevaluation of the atmospheric convection patterns in a deep empty basin would be required (e.g., Murphy et al., 2009; Schneck et al., 2010).

Application I - Sapropel threshold analyses

The estimated freshwater budgets allow us to explore the relationships between Mediterranean sedimentation, runoff and freshwater budget for periods of Earth's history where the dating tools preclude high-resolution dating of individual horizons. Ideally, the RM would drive a biogeochemical model to evaluate sapropel formation. As a first pass, however, we used the simple threshold approach, which assumes that sapropel formation is directly proportional to freshwater input. This takes no account of sedimentation rate changes associated with productivity or the impacts of organic matter preservation or dilution, but does produce a synthetic sapropel log in the time domain, in a similar fashion as the pattern-matching of astronomical tuning. Four threshold analyses were carried out, for two runoff scenarios (RwC and RnC) and two net budgets (PERwC and PERnC). If the curves cross the prescribed threshold, which differs in each scenario, towards wet conditions, we assume a sapropel is deposited. The thresholds are kept constant and are chosen so that the number of predicted sapropels is as close as possible to that seen in the sedimentary record for the time period 6.6-6.0 Ma. The results are compared to the Abad composite (Sierro et al., 2001), an example of a marginal basin in the western Mediterranean and to the Falconara section (Hilgen and Krijgsman, 1999), an example of an intermediate depth basin in the central Mediterranean.

Application II - Box model analyses

Meijer (2006) adopted the notion that the Atlantic-Mediterranean exchange can be parameterized by letting the Mediterranean outflux vary in proportion with the salinity difference between the Atlantic and the Mediterranean. The constant of proportionality is the exchange coefficient, g. Using his one-box representation of the Mediterranean Sea, we calculate the Mediterranean salinity evolution for our net freshwater budget for three restricted scenarios. Prior to 6.7 Ma we set the gateway exchange efficiency to a value suitable for the modern Strait of Gibraltar ($g \sim 10^6$ $(m^3/s)/(g/l)$).

From 6.7 Ma until 5.97 Ma a linear reduction in connectivity is imposed so that exchange efficiencies of 260, 1000 or 10000 $(m^3/s)/(g/l)$ are achieved at the onset of the MSC (Manzi et al., 2013). Thereafter the exchange coefficient for each scenario is kept constant until 5.6 Ma, which marks the end of the PLG phase Roveri et al. (2014a). Both the freshwater budgets with Chad (PERwC) and without (PERnC) are considered.

3.3 Results

Quantifying the Mediterranean freshwater budget

The RM calculated coefficients are listed in Table 3.1. The five different freshwater budget combinations on the left can be calculated by summing up the products of the coefficients and the orbital curves calculated by Laskar et al. (2004):

$$freshwater\ budget\ =\ \sum_{1-10}\ coefficients\ *\ orbits \tag{3.1}$$

Figure 3.4 shows the freshwater budget evolution for the Messinian Stage (7.25-5.33 Ma). Whether the Chad-Eosahabi drainage is included or not, the annual mean freshwater budget of the Mediterranean is negative throughout the late Miocene. The freshwater budget does not simply depend linearly on the three orbital components (precession, obliquity and eccentricity): (1) the difference between evaporation and precipitation (E-P) across the whole basin varies $\pm 0.5 * 10^{15}$ l/year about a value of around $-2.58 * 10^{15}$ l/year, (2) the two runoff curves (RnC, RwC) do not oscillate around a mean, but start from a base of around $2.5 * 10^{14}$ l/year and extend towards positive values (RnC $\sim 1.14 * 10^{15}$ l/year and RwC $\sim 2.96 * 10^{15}$ l/year) and (3) the strong and relatively constant difference in evaporation and precipitation causes the net freshwater budgets ($PERnC$, $PERwC$) to attain negative values with an oscillatory behaviour similar to the runoff curves.

Using the three additional and independent GCM simulations, we estimate an uncertainty of the RM results relative to the GCM results (Table 3.1). This uncertainty is of the order of $\sim 10^{13}$ l/year, which is small relative to the budget variability of the order of $\sim 10^{15}$ l/year. Larger uncertainties ($\sim 10^{14}$ l/year) are found in the regressions including the Chad-Eosahabi drainage, as the positive freshwater excursions towards at insolation maxima are highly non-linear. Generally, this uncertainty is unlikely to cause large changes at eccentricity maxima, but may be more significant at low eccentricities due to the smaller amplitude of the freshwater budget. There is no evidence that this uncertainty affects the freshwater budget peak spacing.

The RwC regression equation sometimes shows negative excursions (e.g. 7.2-7.0 Ma and ~ 6.1 Ma). This is clearly a model artefact, since rivers can only add water to the Mediterranean, but cannot extract it. It develops due to the extremely non-linear nature of the freshwater budget around eccentricity maxima, where curve excursions to the negative are not very large, but excursions to the positive are significant. To counter this, when RwC $<$ RnC we set RwC equal to RnC. Nevertheless, this correction has no impact on the follow up analysis in this manuscript, because (1) peak

Freshwater Budget	Intercept	P	O	E	P^2	O^2	E^2	$P*O$	$P*E$	$O*E$	R^2	*Uncertainty*
P-E+RwC	-2.142	0	0	0	0.665	0	0.256	0	-1.244	-0.071	0.99	$O(10^{14})$
P-E+RnC	-2.293	0	0	0	0.181	0.584	-0.109	0	-0.378	0	0.96	$O(10^{13})$
RwC	0.657	0	0.105	-0.713	0.616	-0.845	1.274	0	-1.252	-0.104	0.99	$O(10^{14})$
RnC	0.384	0	0.005	-0.211	0.201	-0.121	0.375	0	-0.421	0	0.99	$O(10^{13})$
P-E	-2.747	-0.079	0.131	0.484	0.004	0.863	-0.772	0	0.039	-0.396	0.90	$O(10^{13})$

Table 3.1 Overview of resulting coefficients to calculate an annual mean freshwater budget ($*10^{15}$ $l/year$) evolution for the entire Mediterranean. The rows present the five equations, where P is precipitation, E is evaporation, RwC are all rivers draining into the Mediterranean including the Chad-Eosahabi catchment and RnC are all rivers draining into the Mediterranean excluding the Chad-Eosahabi catchment. The columns are the 10 coefficients needed for the calculation, the R^2 value for each regression and an estimate of the budget uncertainty.

spacing, (2) wet excursions, relevant for the threshold analyses and (3) net budgets, relevant for the MSC salinity evolution, are all unaffected.

The main periodicities lie around 20 kyr and are amplitude modulated by an approximately 100 kyr periodicity suggesting that the oscillations are dominantly precession and eccentricity related. Obliquity, which is visible in the Mediterranean sedimentary record at low eccentricities (Hilgen and Krijgsman, 1999; Lourens et al., 1996), is not manifest in the spectral analysis of the freshwater budget (see detailed discussion in Section 3.6).

The peak phasing of different freshwater budget curves relative to each other and to the astronomical curve, changes through time. While the two runoff curves (RwC and RnC) are in-phase with summer insolation at 65^oN throughout (Figure 3.4), the net freshwater evolution of $P - E + RwC$ and $P - E + RnC$ differ from each other, and peaks in these budgets are not always in-phase with insolation. Slight leads and lags characterise the entire period, but are more significant at the start and end of the Messinian ($\sim$ 7.2 Ma and $\sim$ 5.3 Ma; Figure 3.4), and are opposite (out-of-phase) at $\sim$ 6.1 Ma (Figure 3.4). The most likely cause of these phase offsets is the interaction of evaporation and precipitation over the Mediterranean and the rivers draining into it at times of low runoff. Although the runoff is dominated by north African rivers which are in phase with insolation, $E - P$ is not always in phase with insolation.

Figure 3.4 (right page.) Result overview for the Messinian stage ($7.25 - 5.33$ Ma). Plotted are the overall Mediterranean run-off (RnC and RwC), the evaporation minus precipitation ($E - P$) and the net Mediterranean budget ($P - E + RnC$ and $P - E + RwC$). On the left, summer insolation at 65^oN (Laskar et al., 2004), $P - 0.5 * T$ (Lourens et al., 1996) and SITIG (Bosmans et al., 2015b) are shown for reference. If $RwC < RnC$ we set RwC equal to RnC.)

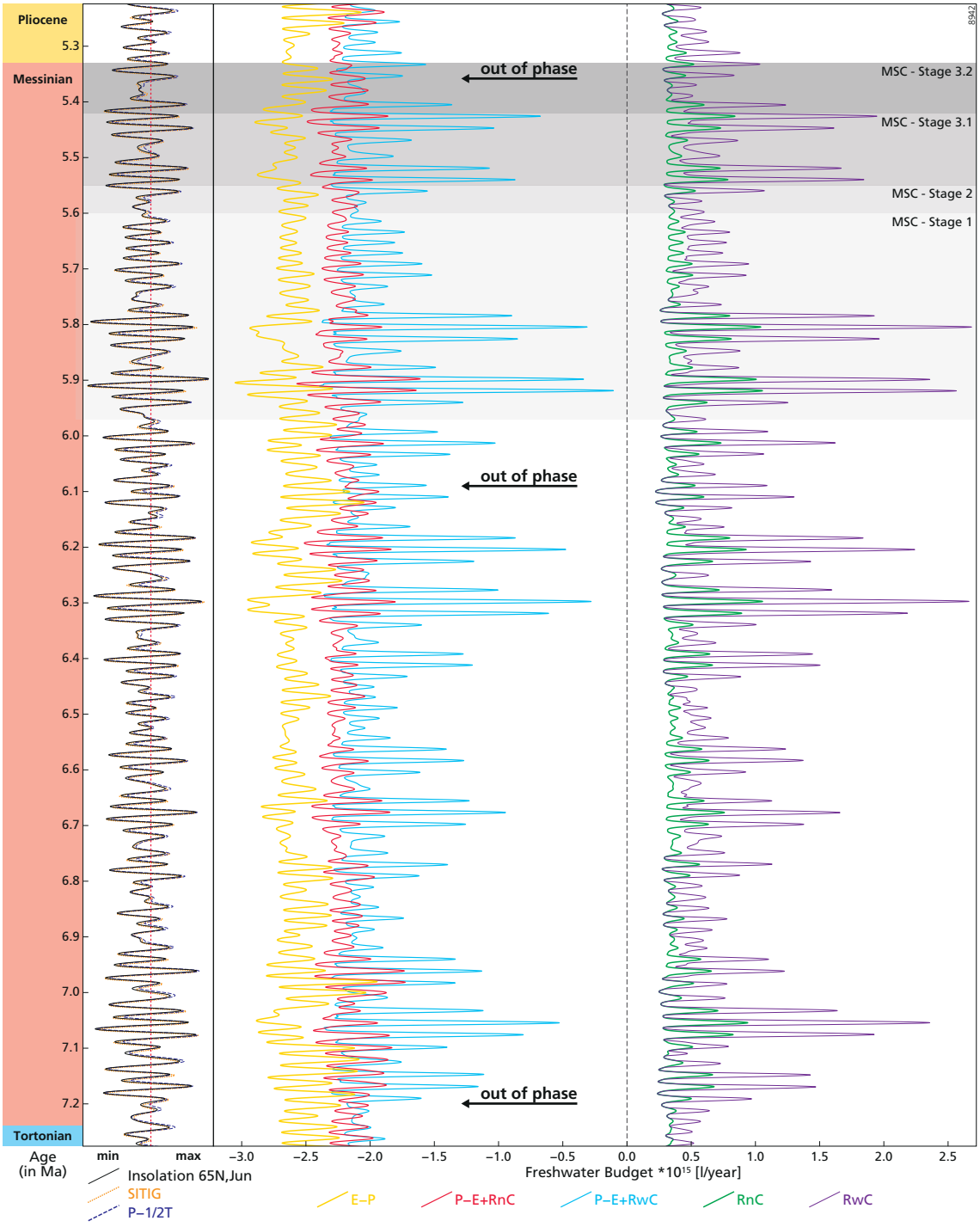
Pliocene
Messinian
Tortonian
5.3
5.4
5.5
5.6
5.7
5.8
5.9
6.0
6.1
6.2
6.3
6.4
6.5
6.6
6.7
6.8
6.9
7.0
7.1
7.2
out of phase
out of phase
out of phase
MSC - Stage 3.2
MSC - Stage 3.1
MSC - Stage 2
MSC - Stage 1
8942
Age (in Ma)
min
max
Insolation 65N,Jun
SITIG
P–1/2T
−3.0
−2.5
−2.0
−1.5
−1.0
−0.5
0.0
0.5
1.0
1.5
2.0
2.5
Freshwater Budget *10¹⁵ [l/year]
E–P
P–E+RnC
P–E+RwC
RnC
RwC

Application I - A synthetic sapropel record

The runoff (RnC and RwC) and the net budget ($PERwC$) synthetics are in phase with insolation throughout, with the exception of the interval $\sim 6.25\ Ma$ where $PERwC$ demonstrates a phase lag of half a cycle. The different phasing of the $PERnC$ relative to insolation is particularly noticeable between $6.06 - 6.14\ Ma$, $\sim 6.25\ Ma$ and $\sim 6.38\ Ma$. The duration of sapropels is predicted differently, depending on the freshwater curve used. The mean sedimentation rate of the Abad marls is approximately twice that of the Falconara section. This is due to the marginal character of the Sorbas basin compared to the more central deeper basin setting of Falconara. Despite this fact, the sedimentary changes follow a similar pattern.

If the sedimentation rate is assumed to be constant within a sapropel, our analyses predict thicker sapropels during eccentricity maxima and thinner sapropels during eccentricity minima. This is in agreement with field observations, but does not match with the observed precession-obliquity interference pattern (see detailed discussion in Section 3.6).

Another way to look at the problem is to retune the observed sapropels (Figure 3.5). We follow Sierro et al. (2001) and Manzi et al. (2013) in that we take the transition from the Abad composite to the Yesares Member to be continuous and tune downwards from the Yesares Member (Abad) and the limestones (Falconara), respectively, by correlating midpoints of synthetics and observed sapropels. At $\sim 6.35\ Ma$, an aberrantly thick whitish marl is present in the Abad composite, which encompasses the main sinistral to dextral coiling change of *N. acostaensis* (Sierro et al., 2001). The same coiling change is also found in the Falconara and Capodarso sections on Sicily (Hilgen and Krijgsman, 1999). However, these sections contain a very thin sapropel, which is missing in the Abad composite (marked "missing cycle" on Figure 3.5). Due to its weak expression and its very unusual position directly underlying a homogeneous marl, this sapropel is not taken into account when cycles were retuned to the freshwater budget curves.

Figure 3.5 (right page.) Model-Data comparison for the pre-MSC Mediterranean sedimentary record ($6.6 - 6.0\ Ma$). Left: the Abad composite (Sierro et al., 2001); right: the Falconara section (Hilgen and Krijgsman, 1999). We follow Sierro et al. (2001) and Manzi et al. (2013) that the transition from the Abad composite to the Yesares Member is continues. The freshwater budget curves (RnC, RwC, $PERnC$ and $PERwC$) and their synthetics are used to retune these two sections. This tuning is done downwards from the Yesares Member and the limestones, respectively, by correlating midpoints of synthetics and observed sapropels. This results in four sedimentation rates for the Abad composite (left) and four sedimentation rates for the Falconara section (right). These sedimentation rates are compared to the sedimentation rates of the original tuning with summer insolation at 65^oN. Obliquity, precession and eccentricity are plotted in the bottom panel for reference.

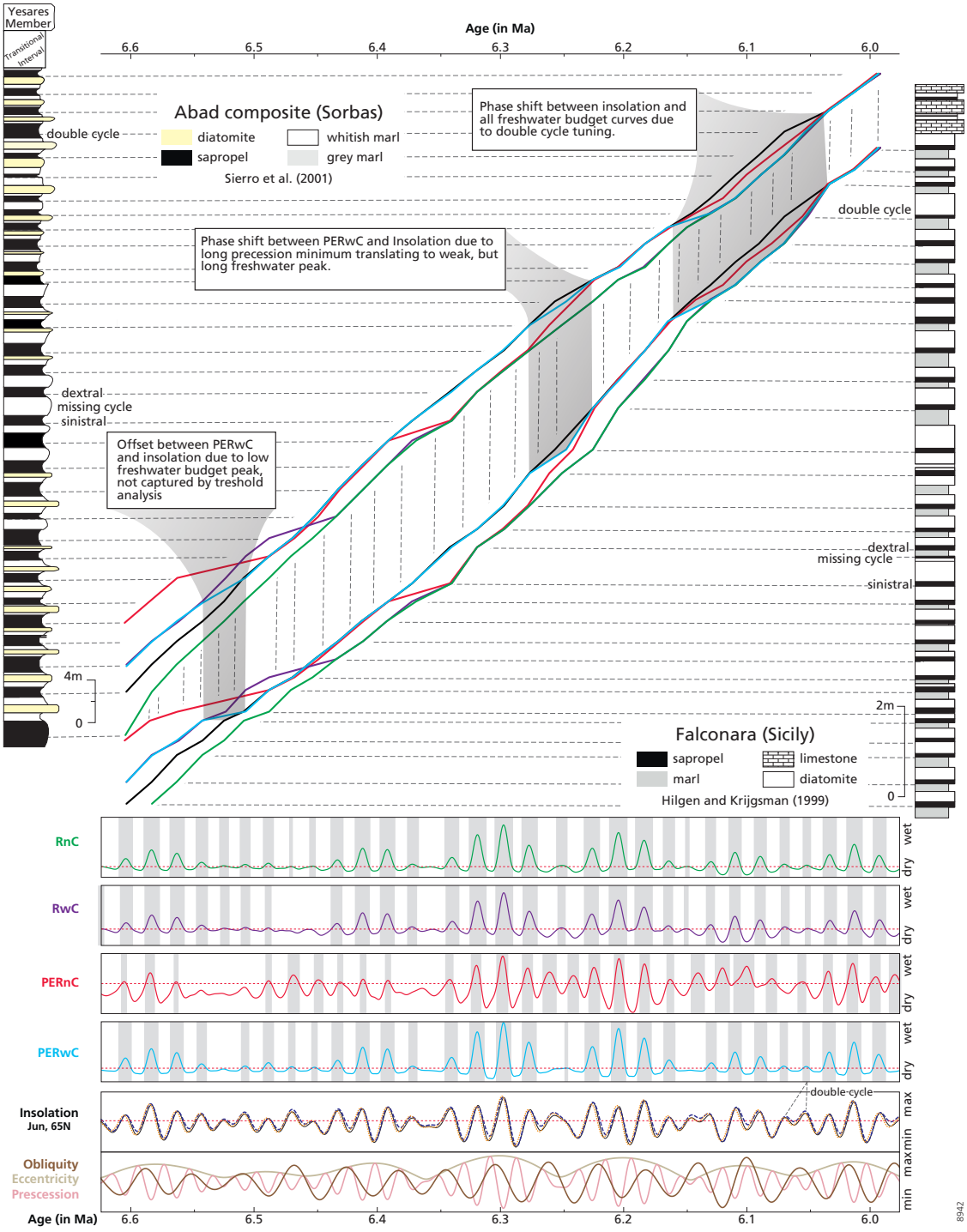
Yesares Member
Transitional Interval
Age (in Ma)
6.6
6.5
6.4
6.3
6.2
6.1
6.0
Abad composite (Sorbas)
diatomite
whitish marl
sapropel
grey marl
Sierro et al. (2001)
double cycle
Phase shift between insolation and all freshwater budget curves due to double cycle tuning.
Phase shift between PERwC and Insolation due to long precession minimum translating to weak, but long freshwater peak.
dextral
missing cycle
sinistral
Offset between PERwC and insolation due to low freshwater budget peak, not captured by treshold analysis
4m
0
2m
Falconara (Sicily)
sapropel
marl
limestone
diatomite
Hilgen and Krijgsman (1999)
RnC
RwC
PERnC
PERwC
wet
dry
Insolation
Jun, 65N
max
min
Obliquity
Eccentricity
Precession
Age (in Ma)
8942

The resulting sedimentation rates reveal variable distinct steps, which indicate abrupt changes in sedimentation rate:

1. At $\sim$ 6.06 Ma the original double-peak insolation tuning to one sapropel introduces a phase shift between the original and all new tunings and consequently a change in the sedimentation rate. This offset is removed at $\sim$ 6.14 Ma ($PERnC$) and $\sim$ 6.16 Ma (PERwC), where both net budget curves predict one sapropel less. Although this introduces a small change in the age model, it provides an explanation for the double cycle assumption made in the original tuning.

2. At $\sim$ 6.25 Ma, both ($PERnC$ and $PERwC$) show diversions in the sedimentation rate from the original one. For $PERwC$ this diversion only lasts for one cycle, because it is due to a long precession minimum translating into a wide insolation peak and a narrow freshwater peak. It demonstrates that sapropel midpoint tuning to orbital peaks needs to be reconsidered. For $PERwC$ this diversion lasts longer, until $\sim$ 6.4 Ma.

3. The offset in the oldest part of the section (older than 6.52 Ma) can be explained due to the simplicity of the threshold analyses and can be overcome by slightly lowering the threshold value used for PERwC.

This lets us conclude that the synthetics based on the net budgets ($PERwC$ tuning being closest to insolation tuning) lead to an age model closest to the original one. Implications of this result are discussed in Section 3.4.

Although this procedure might be even more valuable for more recent times, our motivation and the setup of the GCM are specific for the late Miocene period. The Holocene sapropel record would be an interesting time frame to apply this method to, given the large amount of available data, but a full set of new numerical simulations would be required.

Application II - The MSC salinity evolution

During the pre-restriction phase, the box model estimates Mediterranean salinity to be oscillating in parallel with the freshwater budget. Mediterranean salinity is slightly higher than (37.6-38.2 g/l, Figure 3.6B), but close to the prescribed Atlantic salinity of 36.5g/l, which is similar to todays Mediterranean situation (Rohling et al., 2015). With decreasing Atlantic exchange, the basin increases its sensitivity to freshwater oscillations greatly, and, irrespective of the freshwater budget used, Mediterranean salinity starts to rise, reaching concentrations suitable for gypsum concentration (e.g. 105 g/l, Grothe (2016); 130 g/l Lugli et al. (2010) with a gateway efficiency of 260 $(m^3/s)/(g/l)$; Figure 3.6A).

Between 5.97 Ma and 5.96 Ma our model predicts a sudden increase in salinity, which we interpret as the model expression of the Transitional Interval (Manzi et al., 2013). This interval is identified between the PLG and the pre-evaporite phase and contains a highly discontinuous gypsum bed (Manzi et al., 2013). Meijer (2012) already demonstrated that the increase in Mediterranean salinity is highly non-linear

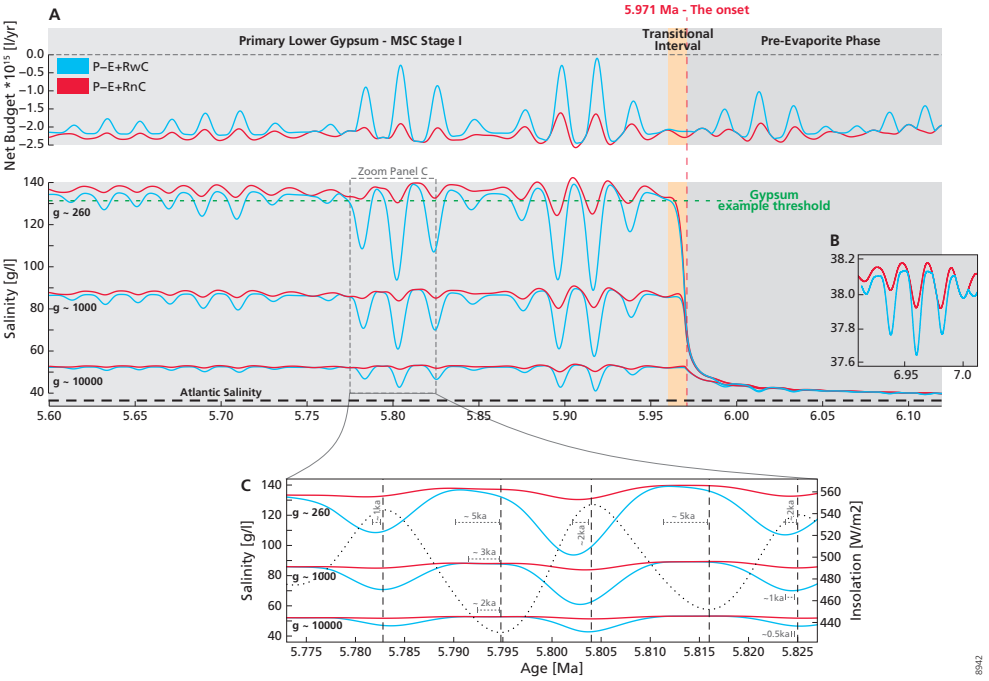

Figure 3.6 A: Calculation of the Mediterranean salinity in a box model, following Meijer (2006), for the time period $6.1 - 5.6\ Ma$. Shown are the two net freshwater budget ($PERnC$ and $PERwC$) and their salt concentration for 3 restriction scenarios. The green line illustrates a gypsum threshold scenario, where gypsum deposits at 130 g/l. B: Close-up of A for a time period prior to the MSC. C: Close-up of A for the time period $5.825 - 5.775\ Ma$ to illustrate the importance of the salinity peaks lagging behind the insolation curve.

relative to the reduction in exchange so that even gradual restriction leads to sudden changes in the sedimentary record, as described by Kouwenhoven et al. (2003).

The extra freshwater from the Chad-Eosahabi catchment has two effects on Mediterranean salinity: (1) a slightly lower Mediterranean salinity for the same exchange coefficient and (2) more extreme salinity fluctuations in each precessional cycle (Figure 3.6B), driven by higher amplitude changes in the freshwater budget.

Figure 3.6C shows phase lags between the freshwater budget and the insolation curve. The greater the restriction of the Mediterranean from the global ocean, the longer the lag of the salinity peak behind the insolation minima (up to 5 $kyrs$) and of the salinity troughs behind insolation maxima (up to 2 $kyrs$, Figure 3.6C). This has already been demonstrated in the idealized model analysis of Topper and Meijer (2015b) and again shows that we have to be careful in identifying tie points in the sedimentary succession.

3.4 Relevance for astronomical tuning and sapropel formation

In the Mediterranean, many Miocene and Plio-Quaternary sections have been astronomically tuned. To some extent, this tuning is based on the observation that cyclicity in the sedimentary succession mimics the insolation curve without clear identification of the processes that link insolation and lithology. Sapropel formation is linked to both productivity and stratification mechanisms and sapropels are assumed to form in-phase with summer insolation, given that a key driver of these mechanisms is thought to be fluvial discharge which is dominated by monsoon runoff (Rossignol-Strick, 1983). Consequently, the mid-point of sapropels is commonly used to tie Mediterranean successions to insolation maxima for astronomical tuning (e.g., Hilgen and Krijgsman, 1999). The temporal relationship between monsoonal runoff and insolation has been confirmed by transient modelling studies over the last 650 $kyrs$ (Weber and Tuenter, 2011), by a model investigation of a full Miocene precession/insolation cycle Marzocchi et al. (2015, 2016), and by idealized simulations Bosmans et al. (2015b). Our calculated runoff evolutions also indicate in-phase agreement (Figure 3.4 and Figure 3.5), which provides additional support. The sapropel retuning to $PERwC$ results clearly in the smoothest sedimentation rate curve (Figure 3.5). We assume that the variable which gives the smoothest implied sedimentation curve, is the one most likely to control sedimentation (Occam's razor). It is most similar to the sedimentation rate curve based on the original tuning to summer insolation 65^oN. This holds for both sedimentary records shown in Figure 3.5. As they represent both the western and central Mediterranean these new insights are likely to be relevant for the entire Mediterranean basin. This indicates that the stratification and upwelling-induced productivity processes that lead to sapropel formation, are a function of the freshwater budget as a whole and not of fluvial discharge alone. Moreover, the importance of other contributors to the Mediterranean freshwater budget is illustrated by recent sapropels S1 and S5 both of which follow major deglaciations, and both of which lag insolation by ~ 3 kyrs, either due to cold spells that interrupt the monsoonal intensification (Ziegler et al., 2010) or as a result of persistent meltwater pulses in the North Atlantic (Grant et al., 2016).

Faunal evidence (Kouwenhoven et al., 2003, e.g.) suggests that the late Miocene Mediterranean experienced salinity higher than today, already prior to the onset of the Primary Lower Gypsum. The interaction of increased freshwater input with this saltier, and therefore denser, water may have led to increased stratification, making stagnation of the basin more extreme and therefore potentially leading to sapropels at shallower water depths.

3.5 How much extra monsoonal runoff drains into the Mediterranean?

During the 400 $kyrs$ eccentricity minimum at ~ 6.1 Ma, Nile runoff alone is not sufficient to impose the temporal periodicity of its North African monsoonal precipitation on the net Mediterranean freshwater budget, because evaporation and precipitation across the Mediterranean are too strong (Figure 3.4 and Figure 3.7). This interaction

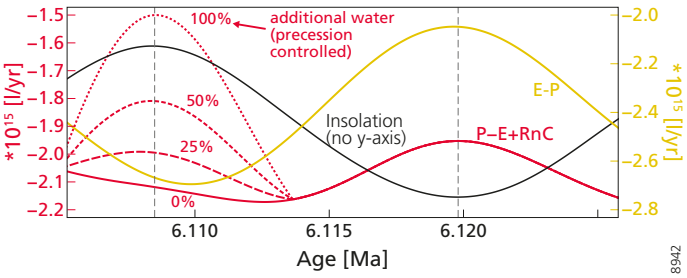

Figure 3.7 Close-up of the $6.125 - 6.105\ Ma$ cycle. The black curve is summer insolation $65^{o}N$ (Laskar et al., 2004), which is plotted without a y-scale. The yellow curve is the evaporation minus precipitation across the whole Mediterranean basin. The red curve is the net freshwater budget of the Mediterranean plus a percentage fraction of the Chad-Eosahabi runoff (0%, solid; 25%, 50% and 100%, various dotted lines).

of contributors to the $P-E+RnC$ freshwater budget means that its peaks correspond well with insolation maxima at high eccentricities, but, at low eccentricities, it either fails to reach the sapropel threshold or predicts sapropel formation out-of-phase with insolation maxima. This phase-offset could mean that during the late Miocene more freshwater was supplied in-phase with precession. This extra water is parameterized in our model with the Chad-Eosahabi catchment. But, how much additional water volume is needed to match the phasing of the net freshwater budget and insolation and does it come from the Chad-Eosahabi basin? Reiterating that our synthetics are based on the assumption that sapropel formation is proportional to freshwater input, we will tackle this question with Figure 3.7. Assuming that only the Nile catchment drains from North Africa into the Mediterranean, the maximum freshwater budget of this cycle occurs exactly at the insolation minimum rather than insolation maximum, which is when North African monsoonal precipitation is at its maximum. By gradually adding more freshwater, which we scale relative to the Chad-Eosahabi catchment (25%, 50% and 100%), an in-phase-peak with insolation can be generated. Figure 3.7 illustrates that approximately 50% more water volume than the maximum freshwater added by the Nile in the analysed time period is needed to match the freshwater budget peaks at the insolation minimum and maximum. To actually cause a significant effect, the volume needed is likely to be even larger. It is important to realise that water flux and drainage basin size do not scale linearly so that we cannot directly infer from these results the size of Chad-Eosahabi basin during the Messinian.

Another potential source of additional and precession-driven freshwater would be the Atlantic-Mediterranean winter storm tracks (e.g., Toucanne et al., 2015; Kutzbach et al., 2014), which may be especially significant for the western basin (Hoffmann et al., 2016). This contribution could be underestimated in the simulations of Marzocchi et al. (2015), as these indicate that the freshwater budget of the entire Mediterranean Sea would still be strongly dominated by summer monsoonal runoff into the eastern

basin (Mayser et al., 2017, see their Figure 8).

Yet another precessional source that could potentially freshen the Mediterranean surface would be brackish Paratethys or "fresher" Atlantic water. African runoff changes Mediterranean density in a cyclic fashion, as described in this study. This cyclicity is therefore likely to be found in the exchange strength of Mediterranean with its neighboring basins. Evidence outside the Mediterranean (e.g., Bahr et al., 2015) also hints at this process and forms an interesting objective for future work.

Due to the large volume of water needed to cause the phase-adjustment, we speculate that monsoonal-driven freshwater off the African continent is the most likely source. The route by which this freshwater reached the Mediterranean is difficult to be sure of. Because of the large volume required, it may have derived from Megalake Chad and drained via the Chad-Eosahabi river. Alternatively, it might have drained into the Mediterranean via the Nile or ephemeral wadi systems (see discussion in Coulthard et al., 2013) or via a combination of all three of these fluvial systems.

3.6 The precession-obliquity interference pattern

GCM experiments by Bosmans et al. (2015a) and Tuenter et al. (2005) conclude that both precession and obliquity influence African Monsoon precipitation and therefore runoff into the Mediterranean Sea. Bosmans et al. (2015b) recently suggested that the obliquity signal found in the Mediterranean sedimentary records (e.g., Lourens et al., 1996; Hilgen and Krijgsman, 1999) can be explained by the low-latitude southern winter component in the insolation gradient that triggers cross-equatorial moisture transport and drives the North African monsoon. However, this conclusion only holds if the sedimentation rate is taken to be constant. The precipitation pattern across northern Africa from Bosmans et al.'s (2015a,b) idealised GCM experiments is very similar to that from Marzocchi et al. (2015) late Miocene runs. Both demonstrate an obliquity effect. In addition, a recent study, that reconstructs the central North African rainfall record during the last glacial period (Hoffmann et al., 2016), suggests that obliquity played a role in positioning the ITCZ, however with different phasing than what was thought previously (e.g., Ziegler et al., 2010; Lourens et al., 1996). Despite this, the freshwater hydrologic budget calculations for the Mediterranean GCM simulation (Figure 3.3) do not show an obliquity influence. Processes like precipitation depend on convection within the atmosphere, which occurs on sub-kilometer scale. As the spatial resolution of most GCMs is not high enough to capture convection, it is parameterised. The modern precipitation in the HadCM3 family of models (used here) has been assessed by Pope et al. (2011). The modern African monsoon seasonality in HadCM3 has been assessed by Marzocchi et al. (2015). Pope et al. (2011), as well as Marzocchi et al. (2015), found that it is in good agreement with observations. Dabang et al. (2005) assessed the accuracy with which a range of GCMs generated Asian monsoon precipitation, and found HadCM3 to be the best performing GCM. We are therefore confident that the GCM produces reliable results and discuss various possible reasons for the absence of an obliquity influence on the freshwater budget:

1. One possibility is that the obliquity signal in the Mediterranean freshwater budget may be underestimated because of interactive vegetation feedbacks. While the simulations of Bosmans et al. (2015b) and Tuenter et al. (2005) had fixed vegetation, HadCM3L is coupled to a vegetation model in all orbital experiments used for the RM. In our simulations, the expansion of the tree fraction at times of enhanced North African monsoon would modify the soil's capacity to retain water (see Tuenter et al. (2005) for further discussion) and could reduce the water available to be transferred to the Mediterranean basin as runoff. In the sensitivity experiments by Bosmans et al. (2015b), a reduced tree fraction across North Africa (fixed to present day conditions) may allow more runoff into Mediterranean than the coupled model used by Marzocchi et al. (2015) and consequently the RM here.

2. The catchment areas for North Africa differ slightly between Bosmans et al. (2015b; Figure 3.5) and Gladstone et al. (2007, see their Figure 1b) resulting in different runoff to the Mediterranean. However, comparison of more similar drainage basins suggests that small deviations in the African drainage basins will only play a minor role on the resulting Mediterranean runoff (not shown).

3. The precession-obliquity interference pattern in Mediterranean sapropels may also be explained by glacio-eustatic sea-level changes affecting Mediterranean-Atlantic connectivity. Such a connectivity change interacts with the $P - E + R$ evolution to determine the biogeochemical response of the Mediterranean and hence the sedimentary succession formed. However, the obliquity signal in the Mediterranean's sedimentary record is found consistently throughout the Mediterranean's sapropel-bearing successions of the last 14 million years, while obliquity-induced glacial cycles occur only episodically and are most developed in the past 1 million years.

4. If obliquity has an effect on the African monsoon, this should be visible by comparing two simulations that have similar values for precession, but different obliquities. Such experiments can be selected from Figure 3.3 with ages 6.568 Ma and 6.589 Ma, but these result in only minor differences in runoff. Comparing our results to Bosmans et al. (2015b) is difficult, as their idealized obliquity extreme experiments are run at zero eccentricity.

We conclude that obliquity does not influence North African-derived runoff to the Mediterranean sufficiently to cause a significant effect at eccentricity maxima. Additional HadCM3L experiments with zero precession and various eccentricity and obliquity values are needed to clarify this issue during eccentricity minima. This suggests that care should be taken when interpreting our results during eccentricity minima.

3.7 The onset of the MSC and the PLG stage

The focus of the box model study (Figure 3.6) is the onset of the MSC (5.971 Ma, Manzi et al., 2013), at which time the lithology changes from foraminiferal-bearing

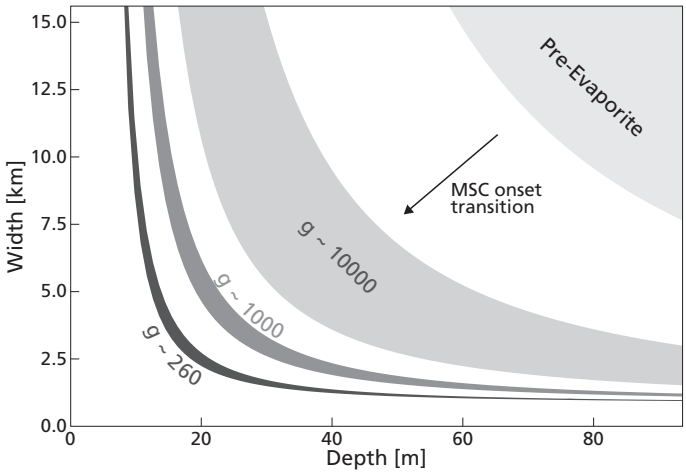

Figure 3.8 The restriction coefficients presented in Figure 6 are translated into gateway dimensions at the onset of the MSC, by combining the theory of Meijer (2006) and Meijer (2012).

marls, to successions comprising alternations of evaporites and barren marls (Figure 3.5). Several authors have hypothesized that this change is due to a restriction in the gateway connectivity (e.g., Flecker et al., 2015). Figure 3.8 shows that even if the lower salinity threshold for gypsum precipitation is used (Grothe, 2016), the gateway needs to be significantly more restricted than at present. The wider the gateway is, the stronger the effect of changing its depth. Even a relatively wide corridor of 15 km would need to shallow by at least 20 m to raise the basin salinity from present-day values to about 50 g/l (see Chapter 2, Simon and Meijer, 2015 for further discussion on gateway dimensions). For narrower gateways and higher salinities, even more shallowing would be needed. Eustatic sea-level fall could be thought of as a possible mechanism for generating this gateway shallowing. However, the low resolution of the late Miocene benthic $\delta^{18}O$ record (e.g., Shackleton and Hall, 1997) makes it difficult to identify precessional or obliquity periods. Also, if restriction is sea-level related the salinity should decrease again during the time-span of the PLG. We conclude that although eustatic sea-level will affect some of the details of the Mediterranean salinity evolution, the actual onset of the MSC was driven by tectonics.

PLG deposits are well-preserved in the Mediterranean (Sorbas, Vena de Gesso, Sicily, Roveri et al., 2014). The 17 and 16 evaporite (gypsum) cycles in Italy and Spain, respectively, correspond well with each other and imply a total duration of approximately $350 - 370$ $kyrs$ for the PLG (Roveri et al., 2014). This assumes the periodicity of the cycles is, like the pre-MSC marls, precessionally forced. Our modelled salinity evolution has 16 excursions towards fresher Mediterranean conditions and 16 or 17 higher salinity excursions (depending on whether the maximum at 5.6 Ma is counted, Figure 3.6A). The green threshold line (Figure 3.6A) illustrates how

such salinity oscillations can oscillate in and out of a regime in which the Mediterranean reaches brine concentration suitable for precipitating gypsum (e.g. salinity concentration 130 g/l). Based on this example, the PLG salinity evolution can be matched to either of the hypotheses for gypsum formation e.g. saltier (Lugli et al., 2010) or fresher (Grothe, 2016), for different thresholds and can be linked to the observed number of gypsum cycles. This agrees with the previously used tuning assumption and quantitatively justifies, for the first time, that the PLG sediments are precessional-driven.

While we cannot use our results to identify whether the gypsum is linked to the dryer (Lugli et al., 2010) or wetter (Grothe, 2016) phases of the freshwater budget, we can argue that both scenarios benefit from having additional runoff from the Chad-Eosahabi basin: (1) If gypsum is in-phase with insolation minima (dryer and therefore saltier), the greater fluctuations in salinity mark a more defined distinction for moving in an out of the gypsum saturation concentration; (2) if gypsum is in-phase with insolation maxima (wetter and therefore fresher), greater monsoonal runoff from north Africa will prompt additional sulphate production in the Mediterranean, making gypsum precipitation more likely.

3.8 Conclusions

For the first time we have generated an estimate of the Mediterranean freshwater budget evolution throughout the late Miocene. This has been achieved via a novel multi-model technique by extending GCM results with a regression model and makes us conclude: (1) Wetter climates occur during eccentricity maxima and precession minima, which is in good agreement with hypotheses for the Mediterranean sapropel-bearing sedimentary record. (2) At low eccentricities, differences can be identified in freshwater budget phasing due to differing $E - P$ and R contribution through time. (3) When using the calculated synthetic sapropel record as a tuning target and comparing it to the original tuning we identify that the net freshwater budget is the most likely mechanism causing sapropel formation in the late Miocene. This is best achieved with enhanced monsoonal runoff. These first three conclusions may be taken to endorse the existing paradigm for sapropel formation. (4) As this additional runoff needs to be at least half the amount of the river Nile, we speculate that the Chad-Eosahabi supplied this enhanced discharge to the Mediterranean. (5) Models differ in their sensitivity to obliquity with respect to the freshwater signal. Therefore, results at low eccentricity should be considered with care. Additional HadCM3L experiments with zero precession and various eccentricity and obliquity are required to investigate the obliquity effect on the African monsoon in greater detail. (6) Exploring our new freshwater budget evolution in a box model has shown that gypsum-marl cycles during the PLG are quantitatively consistent with precessional control. (7) Greater monsoonal runoff from north Africa helps to explain the PLG observations. (8) Furthermore, our freshwater results allow us to disentangle the climatic and tectonic controls on Mediterranean environmental changes. We successfully demonstrate that the lithology change at the onset of the MSC can be linked to gateway restriction, which was most likely of tectonic nature.

4

Salinity stratification of the Mediterranean Sea during the Messinian crisis: A first model analysis

In the late Miocene, a thick and complex sequence of evaporites was deposited in the Mediterranean Sea during an interruption of normal marine sedimentation known as the Messinian Salinity Crisis. Because the related deposits are mostly hidden from scrutiny in the deep basin, correlation between onshore and offshore sediments is difficult, hampering the development of a comprehensive stratigraphic model. Since the various facies correspond to different salinities of the basin waters, it would help to have physics-based understanding of the spatial distribution of salt concentration. Here, we focus on modelling salinity as a function of depth, i.e., on the stratification of the water column. A box model is set up that includes a simple representation of a haline overturning circulation and of mixing. The model is forced by Atlantic exchange and evaporative loss and is used to systematically explore the degree of stratification that results under a wide range of combinations of parameter values. The model demonstrates counterintuitive behaviour close to the saturation of halite. For parameter values that may well be realistic for the Messinian, we show that a significantly stratified Mediterranean water column can be established. In this case, Atlantic connectivity is limited but may be closer to modern magnitudes than previously thought. In addition, a slowing of Mediterranean overturning and a larger deep-water formation region (both in comparison to the present day) are required. Under these conditions, we would expect a longer duration of halite deposition than currently considered in the stratigraphic consensus model of the Messinian Salinity Crisis.

4.1 Introduction

The Mediterranean sedimentary record hosts a kilometer-thick salt giant, deposited during the Messinian Salinity Crisis (MSC, Roveri et al., 2014a, and references therein). The occurrence of evaporites indicates that, overall, basin salinity must have been high. Several different evaporitic lithologies are found in outcrops and are interpreted from seismic profiles. Most notable elements are a gypsum/marl alternation (e.g., Lugli et al., 2010) and halite (e.g., Lofi et al., 2011). Considerable attention has been paid to establishing the stratigraphy of the MSC, both vertically and laterally (e.g., Ochoa et al., 2015; Lugli et al., 2010). Although a stratigraphic consensus model has been proposed (Figure 4.1, summarized by Roveri et al., 2014a), which correlates the deep sequence (the Messinian trilogy of Montadert et al., 1970) to the onshore erosional surfaces and evaporites, much is still uncertain for the simple reason that most of the deposits are hidden from scrutiny below the present sea. It is therefore difficult to establish a definitive correlation between marginal sequences studied in the field and the deep record as seen in seismics. While the halite mined on Sicily is commonly considered an exposed representative of the deep-basin record (the only, in fact), also this is uncertain.

Given that the different evaporitic facies correspond to different salinities of the waters from which they precipitated (e.g., Warren, 2016), it would help to have insight from physics as to which spatial distribution of salinity is most likely at any one point in time. Is it possible that the shallow waters of the marginal basins reside at gypsum saturation while, at the same time, the deeper waters reach levels high enough for halite precipitation? Or, are there reasons to expect the basin to be always well mixed? In the latter case, for example, marginal gypsum and deep halite are not expected to be lateral equivalents and the physics would support the consensus model (Figure 4.1) that has the halite following in time after a first series of gypsum/marl cycles (Roveri et al., 2014b).

In the literature one almost exclusively finds qualitative ideas about the spatial distribution of salinity during the MSC. An early example (Sonnenfeld and Finetti, 1985) suggests various precipitation cycles in which gypsum forms in the shallow parts of the basin and halite at greater depth. More recently this configuration was envisaged by de Lange and Krijgsman (2010), who present a chemical mechanism that allows for synchronous deposition of gypsum at the surface and dolomite at depth and take stratification to be more stable due to the presence of deep brines. Roveri et al. (2014a) numerically simulate the notion that cascading explains the Messinian erosional surface and forms deep supersaturated brines. Also Yoshimura et al. (2016) propose that the deep basin is density stratified and that halite-oversaturated brines transport salt from the margins to depth. While Meijer (2006) and Topper and Meijer (2013) investigated the effect that an imposed stratification has on their model results for the MSC, they did not study how and whether stratification arises in the first place.

The purpose of this chapter is to gain quantitative, physics-based, understanding of the factors that controlled the vertical distribution of salinity in the Messinian brine basin. For this we use a simple box model. Although general circulation models

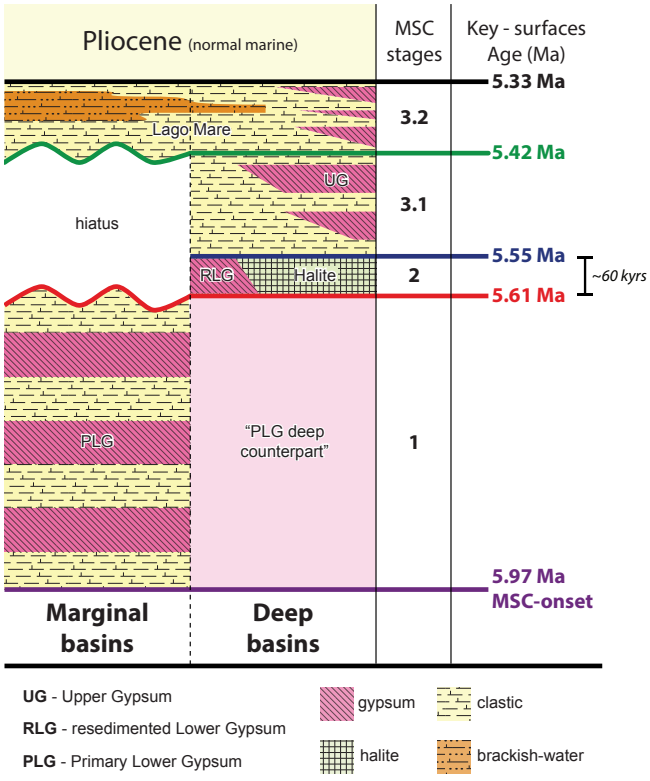

Figure 4.1 The MSC stratigraphic consensus model (linear in time), simplified from Roveri et al. (2014).

(e.g., Topper and Meijer, 2015a) certainly provide insight about stratification, their long computation time and the extreme ocean salinity during the MSC preclude their use for our purposes. These limitations do not affect box models and these have proven to be valuable tools for testing the sensitivity of Mediterranean parameters to external forcing. In this first study of this kind we explore a box model that includes a deep-water formation region feeding a basin-wide circulation, which can be thought of as a simple representation of a haline overturning circulation. In addition, exchange with the Atlantic, evaporative surface forcing and mixing within the basin are taken into consideration. The model calculates surface and deep Mediterranean salinity through time, which provides a crude quantitative measure for the degree of stratification. Our findings will be discussed in terms of their potential implications for the stratigraphical relationships within the Messinian sedimentary record. What makes the analysis timely is the recent suggestion that the Sicily halite may not have been deposited in the deepest parts of the basin after all (Lofi et al., 2016, on the basis of Maillard et al., 2014). Also, industry data from the Levantine basin are now

starting to reveal more details about the deep record of the eastern Mediterranean (Feng et al., 2016; Madof and Connell, 2016; Meilijson et al., 2016). Furthermore, for many years now, the scientific community has been working towards drilling the deep Messinian record (e.g., MEDSALT initiative, https://medsalt.eu).

4.2 Model description

Consider the following thought experiment: an ocean basin subject to evaporation is represented as a single water column. The evaporation will cause salinity of the surface water to increase. As a result, surface density is enhanced and a gravitational instability is created, which leads to mixing of the water column. As long as evaporation continues, these steps will repeat themselves and the column will be essentially homogeneous at all times. This effect is exemplified by the recent Dead Sea, apart from the fact that here a stable stratification is installed seasonally due to heating (e.g., Sirota et al., 2016). We learn from this thought experiment that, in order to create persistent (i.e., lasting longer than one year) stratification, a single-column representation does not suffice and that lateral variation is crucial.

In this study we are using a box model, as show in Figure 4.2. In the Mediterranean Sea evaporation exceeds precipitation and river input. We denote net evaporation as e and take it to act uniformly across the basin. Exchange with the Atlantic adds "fresher" water to, and removes saltier water from, the Mediterranean Sea at its western side. Instead of considering the drivers of exchange — Atlantic-Mediterranean density difference and the gateway dimensions (e.g., Chapter 2, Simon and Meijer, 2015) — we prescribe a value for the outflow from the Mediterranean (q). Volume conservation then implies the Atlantic inflow equals ($q + e * A$).

Wåhlin and Cenedese (2006) investigate the response of ocean stratification to the inflow of dense water from an adjacent marginal sea by solving the advection-diffusion equation which allows them to obtain a continuous depth variation of water properties. As a first step towards this, we consider the simpler case where the basin is divided into a surface layer (subscript "*Surf*") and a deep layer (subscript "*Deep*"). Turbulent mixing between the surface and deep box is represented as a diffusive process, following the models for the Mediterranean Sea of Tziperman and Speer (1994) and Matthiesen and Haines (2003). Mixing is controlled by a constant diffusivity κ and a vertical length scale equal to the vertical distance between the middle of the two layers.

In the present-day Mediterranean circulation (e.g., Tsimplis et al., 2006), Atlantic surface water flows towards the east and increases in salinity due to evaporation. In the Levantine basin the water becomes dense enough to sink to intermediate depth, at which level it spreads westwards throughout the basin. On its path to the west, the salt-preconditioned water passes through regions where it is subject to cold and dry winds (e.g., Schroeder et al., 2012). This leads to further increase in density and forms deep water. Modern deep-water formation occurs at the northern rim of the Mediterranean Sea in shallow, restricted, basins, like the Adriatic Sea (Malanotte-Rizzoli et al., 1997) or the Aegean Sea (Roether et al., 1996), and in open-ocean convection sites (e.g., Stommel, 1972). The dense water produced charges the Mediterranean

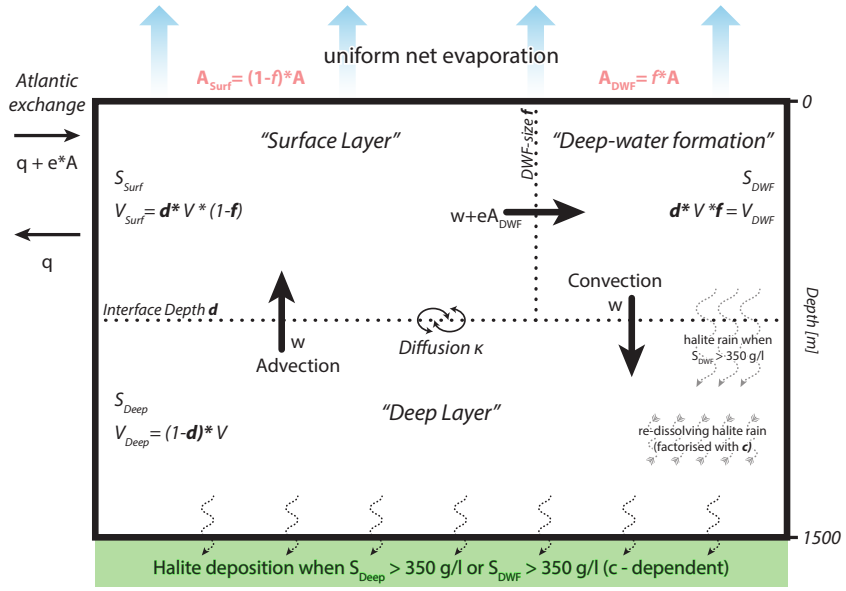

Figure 4.2 Illustration of all parameters in the box model (e.g., salinity, volume, area or halite rain). The basin is split up into three boxes ("*Surf*", "*DWF*" and "*Deep*"). Parameters, related to water fluxes, are represented as arrows (not to scale).

overturning circulation. In our model the deep-water formation-box (DWF) represents such a region. The production of deep water (to which we will refer as "convection") is parametrised as a constant volume flux w. The same volume of water per unit of time is advected upwards outside the DWF. Convection and advection together lead to a simple basin-wide circulation (Figure 4.2).

When the DWF-box reaches halite saturation, which we define to be when S_{DWF} = 350 g/l, halite starts to crystallize, causing halite rain into the deep box (e.g., Yoshimura et al., 2016; referred as "rain from heaven" in Warren, 2016). In the deep box it may partly or entirely re-dissolve and the remainder is removed from the system by sedimentation. How much of the halite raining down is re-dissolved is set by the factor c ($c = 0$, no re-dissolution; $c = 1$, full re-dissolution). All halite that forms in the deep box (when $S_{Deep} = 350\ g/l$) is deposited equally across the Mediterranean surface (A), allowing us to estimate its sedimentation rate (cm/yr) under the assumption of a uniform density for the halite (2160 kg/m^3). Because, in reality, the deposits are unlikely to cover the entire surface area of the basin, our sedimentation rate is a conservative estimate.

The salt concentration of the three boxes evolves as:

$$V_{Surf}\frac{dS_{Surf}}{dt} = \overbrace{q * \Delta S_{AtlSurf}}^{\text{Exchange related}} + \underbrace{w * \Delta S_{DeepSurf}}_{\text{Con/Advection related}} + \overbrace{e * (A * S_{Atl} - A_{DWF} * S_{Surf})}^{\text{Evaporation related}} - \underbrace{\kappa * A_{Surf} * \frac{\Delta S_{SurfDeep}}{0.5 * V/A}}_{\text{Diffusion related}} \quad (4.1)$$

$$V_{DWF}\frac{dS_{DWF}}{dt} = \underbrace{w * \Delta S_{SurfDWF}}_{\text{Con/Advection related}} + \overbrace{e * A_{DWF} * S_{Surf}}^{\text{Evaporation related}} - \overbrace{\underbrace{dDWF_{sink}}_{\text{when } S_{DWF} > 350g/l}}^{\text{Halite crystallization}} \quad (4.2)$$

$$V_{Deep}\frac{dS_{Deep}}{dt} = \underbrace{w * \Delta S_{DWFDeep}}_{\text{Con/Advection related}} \overbrace{- \kappa * A_{Surf} * \frac{\Delta S_{DeepSurf}}{0.5 * V/A}}^{\text{Diffusion related}} + \overbrace{c * dDWF_{sink}}^{\text{Halite re-dissolution}} - \overbrace{\underbrace{dDeep_{sink}}_{\text{when } S_{Deep} > 350g/l}}^{\text{Halite crystallization}} \quad (4.3)$$

The subscript "*Atl*" stands for the Atlantic. S represents the salinity and $\Delta S_{xy} = S_x - S_y$. The limitations imposed on our model as a result of the various assumptions and simplifications will be treated in the discussion (Section 4.4).

4.3 Model analysis and results

4.3.1 Setup of the analysis

With the model outlined in the previous section we systematically explore the effect on salinity and salinity stratification of all parameters. Only basin volume and surface area are kept constant. Since the late Miocene hypsometry was already close to that of the present day (Meijer and Krijgsman, 2005), we set the volume and surface area of the entire box-system to modern values ($3.75 * 10^{15}$ m^3 and $2.48 * 10^{12}$ m^2). In order to allow for a clear presentation of our findings, we will first present only a subset of the experiments (Figures 4.3-4.8), followed by a summary (Figure 4.9). We start by reporting the impact of different strengths of flux-related parameters (Section 4.3.2). This is followed by the relevance of the box sizes and the extent of re-dissolution of halite rain in the deep basin (Section 4.3.3). Section 4.3.4 summarises all findings, which sets the basis to form implications for the MSC (Section 4.3.5).

Three net evaporation values (e = 0.25 m/yr, 0.5 m/yr, 1.0 m/yr) are tested. These cover the range of estimates for the late Miocene (e.g., Chapter 3; Simon et al., 2017; Topper et al., 2011; Gladstone et al., 2007). For reference, the present-day value amounts to $\sim$ 0.5 m/yr (Mariotti et al., 2002). If we consider a single-box representation of the Mediterranean and combine the conservation of salt mass

(Figure 2.2, Chapter 2, Simon and Meijer, 2015) with the conservation of water mass, it is straightforward to calculate the outflux q required to increase salinity to large values (the expression for q reads $q = eS_{Atl}/\Delta S_{MedAtl}$, e.g., Bryden and Stommel, 1984). For the three e values considered, halite saturation ($S_{Med} = 350\ g/l$) would be reached for a q of 0.002 Sv, 0.004 Sv and 0.009 Sv, respectively. These are clearly much lower than the present-day exchange at Gibraltar, which has an annual mean of about $0.7 - 0.8\ Sv$ (Soto-Navarro et al., 2010). In our sensitivity analysis we consider three values for q (0.001 Sv, 0.01 Sv, 0.1 Sv). This is followed by results related to the vigour of circulation (w) and mixing (κ). It is difficult to identify a single number for annual mean present-day overturning. However, zonal overturning streamfunctions based on observations (e.g., Sevault et al., 2014) and on modelling (Mikolajewicz et al., 1993; Topper and Meijer, 2015a; Grimm et al., 2015) indicate strength of the order of $1 - 2\ Sv$. Slightly weaker deep-water formation fluxes (mostly between $0.1 - 0.6$ Sv) are reported by (Béranger et al., 2010). Our analysis shows that $w > 0.1\ Sv$ will never yield significant stratification, which, in fact, is a first important result. We thus consider lower values ($w = 0.1\ Sv$ and 0.01 Sv, Figure 4.4). We test the mixing strength for κ values of $10^{-5}\ m^2/s$ (Figure 4.3 and 4.4) and $10^{-4}\ m^2/s$ (Figure 4.5). These values have been inferred for the general background mixing of the global ocean interior (Jayne, 2005; Munk, 1966) and have been applied in other studies of the Mediterranean (e.g. Tziperman and Speer, 1994). The flux-related parameters are explored for the case of a surface layer thickness of 160 m ($d = 160/1500$), a DWF-box with a surface area that is 1/3 of the entire Mediterranean area ($f = 1/3$) and full re-dissolution of halite in the deep basin ($c = 1.0$; Figures 4.3–4.5). This specific combination of settings is chosen as our starting point because it allows for the best visual presentation of the model behaviour. The effect of $c < 1.0$ will be investigated in second instance, together with that of other values for d and f.

Figures 4.3–4.5 present changes in time of salinity of the three boxes (S_{Surf}, dashed; S_{DWF}, solid, S_{Deep}, dotted) and the degree of stratification (shaded). Each simulation is calculated for a different set of parameters. Figure 4.3 shows a matrix of experiments with a different e in each column and different q in each row.

4.3.2 Sensitivity of salinity to flux-rated parameters

All our model experiments start at a salinity of 36 g/l, which is about equal to the salinity of the presently inflowing Atlantic water. Through time, salinity in the basin will increase due to the net evaporative loss and the restriction from the Atlantic. The salinity in the DWF-box evolves consistently to be the highest of all boxes, because the water in this box has been subject to evaporation the longest. The second highest salt concentration is hosted by the deep box, because it is directly fed by the DWF-box. The lowest salinity is reached by the surface box, because it is under the most direct influence of the Atlantic exchange.

Figures 4.3G, 4.3H and 4.3I show that greater evaporation leads to faster salinity increase and to higher equilibrium salinity in each box. The degree of stratification is also greater for a larger evaporation, because the salt concentration in the deep box is impacted more than surface salinity. This holds true for all panels presented.

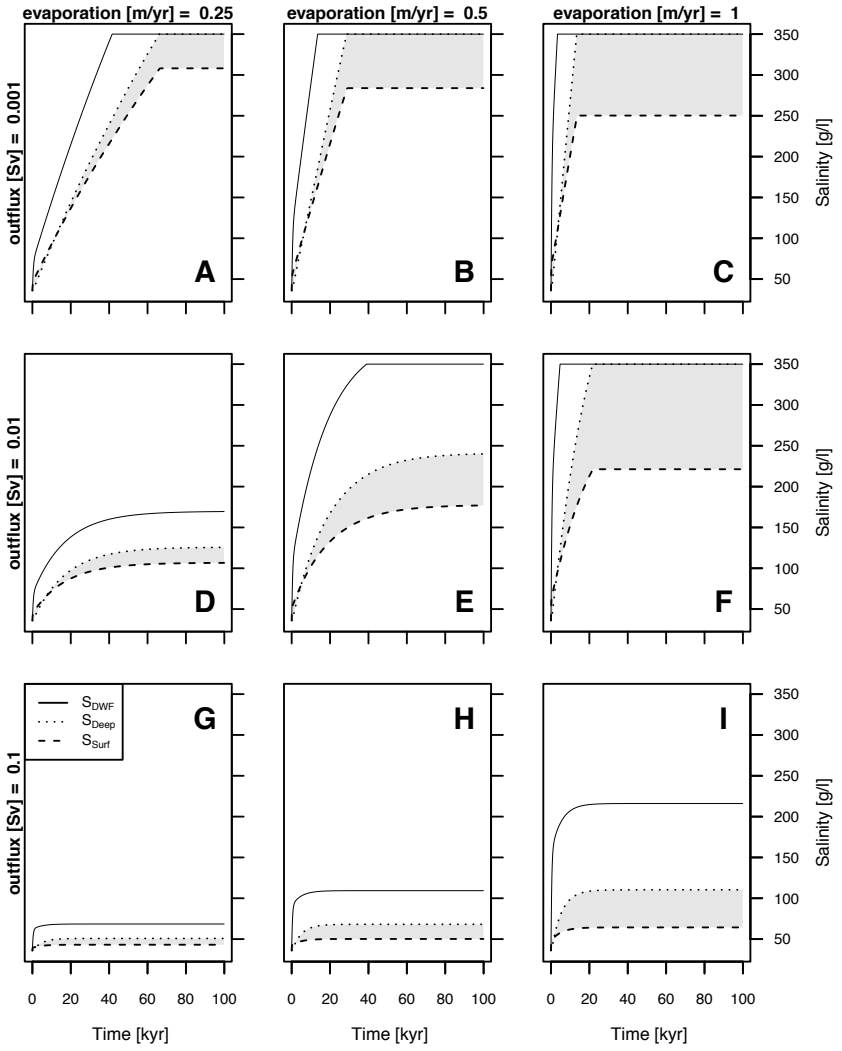

Figure 4.3 All nine panels follow the same layout and the standard setup ($f = 1/3$, $d = 160/1500$, $c = 1.0$). The experiments plotted in each column of panels are forced with a different net evaporative forcing (0.25 m/yr, left; 0.5 m/yr, center; 1.0 m/yr, right). The experiments plotted in each row are forced with a different exchange flux with the Atlantic (0.001 Sv, top; 0.01 Sv, middle, 0.1 Sv, bottom). The diffusivity κ is set to a value of 10^{-5} m^2/s and con-/advection w is 0.01 Sv. The x-axis is time and the y-axis is salinity. Each line represents one box of our model (Figure 4.2): Deep-water formation (DWF), solid line; $Deep$, dotted line; $Surface$, dashed line. The salinity difference between surface and deep box is the "degree of stratification" (shaded in grey).

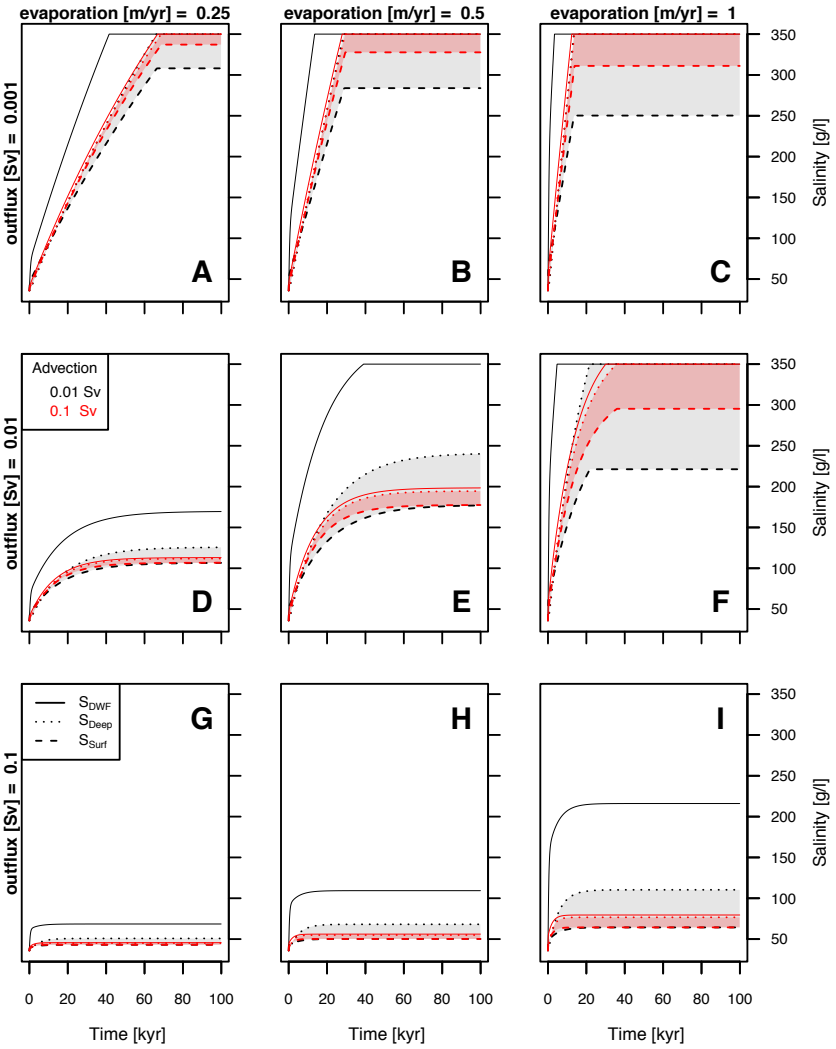

Figure 4.4 Presented experiments have an identical setup to the ones in Figure 4.3. However, per panel, two experiments are shown with different advection fluxes (0.01 Sv, black; 0.1 Sv, red).

However, when the deep basin reaches halite saturation, the deep salinity stays constant, but the surface water is fresher for stronger evaporation (Figure 4.3A, 4.3B, 4.3C). This is because a greater e will increase the Atlantic inflow, which increases the salt intake by the basin as a whole, but dilutes the surface layer. Steady state is reached fastest for low evaporation values, when water does not saturate for halite (comparing Figure 4.3G to 4.3I). This trend would continue if salinity were allowed to rise unlimitedly. However, when a box reaches 350 g/l its salinity is capped, forcing the system to steady state at that instant (time-dependent terms on the left-hand side of equations 4.1–4.3 go to zero). Therefore, when S_{DWF} is at 350 g/l, steady state is reached fastest for high evaporation values.

Comparing Figures 4.3A to 4.3D and 4.3G shows that a smaller exchange causes salt concentration in all boxes to reach higher values (also observed by comparing Figures 4.3B with 4.3E and 4.3H and 4.3C with 4.3F and 4.3I). Similar to the response to evaporation, variation of the exchange impacts the deep box stronger than the surface box, causing greater stratification for smaller q values. This holds true until the deep basin hits halite saturation. That moment S_{Deep} is fixed, a lower q can only further raise S_{Surf}, leading to a decreased stratification (compare Figure 4.3I to 4.3F and 4.3C, for example). This demonstrates that the value of Atlantic exchange that causes the deep basin to just reach to halite saturation will create the strongest stratification. The exact magnitude depends on the value of the other model parameters (see Figure 4.9 and supplementary Figures 4.11 - 4.13, which will be discussed in Section 4.3.4 and 4.3.5). When exchange is restricted, more time is needed to reach equilibrium (when $S_{Deep} < 350$ g/l, compare D and G in Figure 4.3). For $S_{Deep} = 350$ g/l, the opposite is the case (compare C and F in Figure 4.3).

To evaluate the effect of circulation on salinity, we add to Figure 4.3 an additional set of experiments with a larger w value (red in Figure 4.4). Stronger advection causes faster redistribution of salt, leading the salinity of the boxes to approach each other (i.e. reduced stratification). Again, the reaching of halite saturation will change the response to this parameter. When $S_{DWF} < 350$ g/l, the surface salinity is not affected by the magnitude of w; however, the deep salinity is and it is larger for smaller w, causing greater stratification (e.g., Figure 4.4I). When $S_{DWF} = 350$ g/l (e.g., Figure 4.4C), only the surface salinity is affected and is lower for smaller w values, causing enhanced stratification. Time to equilibrium is hardly affected by the circulation strength. Larger w values cause salinity to reach equilibrium earlier, when $S_{DWF} < 350$ g/l. A reversed behaviour is seen in the case, when $S_{DWF} = 350$ g/l.

The experiments in Figure 4.5 have an identical setup to experiments in Figure 4.4 but correspond to a larger κ of 10^{-4} m^2/s representing increased mixing. Larger values of κ decrease the difference in salinity between the surface and the deep basin (i.e., lead to lower stratification). S_{DWF} is hardly impacted by κ (compare 4.4A with 4.5A). Less mixing leads to greater S_{Deep} (when $S_{Deep} < 350$ g/l, S_{Surf} is not affected) and to lower S_{Surf} (when $S_{Deep} = 350$ g/l). If the water column is particularly stable, an even less restricted gateway could lead to significant stratification (mixing very weak, $\kappa = 10^{-6}$ m^2/s, see supplementary Figure 4.10). The time to equilibrium, although hardly impacted, is reached faster when κ is larger.

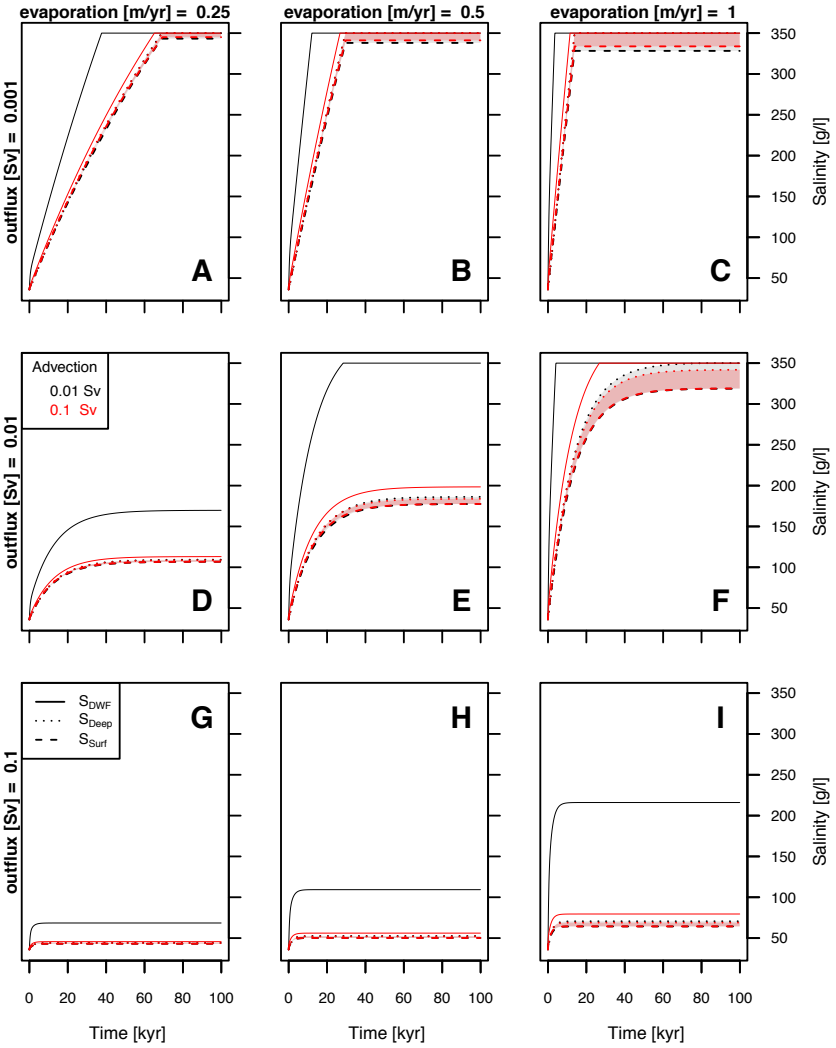

Figure 4.5 Presented experiments have an identical setup to the ones in Figure 4.4. However, the diffusivity κ is set to a value of $\kappa = 10^{-4}\ m^2/s$. Supplementary Figure 4.10 plots the same experiments for $\kappa = 10^{-4}\ m^2/s$.

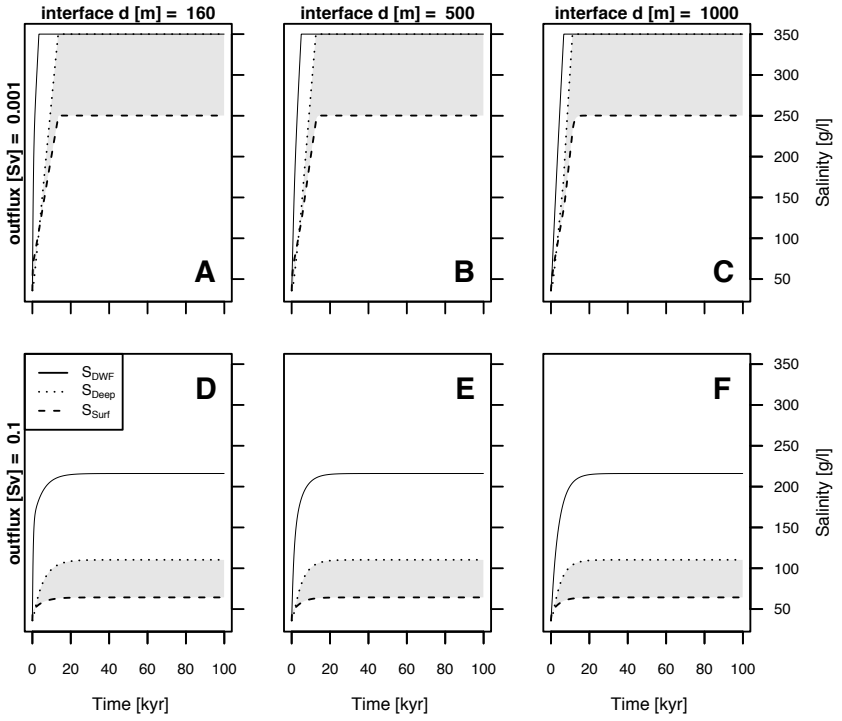

Figure 4.6 Panels A and D are identical to Figure 4.3C and 4.3I, respectively. Panels B/E and C/F differ to A/D in value the horizontal interface depth d (B/E, 500 m; C/F, 1000 m).

4.3.3 Effect of variation of d, f and c

Following the analysis on the response to flux-related parameters, we now consider how the established insight is affected by other choices for the parameters d, f and c. For the sake of clarity, we choose one experiment from Figure 4.3 and consider how it is affected by a different horizontal interface depth (d, Figure 4.6), DWF-area (f, Figure 4.7) and strength of re-dissolution of halite in the deep basin (c, Figure 4.8). The selected experiments are chosen so that the impact of d, f and c is clearly illustrated.

The horizontal interface depth impacts the volume distribution of the boxes. The steady-state salinity is independent of the position of d (comparing Figure 4.6A with 4.6B and 4.6C and 4.6D with 4.6E and 4.6F). Considering equations 4.1–4.3 it becomes clear that d can only affect the salinity evolution prior to equilibrium. The shallower d is, the longer it takes to reach a certain salinity in both surface and deep box. This is the case because with a shallower d, the deep box has a larger volume, which implies more Mediterranean water needs to be raised in salinity, which takes longer (compare Figure 4.6A and C). This response of the system to d holds true across the entire parameter space.

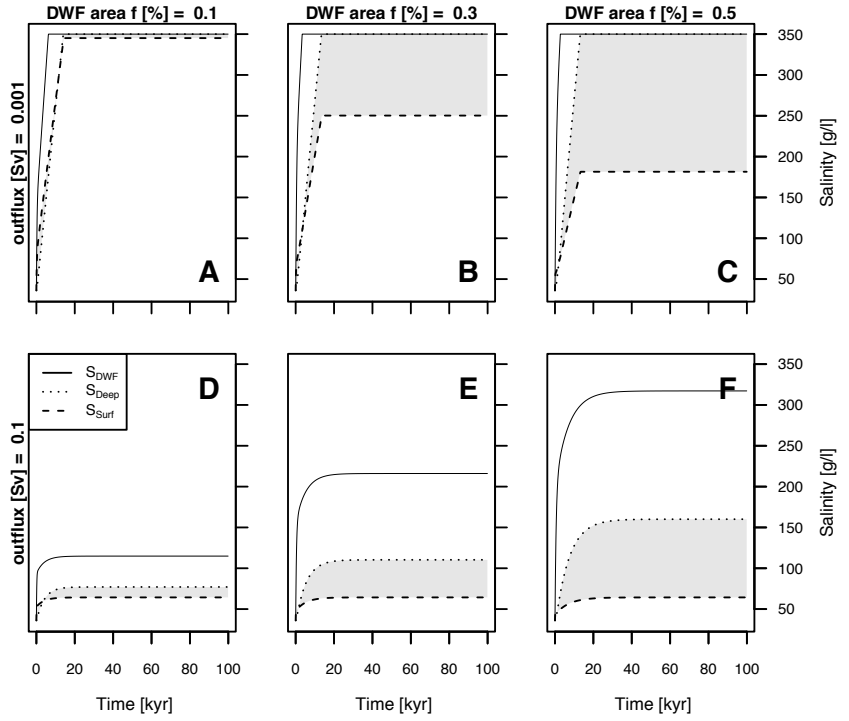

Figure 4.7 Panels B and E are identical to Figure 4.3C and 4.3I, respectively. Panels A/D and C/F differ to B/E in value the DWF-size f (A/D, 0.1; C/F, 0.5).

The larger the DWF-surface-area, the greater is the calculated degree of stratification (Figure 4.7). When $S_{Deep} < 350$ g/l, this is because S_{Deep} is larger, while S_{Surf} is relative constant (compare panels D with E and F in Figure 4.7). When $S_{Deep} = 350\ g/l$, it is because S_{Surf} is lower, while S_{Deep} is relatively constant (compare panels A with B and C in Figure 4.7). This behaviour of the surface salinity makes sense, because even while depositing halite the deep box can recycle salt to the surface via advection.

So far, our results (Figures 4.3 - 4.7) only considered the scenario in which any halite that crystallizes at the surface is fully re-dissolved in the deep basin. When none or partial re-dissolution occurs, salt is removed from the system by deposition at an earlier stage, leaving the deep basin less saline and therefore leading to weaker stratification (compare Figure 4.8A-C). Analysing the response to c also demonstrates that if not all salt is re-dissolved, halite deposition starts earlier (up to several thousand years). Moreover, parameter c affects the described response to circulation. Each panel of Figure 4.9 presents results of 10^4 model experiments for a range of w and q values. Panels A and B correspond to $c = 0$ while C and D have $c = 1$. In panels A and C, κ equals $10^{-5}\ m^2/s$ and in B and D it is $10^{-4}\ m^2/s$. The other parameters

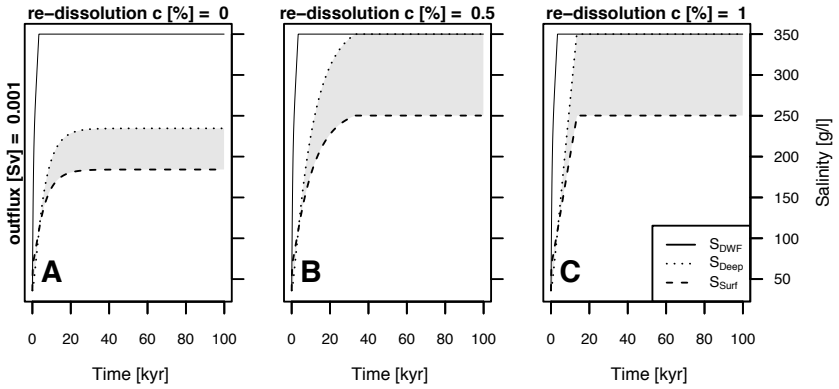

Figure 4.8 Panel C is the identical experiment to Figure 4.3C. Panels A and B differ to C in the strength of re-dissolution of halite rain c, which is 0.0 and 0.5, respectively.

are the same in all experiment panels: $e = 1.0\ m/yr$, $f = 0.3$ and $d = 160\ m$. The model runs are calculated for 1000 $kyrs$, rather than 100 $kyrs$, to guarantee that all experiments reach a steady state. In addition to the level of stratification, we also extract the sedimentation rate at which halite is deposited (indicated by contours), once an experiment reaches steady state. This shows that, when w is approaching zero, the stratification may again decrease slightly (e.g., Figure 4.9A). This effect is also there in Figures 4.3-4.5 but not observable because it is overprinted by halite rain re-dissolving in the deep basin.

4.3.4 Summary of the sensitivity analysis

Strongest stratification occurs when the deep basin just reaches halite deposition and when the surface salinity sits as close as possible to that of the Atlantic. The existence of strong stratification implies a marked distribution of salt within the basin and can involve halite deposition in a situation in which the mean Mediterranean salinity is below halite saturation. An important finding is that our experiments divide into two sets. Depending on whether water passes the saturation threshold, the system demonstrates different sensitivity to the model parameters. For example, if salt concentrations stay below 350 g/l then equilibrium is reached fastest when q is high, e is low and w and κ are high. However, if halite saturation is reached in the deep box, then equilibrium is reached fastest when q is low, e is high and w and κ are low. The reason for this is the salinity capping due to the crystallization of halite.

Figure 4.9, together with the supplementary Figures 4.11 - 4.13, summarize the systems behaviour in terms of the level of stratification that is reached in steady state. The response to some of the parameters proves to be relatively straightforward: the interface depth has no impact on the level of stratification and stronger evaporation causes stronger stratification. Also, a larger DWF-region (larger f) increases stratification and a stronger mixing, naturally, reduces stratification. The other parameters

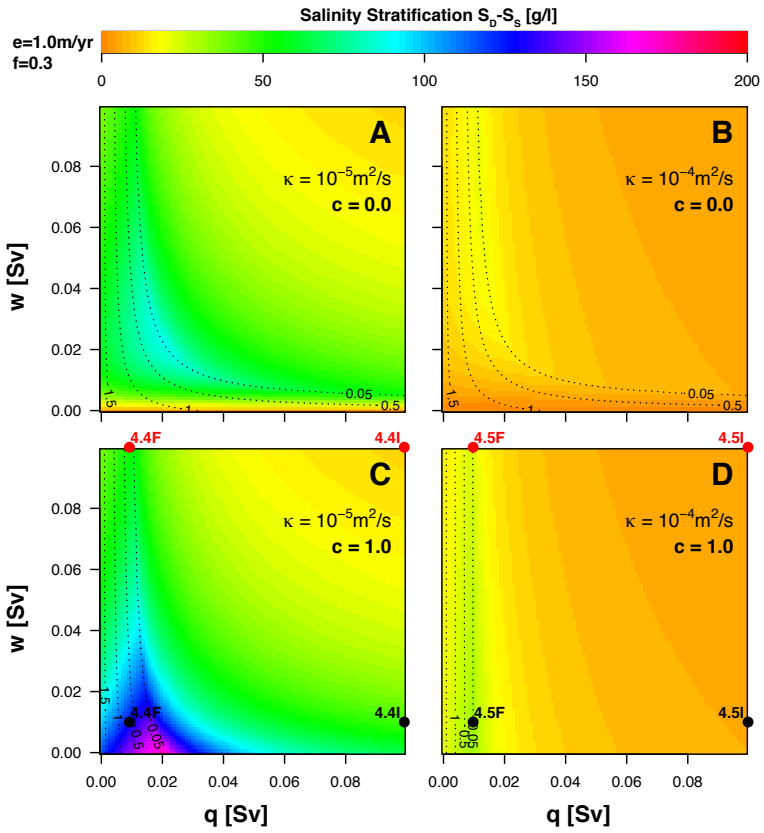

Figure 4.9 Degree of stratification plotted for 4 sets (2 κ-values by 2 c-values) of 10^4 experiments for various w (y-axis) and q (x-axis). All other parameters are constant and set to $e = 1.0\ m/yr$, $f = 0.3$ and $d = 160\ m$. Contour lines indicate the halite sedimentation rate for the same parameter space. Red and Black dots on panel C and D link to individual experiments presented on Figure 4.4 and 4.5. Three equivalent figures are placed in the Supplementary Figures 4.11 - 4.13, which differ in e and f values.

q, w and c are more complex. Generally, high w and q values create weak stratification and small w and q values cause larger stratification (Figure 4.9). However, largest stratification is formed when w and q are just allowing for halite saturation (dependent on the strength of the diffusivity, supplementary Figure 4.14). Another interesting observation is that, although for large c only very low q values will cause the deposition of halite (consider contours on Figures 4.9C and 4.9D), for small c also large q values (e.g., present-day) result in deposition when w is small (consider contours on Figures 4.9A and 4.9B). Halite deposition during such a scenario (small c, large q and small w) would entirely be created from halite rain and the deep basin would not be at halite saturation yet.

4.3.5 Was there significant stratification during the MSC?

We now use the model to try and answer the question outlined in the introduction: would we expect significant stratification of the Messinian basin? In order to achieve, for example, a stratification of $\sim 200\ g/l$ it follows from our analysis that this occurs when evaporation is strong ($e = 1.0\ m/yr$), mixing is weak ($\kappa = 10^{-5}\ m^3/s$), halite is re-dissolving ($c = 1.0$), deep-water flux is below $0.01\ Sv$ and exchange is between $0.01 - 0.03\ Sv$ (Figure 4.9C). If no halite re-dissolves ($c = 0.0$), a weaker but still significant stratification (e.g., $\sim 100\ g/l$) is created, for w in the range $\sim 0.01 - 0.04$ Sv (Figure 4.9A). By halving evaporation ($e = 0.5\ m/yr$, supplementary Figure 4.11) maximum stratification is reduced by approximately 50% with an exchange range of lower values ($\sim 0.005 - 0.01\ Sv$ supplementary Figures 4.11A and 4.11C). Such a linear response between evaporation and salinity was previously documented (Chapter 2, Simon and Meijer, 2015). These ranges are for a DWF-size of $f = 1/3$. If the two evaporation values are considered for an f value of 0.1, the maximum degree of stratification, which now occurs at when exchange and overturning are approximately halved, is reduced by about 50% (compare Figures 4.9 with 4.11 and Figures 4.12 with 4.13).

The question now is whether these combinations of parameters are realistic for the Messinian crisis. Recently derived estimates of late Miocene net evaporation in the Mediterranean range between $\sim 0.79\ m/yr$ and $\sim 0.88\ m/yr$ (including and excluding the drainage of the Chad-Eosahabi catchment, respectively; Chapter 3, Simon et al., 2017). These values are positioned within the parameter range that would allow for significant stratification. Present-day estimates of turbulent diffusivity, as a measure of mechanical mixing, are of the order of $\sim 10^{-5}$ - $10^{-4}\ m^2/s$ (e.g., Jayne, 2005; Munk, 1966). To create significant stratification during the MSC we found that κ needs to be at the lower end of this range. Although corresponding values for diffusivity are not known it has been pointed out that in marginal settings (Bryden et al., 2014) or when strong water column stability is present (e.g., Marzeion and Levermann, 2009), mixing may indeed be minor. If κ would be less than $10^{-5}\ m^2/s$, even larger w and q or lower f values than those reported at the start of this section would allow for significant stratification (see supplementary Figure 4.14). As to the required reduction in the exchange (down to the order of 0.01 Sv) this can ascribed to the greater constriction of the Messinian gateway. Meijer (2012), Rohling et al. (2008) and Simon and Meijer (2015) addressed the strait dimensions that would be associated with such limited exchange. Thus, with regards to e, κ, and q a significant Mediterranean stratification during the Messinian would seem possible to achieve. However, this is true only if overturning (w) is weak and the size of the deep-water formation region (f) is large and these are much harder to constrain for the MSC. In itself, the required combination is surprising, because a large f might intuitively not be associated with a small w. The reason for this specific combination is that a large f leads to low surface salinity and high salinity in the DWF-box, which is needed to increase the deep salinity and therefore stratification. However, if the salt is transported by water and not as halite rain, only a small amount of water should convect, because it would otherwise lead to a more mixed basin. As to w, if the strength of overturning is coupled to Atlantic exchange then a smaller w would indeed be expected during the Messinian.

The alternative, that the overturning is exclusively set by the atmospheric forcing, resulting in a basin that is ever more overmixed when the exchange is reduced, seems unlikely (cf. Topper and Meijer, 2015a). Also, to the extent that convection depends on the density difference between DWF and *deep*-box, the moment that both are close to halite saturation, w will be small. The value of f required to obtain significant stratification proves large compared to the value that would describe the present-day area of intermediate and deep-water formation. For reference, the site of open-ocean convection in the Gulf of Lions corresponds to an f of about 0.004 (Herrmann et al., 2009). Taken together, present-day regions of deep mixing do not occupy more than 1% of the Mediterranean surface (e.g., Pinardi and Masetti, 2000; D'Ortenzio et al., 2005; Tsimplis et al., 2006). Starting from a case with strong stratification ($\kappa = 10^{-5}$ m^2/s and $e = 1.0$ m/yr, supplementary Figure 4.15), with decreasing f, the parameter space of q and w that leads to significant stratification narrows. When f is below 0.05 only for a diffusivity value lower than 10^{-5} m^2/s, stratification of 50 g/l can be reached. The implication of a relatively large f would be that a large part of the eastern Mediterranean acted like our DWF-box. This would imply that in this region surface waters were very salty, causing, for example, halite rain. Further west, surface waters would decrease in salinity, most likely in gradual fashion towards the Atlantic. One may speculate that this explains the presence of less-saline waters, maybe saturated for gypsum, in areas like the Sorbas basin (Krijgsman et al., 2001) or the Vena del Gesso basin (Lugli et al., 2010). Also, the same lateral distribution of salinity could be the reason that no onshore gypsum is found in the far eastern Mediterranean (e.g., Gavdos, Krijgsman et al., 1999a).

An independent way to decide on the likelihood of stratification during the MSC stems from the fact that the different scenarios prove to imply different rates of sedimentation (see also Topper and Meijer, 2013). The consensus model places the Messinian halite layer within a short time period of ~ 60 kyrs (Figure 4.1, Roveri et al., 2014) and Ryan (2008) estimates the salt volume to be $\sim 2 * 10^{15}$ m^3. By spreading this volume over the Mediterranean surface area employed in our calculations, we arrive at a salt thickness that can be directly compared to the model results. It proves that the implied sedimentation rate of the order of $\sim 1 - 2$ cm/yr can only be reached for a relatively well-mixed basin (Figure 4.9). For a stratified Mediterranean, our results suggest much lower sedimentation rates of below 0.5 m/yr. In order to explain the observed thickness with such low rates, the duration of halite deposition in the deep basin must have been longer — at least $100 - 200$ $kyrs$, but possibly even more — than considered in the consensus model (Roveri et al., 2014). The reason for this is that greater Atlantic-Mediterranean exchange is needed to create significant stratification (about twice the exchange associated with a mixed basin, and even more for lower κ, supplementary Figure 4.14) This corresponds to a lower net salt flux from the Atlantic Ocean into the Mediterranean Sea. The insight that a stratified basin results in a lower halite sedimentation rate can already be inferred from Topper and Meijer (2013) who looked at the effect of an assumed stratification (rather than solving for it). Their Figure 10 shows that the halite thickness created in 60 $kyrs$ is less for increased stratification which also points to a low rate of sedimentation.

4.4 Discussion

The neglect of temperature

The relative importance of salinity and temperature in controlling seawater density is determined by the ratio of the coefficients of haline contraction to thermal expansion which is typically about 4 : 1 (Johnson et al., 2007). Present-day temperature in the Mediterranean ranges from $\sim 10^oC$ during winter in the northern Adriatic Sea to $\sim 30^oC$ during summer in the Gulf of Sirt or the Levantine Sea (Rohling et al., 2015). If this temperature span would be imposed as a variation at a single location at the surface, the density would change by an amount equivalent to a change in surface salinity of $\sim 5\ g/l$. Present-day salinity in the Mediterranean ranges from $\sim 35\ g/l$ in the northern Adriatic or Aegean Sea to $\sim 40\ g/l$ in the Levantine Sea (Rohling et al., 2015) and it follows temperature and salinity both play a role. However, during the MSC the salt concentration reached up to absolute values of $\sim 350\ g/l$, while the Atlantic and rivers added much fresher water ($\sim 36\ g/l$ or less).With increasing temperature the haline contraction coefficient decreases and the thermal expansion coefficient increases (Thorpe, 2005). Despite the fact that its waters have a particular chemical composition, the Dead Sea could be an interesting analog to the MSC. Anati (1997) reports that measurements of the Dead Sea water yield a ratio of 2 : 1 between haline contraction to thermal expansion. Although it is unknown what is the appropriate value for these coefficients for the MSC, the very ranges of temperature and salinity imply that the latter dominated over the former. The role of temperature will not be negligible in a situation where the water column is close to being homogeneous in salinity. Even when salinity is very high, variations in temperature of the surface water would be significant in that they determine the stability. This behaviour has been documented in detail for the Dead Sea (e.g., Sirota et al., 2016). In the context of our model, this particular role of temperature would be captured by the imposed convective flux.

Role of salinity-related feedbacks

In view of the already large number of parameters in our box model, we deliberately assumed the various fluxes of water and salt between the boxes to be independent of salinity. Here we discuss how any feedbacks would impact on our results. Exchange is dependent on the density gradient at the strait — controlled by gateway dimensions (Chapter 2, Simon and Meijer, 2015) and Mediterranean evaporative loss (Chapter 3; Simon et al., 2017). Due to the neglect of temperature, salinity directly represents density. When salinity is still increasing (prior to steady state), the pressure gradient along the strait would increase and enhance exchange. The latter, in turn, would dampen the rise in basin salinity. Steady state results are not impacted by this feedback, because the final basin salinity is in balance with the prescribed outflux.

A higher salinity of a water body will reduce its activity, which lowers the rate of evaporation (Warren, 2016; see also Salhotra et al. (1985)). Myers and Bonython (1958) approximated the effect linearly:

$$e = e_o * 1.0316 * (1 - 8.75 * 10^{-4} * S) \tag{4.4}$$

where e is the net evaporation affected by water salinity S and e_o corresponds to the initial value of e. This relationship shows that water at a salinity of $\sim 130 - 160$ g/l (gypsum saturation) will cause a reduction in evaporation of $\sim 10\%$ and water at a salinity of ~ 350 g/l (halite saturation) of $\sim 28\%$. If we would account for the salinity-dependence of evaporation, stratification would be weaker than now found for a given combination of the other controlling parameters (Figure 4.3). Interestingly, below halite saturation this would result in lower surface salinity, thus increasing evaporation again.

We impose a constant convective flux (w), while in reality this depends on the density in the DWF-area relative to the density of the deep water. A larger density difference (i.e., larger salinity difference) would correspond to a larger w. Therefore, when both the DWF-box and deep box are close to halite saturation, a very low q would be the result, which would continue to decrease with time, making halite rain the dominant supplier of salt to the deep basin. In contrast, if the deep basin has a much lower salinity than the DWF-box (e.g., when c is low), stronger convection may be the case, which would re-distribute salt and in the extreme case even stop halite rain. This complex feedback loop again illustrates that a basin at halite saturation behaves very differently from the present Mediterranean.

If diffusivity (κ) would decrease with increasing stratification, the result would be to further increase stratification, demonstrating a positive feedback loop (compare Figure 4.4 with 4.5). This would hold true up to the moment that diffusivity is so small that mixing is effectively turned off (compare supplementary Figures 4.14C and G with 4.14D and H).

Consequences of the simple evaporite precipitation model

Warren (2016) describes that if marine water rises to a salt concentration of $\sim 40-60$ g/l, carbonates will be precipitated, followed by sulfates at $\sim 130 - 160$ g/l (e.g., gypsum, $CaSO_4$) and chlorides at $\sim 340 - 360$ g/l (e.g., halite, $NaCl$). Ideally, for each ionic salt pair a crystallization threshold would have to be introduced in the model. Whereas Topper and Meijer (2013) treated gypsum and halite separately, we only consider the formation of halite. An inclusion of a gypsum threshold in our model might lead to a slower increase in salinity than predicted now (from $\sim 130-160$ g/l onwards). As this would impact the DWF-box first, it might take the deep and surface slightly longer to reach this threshold. Once the threshold is reached by all boxes, no drastic additional effect is expected. Regarding the halite threshold, if salinity were allowed to rise beyond 350 g/l, the $Deep$ or DWF-box would not force the system to a steady state as sharply as shown. This might allow the surface salinity to increase to higher values than predicted; however, also the other boxes will have higher salinities, which might balance and cause no significant effect on the stratification behaviour. Na^+ and Cl^- are by far the most prominent ions dissolved in marine water. Therefore, density is prominently dependent on dissolved halite. We argue that as a first pass our evaporite precipitation model is a fair approximation.

Limitations imposed by model geometry

The fact that the surface layer (outside the DWF-region) is represented by a single salinity is a simplification. In reality the salinity ranges from the Atlantic value (36 g/l) in the west, to a much elevated salinity adjacent to the DWF-box. This lateral variation would imply lateral variation in vertical stratification and could affect the strength of the exchange and the salinity in the DWF-box.

Representing the water column with only two layers is another imposed simplification. Again, the calculated mean salinities are likely to be more variable in reality. This implies that deep brines could have formed at even less extreme parameter values than found now. This representation could be improved by either adding more layers or by implementing the 1D advection-diffusion equation (e.g., Wåhlin and Cenedese, 2006). Although this would increase the vertical resolution, also other processes would need to be considered in greater detail. For example the settling depth of convecting water would need to be parameterised.

4.5 Conclusions

Our model analysis allows us to gain the first physics-based insight into the factors that determine the extent of water stratification of the Mediterranean Sea during the Messinian Salinity Crisis. Investigating the box model in the parameter space relevant for the Messinian Mediterranean, we conclude that a stratified water column may well have occurred, if the rate of deep-water formation was low while the area across which this happened was relatively large (both in comparison to the present day). In this case, synchronous formation of gypsum and halite could have occurred at different vertical levels within the basin. Halite sedimentation rate would be lower in the stratified case compared to a mixed basin, which would be in disagreement with the duration assigned to the halite in the stratigraphic consensus model of the MSC (Roveri et al., 2014a).

Chapter 4 — Supplementary Figures

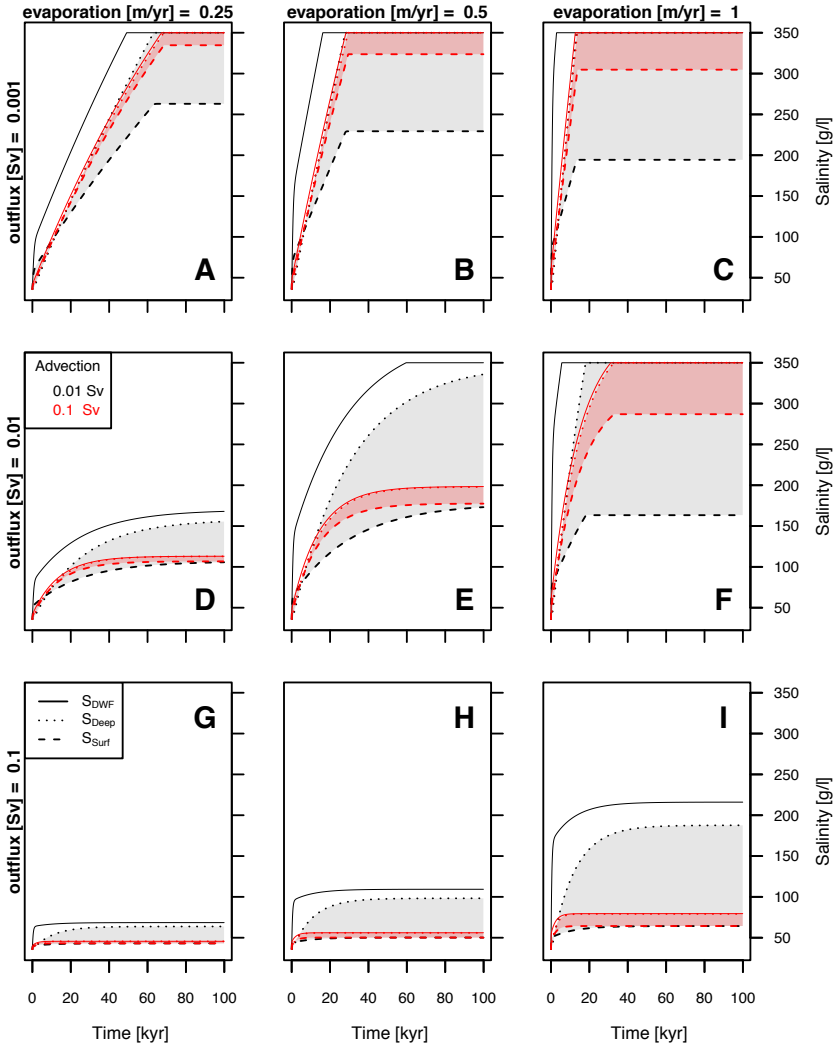

Figure 4.10 Experiments presented are of an equal setup to the ones shown in Figures 4.4 and 4.5. However, the diffusivity is set to $\kappa = 10^{-6}\ m^2/s$. In order to achieve a certain stratification, a lower diffusivity allows for stronger exchange and circulation.

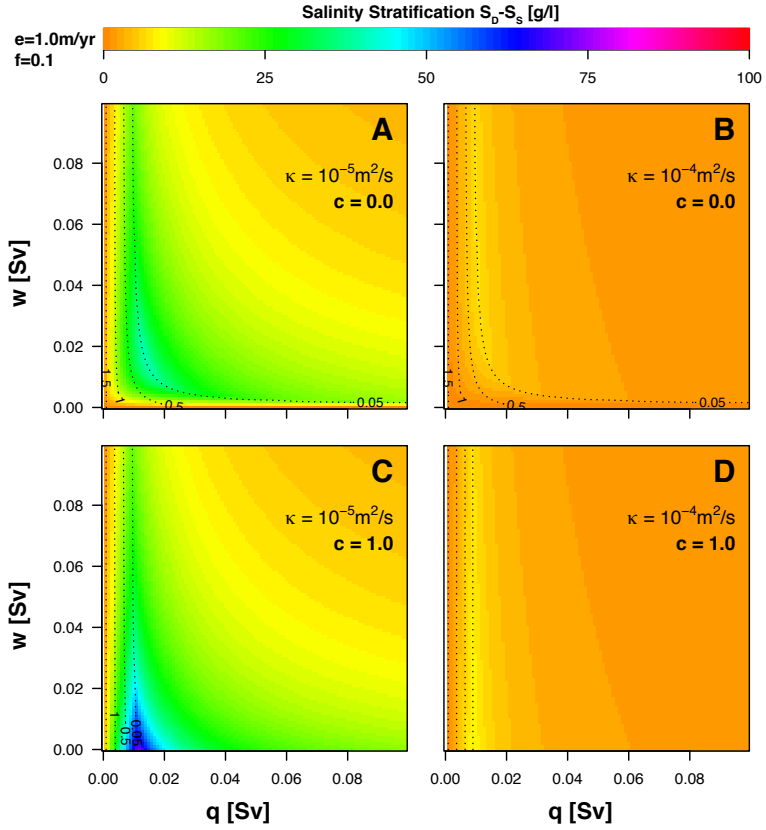

Figure 4.11 Identical to Figure 4.9, however for $f = 0.1$. It shows that a change in the f-parameter produces a similar behaviour in stratification response to the other parameters. However, for a lower f, the magnitude of degree of stratification is reduced. Please note that a different color-scale is used.

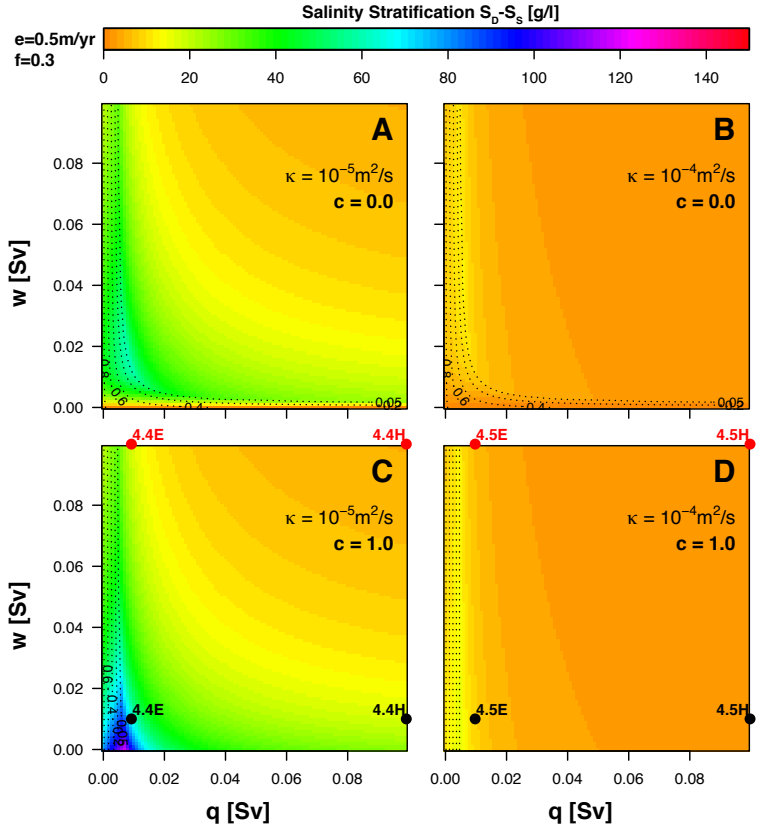

Figure 4.12 Identical to Figure 4.9, however for $e = 0.5\ m/yr$. It shows that a change in evaporation produces a similar behaviour in stratification response to the other parameters. However, for a lower e, the magnitude of degree of stratification is reduced. Please note that a different color-scale is used.

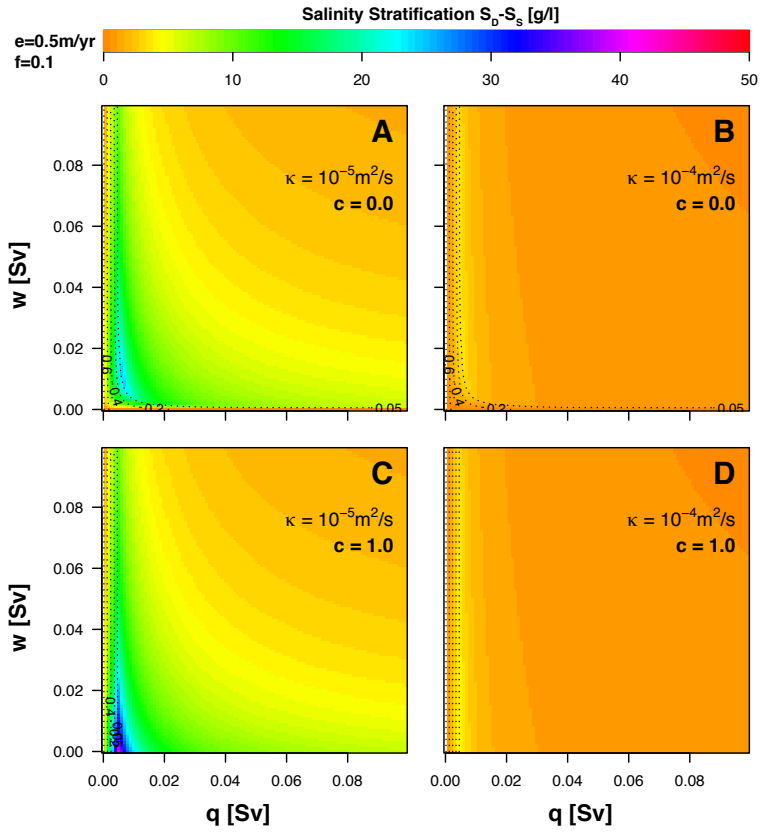

Figure 4.13 Identical to Figure 4.9, however for $f = 0.1$ and $e = 0.5\ m/yr$. Therefore also identical to Figure 4.11, however for $e = 0.5\ m/yr$ and identical to Figure 4.12, however for $f = 0.1$. The integrated effect, demonstrated by Figures 4.11 and 4.12, leads to further reduced stratification. Please note that a different color-scale is used.

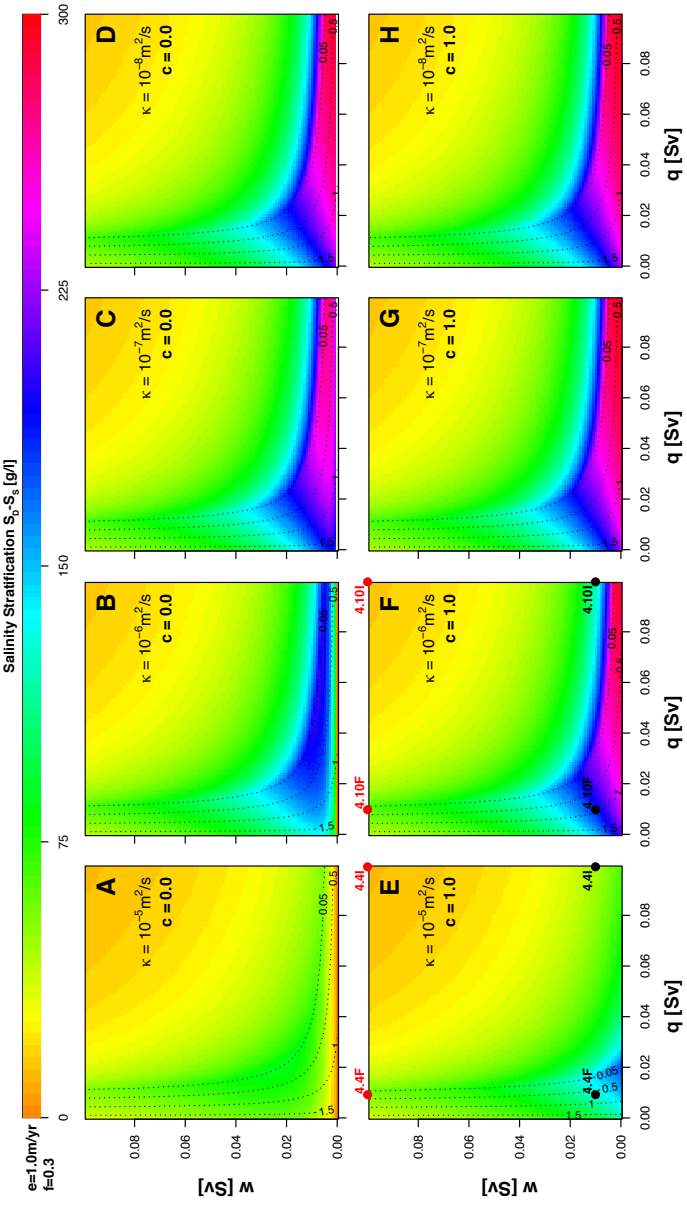

Figure 4.14 Panels A and E are identical to panels A and C in Figure 4.9. Panels B/F, C/G and D/H are the same experiments with different values of the diffusivity, $\kappa = 10^{-6}\ m^2/s$, $\kappa = 10^{-7}\ m^2/s$, $\kappa = 10^{-8}\ m^2/s$, respectively. Comparing panels with $\kappa = 10^{-5}\ m^2/s$ to $\kappa = 10^{-6}\ m^2/s$ shows in order to achieve a certain stratification, lower mixing than present today would allow for stronger exchange and circulation. If mixing is reduced further (C/G and D/H), not many changes are observed, because the mixing is effectively not existent. Red and Black dots on panel E and F link to individual experiments presented on Figure 4.4 and 4.10.

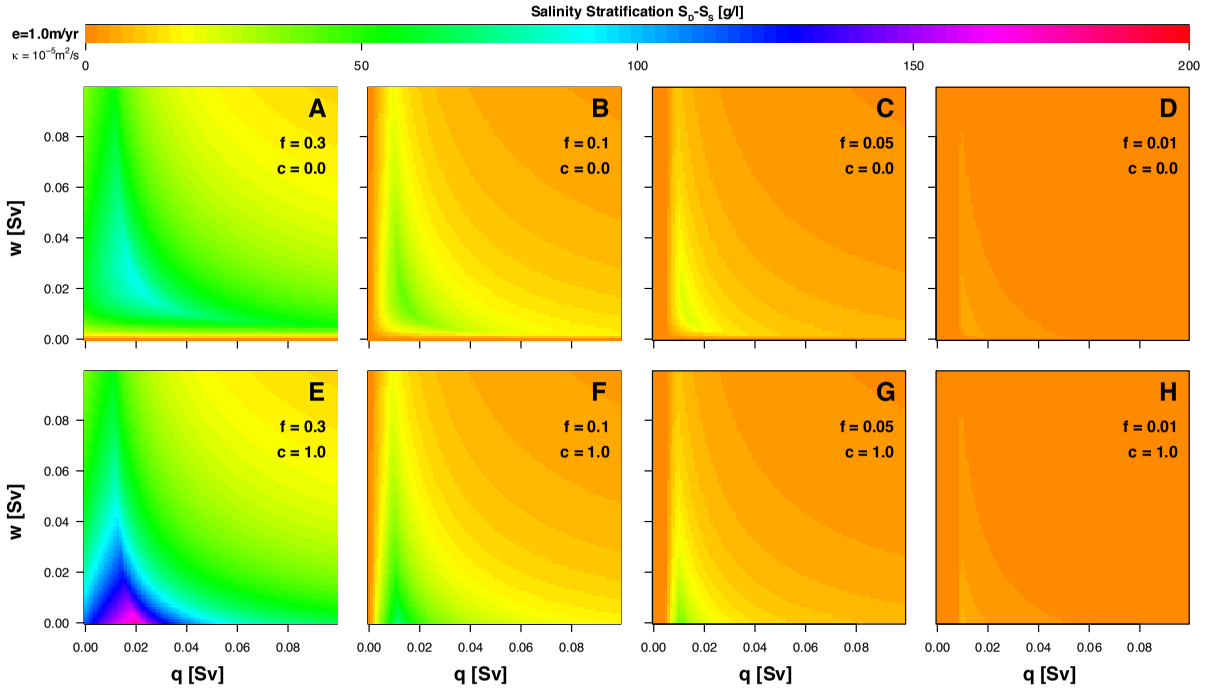

Figure 4.15 Panels A and E are identical to panels A and C in Figure 4.9. Panels B and F are identical to panels A and C in Figure 4.11. Panels C/G and D/H are the same experiments with different size for the DWF-region, $f = 0.05$ and $f = 0.01$, respectively. Lower f-values will cause less stratification, also because the surface salinity is greater. If the diffusivity were reduced further (until $\sim 10^{-7}\ m^2/s$), stronger stratification could be achieved.

References

Aharon, P., S. L. Goldstein, C. W. Wheeler and G. Jacobson (1993), Sea-level events in the South Pacific linked with the Messinian salinity crisis. Geology 21, 771–775.

Anati, D. A. (1997), The hydrography of a hypersaline lake. Oxford monographs on geology and geophysics 36, 89–103.

Anati, D. A., G. Assaf and R. Thompson (1977), Laboratory models of sea straits. Journal of Fluid Mechanics 81, 341–351.

Armi, L. and D. Farmer (1987), A generalization of the concept of maximal exchange in a strait. Journal of Geophysical Research 92, 14679–14680.

Ashley, G. M. et al. (1990), Classification of large-scale subaqueous bedforms: a new look at an old problem-SEPM bedforms and bedding structures. Journal of Sedimentary Petrology 60, 160–172.

Assaf, G. and A. Hecht (1974), Sea straits: a dynamical model. In: Deep Sea Research and Oceanographic Abstracts, vol. 21, Elsevier, 947–958.

Bahr, A., S. Kaboth, F. Jiménez-Espejo, F. Sierro, A. Voelker, L. Lourens, U. Röhl, G. Reichart, C. Escutia, F. Hernández-Molina et al. (2015), Persistent monsoonal forcing of Mediterranean Outflow Water dynamics during the late Pleistocene. Geology 43, 951–954.

Béranger, K., Y. Drillet, M.-N. Houssais, P. Testor, R. Bourdallé-Badie, B. Alhammoud, A. Bozec, L. Mortier, P. Bouruet-Aubertot and M. Crépon (2010), Impact of the spatial distribution of the atmospheric forcing on water mass formation in the Mediterranean Sea. Journal of Geophysical Research: Oceans 115, doi:10.1029/2009JC005648.

Betzler, C., J. C. Braga, J. M. Martín, I. M. Sánchez-Almazo and S. Lindhorst (2006), Closure of a seaway: stratigraphic record and facies (Guadix basin, Southern Spain). International Journal of Earth Sciences 95, 903–910.

Blanc, P.-L. (2000), Of sills and straits: a quantitative assessment of the Messinian Salinity Crisis. Deep Sea Research Part I: Oceanographic Research Papers 47, 1429–1460.

Blanc, P.-L. (2002), The opening of the Plio-Quaternary Gibraltar Strait: assessing the size of a cataclysm. Geodinamica Acta 15, 303–317.

Boguchwal, L. A. and J. B. Southard (1990), Bed configurations in steady unidirectional water flows. Part 1. Scale model study using fine sands. Journal of Sedimentary Petrology 60, 649–657.

Bosmans, J., S. Drijfhout, E. Tuenter, F. Hilgen, L. J. Lourens and E. Rohling (2015a), Precession and obliquity forcing of the freshwater budget over the Mediterranean. Quaternary Science Reviews 123, 16–30.

Bosmans, J., F. Hilgen, E. Tuenter and L. Lourens (2015b), Obliquity forcing of low-latitude climate. Climate of the Past 11, 221–241.

Bowman, S. (2012), A comprehensive review of the MSC facies and their origins in the offshore Sirt Basin, Libya. Petroleum Geoscience 18, 457–469.

Bradshaw, C., D. Lunt, R. Flecker, U. Salzmann, M. Pound, A. Haywood and J. Eronen (2012), The relative roles of CO2 and palaeogeography in determining Late Miocene climate: results from a terrestrial model-data comparison. Climate of the Past 8, 715–786.

Braga, J. and J. Martín (1996), Geometries of reef advance in response to relative sea-level changes in a Messinian (uppermost Miocene) fringing reef (Cariatiz reef, Sorbas Basin, SE Spain). Sedimentary Geology 107, 61–81.

Braga, J. C., J. M. Martín, R. Riding, J. Aguirre, I. M. Sánchez-Almazo and J. Dinarès-Turell (2006), Testing models for the Messinian Salinity Crisis: the Messinian record in Almería, SE Spain. Sedimentary Geology 188, 131–154.

Bryden, H. and H. Stommel (1984), Limiting processes that determine basic features of the circulation in the Mediterranean Sea. Oceanologica Acta 7, 289–296.

Bryden, H., K. Schroeder, M. Borghini, A. Vetrano and S. Sparnocchia (2014), The Mediterranean Sea: Temporal Variability and Spatial Patterns, chap. Mixing in the deep waters of the western Mediterranean. Wiley Online Library, 51–58.

Bryden, H. L., J. Candela and T. H. Kinder (1994), Exchange through the Strait of Gibraltar. Progress in Oceanography 33, 201–248.

Bush, A. B. (1997), Numerical simulation of the Cretaceous Tethys circumglobal current. Science 275, 807–810.

Capella, W. (2017), Gateway to a vanishing ocean: the tectono-sedimentary evolution of the Rifian Corridor (Morocco) and the late Miocene isolation of the Mediterranean, vol. 128. Utrecht Studies in Earth Sciences, Utrecht Univeristy.

Capella, W., F. Hernández-Molina, R. Flecker, F. Hilgen, M. Hssain, T. Kouwenhoven, M. van Oorschot, F. Sierro, D. Stow, J. Trabucho-Alexandre et al. (2017a), Sandy contourite drift in the late Miocene Rifian Corridor (Morocco): Reconstruction of depositional environments in a foreland-basin seaway. Sedimentary Geology , doi:10.1016/j.tecto.2016.09.028.

Capella, W., L. Matenco, E. Dmitrieva, W. M. Roest, S. Hessels, M. Hssain, A. Chakor-Alami, F. J. Sierro and W. Krijgsman (2017b), Thick-skinned tectonics closing the Rifian Corridor. Tectonophysics , doi:10.1016/j.tecto.2016.09.028.

Casford, J., E. Rohling, R. Abu-Zied, C. Fontanier, F. Jorissen, M. Leng, G. Schmiedl and J. Thomson (2003), A dynamic concept for eastern Mediterranean circulation and oxygenation during sapropel formation. Palaeogeography, Palaeoclimatology, Palaeoecology 190, 103–119.

Chumakov, I. (1973), Pliocene and Pleistocene deposits of the Nile valley in Nubia and upper Egypt. Initial Reports of the Deep Sea Drilling Project 13, 1242–1243.

Clauzon, G. (1973), The eustatic hypothesis and the pre-Pliocene cutting of the Rhône valley. Initial Reports of the Deep Sea Drilling Project 13, 1251–1256.

Colin, C., G. Siani, Z. Liu, D. Blamart, C. Skonieczny, Y. Zhao, A. Bory, N. Frank, S. Duchamp-Alphonse, F. Thil et al. (2014), Late Miocene to early Pliocene climate variability off NW Africa (ODP Site 659). Palaeogeography, Palaeoclimatology, Palaeoecology 401, 81–95.

Corbí, H., C. Lancis, F. García-García, J.-A. Pina, J. M. Soria, J. E. Tent-Manclús and C. Viseras (2012), Updating the marine biostratigraphy of the Granada Basin (central Betic Cordillera). Insight for the Late Miocene palaeogeographic evolution of the Atlantic–Mediterranean seaway. Geobios 45, 249–263.

Coulthard, T. J., J. A. Ramirez, N. Barton, M. Rogerson and T. Brücher (2013), Were rivers flowing across the Sahara during the last interglacial? Implications for human migration through Africa. PloS one 8, e74834.

Curry, R., B. Dickson and I. Yashayaev (2003), A change in the freshwater balance of the Atlantic Ocean over the past four decades. Nature 426, 826–829.

Dabang, J., W. Huijun and L. Xianmei (2005), Evaluation of East Asian climatology as simulated by seven coupled models. Advances in Atmospheric Sciences 22, 479–495.

Dalziel, S. B. (1992), Maximal exchange in channels with nonrectangular cross sections. Journal of Physical Oceanography 22, 1188–1206.

de la Vara, A. and P. Meijer (2016), Response of Mediterranean circulation to Miocene shoaling and closure of the Indian Gateway: A model study. Palaeogeography, Palaeoclimatology, Palaeoecology 442, 96–109.

de la Vara, A., R. P. Topper, P. T. Meijer and T. J. Kouwenhoven (2015), Water exchange through the Betic and Rifian corridors prior to the Messinian Salinity Crisis: A model study. Paleoceanography 30, 548–557.

de la Vara, A., C. G. van Baak, A. Marzocchi, A. Grothe and P. T. Meijer (2016), Quantitative analysis of Paratethys sea level change during the Messinian Salinity Crisis. Marine Geology 379, 39–51.

de Lange, G. J. and W. Krijgsman (2010), Messinian salinity crisis: a novel unifying shallow gypsum/deep dolomite formation mechanism. Marine Geology 275, 273–277.

D'Ortenzio, F., D. Iudicone, C. de Boyer Montegut, P. Testor, D. Antoine, S. Marullo, R. Santoleri and G. Madec (2005), Seasonal variability of the mixed layer depth in the Mediterranean Sea as derived from in situ profiles. Geophysical Research Letters 32, doi:10.1029/2005GL022463.

Duggen, S., K. Hoernle, P. Van Den Bogaard, L. Rüpke and J. P. Morgan (2003), Deep roots of the Messinian salinity crisis. Nature 422, 602–606.

Evans, N. P., A. V. Turchyn, F. Gázquez, T. R. Bontognali, H. J. Chapman and D. A. Hodell (2015), Coupled measurements of δ18O and δD of hydration water and salinity of fluid inclusions in gypsum from the Messinian Yesares Member, Sorbas Basin (SE Spain). Earth and Planetary Science Letters 430, 499–510.

Farmer, D. and L. Armi (1986), Maximal two-layer exchange over a sill and through the combination of a sill and contraction with barotropic flow. Journal of Fluid Mechanics 164, 53–76.

Farmer, D. M. and L. Armi (1988), The flow of Atlantic water through the Strait of Gibraltar, vol. 21. Elsevier.

Farr, T. G., P. A. Rosen, E. Caro, R. Crippen, R. Duren, S. Hensley, M. Kobrick, M. Paller, E. Rodriguez, L. Roth et al. (2007), The shuttle radar topography mission. Reviews of Geophysics 45, doi:10.1029/2005RG000183.

Feistel, R. (2008), A Gibbs function for seawater thermodynamics for -6 to 80^oC and salinity up to $120g/kg$. Deep Sea Research Part I: Oceanographic Research Papers 55, 1639–1671.

Feng, Y. E., A. Yankelzon, J. Steinberg and M. Reshef (2016), Lithology and characteristics of the Messinian evaporite sequence of the deep Levant Basin, eastern Mediterranean. Marine Geology 376, 118–131.

Flecker, R., S. De Villiers and R. Ellam (2002), Modelling the effect of evaporation on the salinity — 87Sr/86Sr relationship in modern and ancient marginal-marine systems: the Mediterranean Messinian Salinity Crisis. Earth and Planetary Science Letters 203, 221–233.

Flecker, R., W. Krijgsman, W. Capella, C. de Castro Martíns, E. Dmitrieva, J. P. Mayser, A. Marzocchi, S. Modestu, D. Ochoa, D. Simon, M. Tulbure, B. van den Berg, M. van der Schee, G. de Lange, R. Ellam, R. Govers, M. Gutjahr, F. Hilgen, T. Kouwenhoven, P. Meijer, F. J. Sierro, N. Bachiri, N. Barhoun, A. Chakor-Alami, B. Chacon, J. A. Flores, J. Gregory, J. Howard, D. Lunt, M. Ochoa, R. Pancost, S. Vincent and M. Z. Yousfi (2015), Evolution of the Late Miocene Mediterranean–Atlantic gateways and their impact on regional and global environmental change. Earth-Science Reviews 150, 365–392.

Flower, B. P. and J. P. Kennett (1994), The middle Miocene climatic transition: East Antarctic ice sheet development, deep ocean circulation and global carbon cycling. Palaeogeography, palaeoclimatology, palaeoecology 108, 537–555.

Garcia-Castellanos, D., F. Estrada, I. Jiménez-Munt, C. Gorini, M. Fernández, J. Vergés and R. De Vicente (2009), Catastrophic flood of the Mediterranean after the Messinian salinity crisis. Nature 462, 778–781.

García-Veigas, J., D. I. Cendón, L. Rosell, F. Ortí, J. Torres Ruiz, J. M. Martín and E. Sanz (2013), Salt deposition and brine evolution in the Granada Basin (Late Tortonian, SE Spain). Palaeogeography, Palaeoclimatology, Palaeoecology 369, 452–465.

García-Veigas, J., L. Rosell, D. I. Cendón, L. Gibert, J. M. Martín, J. Torres-Ruiz and F. Ortí (2015), Large celestine orebodies formed by early-diagenetic replacement of gypsified stromatolites (Upper Miocene, Montevive–Escúzar deposit, Granada Basin, Spain). Ore Geology Reviews 64, 187–199.

Garrett, C. (2004), Frictional processes in straits. Deep Sea Research Part II: Topical Studies in Oceanography 51, 393–410.

Ghoneim, E., M. Benedetti and F. El-Baz (2012), An integrated remote sensing and GIS analysis of the Kufrah Paleoriver, Eastern Sahara. Geomorphology 139, 242–257.

Gladstone, R., R. Flecker, P. Valdes, D. Lunt and P. Markwick (2007), The Mediterranean hydrologic budget from a Late Miocene global climate simulation. Palaeogeography, Palaeoclimatology, Palaeoecology 251, 254–267.

Govers, R. (2009), Choking the Mediterranean to dehydration: the Messinian salinity crisis. Geology 37, 167–170.

Grant, K., R. Grimm, U. Mikolajewicz, G. Marino, M. Ziegler and E. Rohling (2016), The timing of Mediterranean sapropel deposition relative to insolation, sea-level and African monsoon changes. Quaternary Science Reviews 140, 125–141.

Griffin, D. L. (2002), Aridity and humidity: two aspects of the late Miocene climate of North Africa and the Mediterranean. Palaeogeography, Palaeoclimatology, Palaeoecology 182, 65–91.

Griffin, D. L. (2006), The late Neogene Sahabi rivers of the Sahara and their climatic and environmental implications for the Chad Basin. Journal of the Geological Society 163, 905–921.

Grimm, R., E. Maier-Reimer, U. Mikolajewicz, G. Schmiedl, K. Müller-Navarra, F. Adloff, K. M. Grant, M. Ziegler, L. J. Lourens and K.-C. Emeis (2015), Late glacial initiation of Holocene eastern Mediterranean sapropel formation. Nature communications 6, doi:10.1038/ncomms8099.

Grothe, A. (2016), The Messinian Salinity Crisis: a Paratethyan perspective, vol. 107. Utrecht Studies in Earth Sciences, Utrecht Univeristy.

Gu, L. and G. A. Lawrence (2001), Frictional exchange flow through a ship canal. In: Proceedings of the congress-international association for hydraulic research, 433–438.

Gu, L. and G. A. Lawrence (2005), Analytical solution for maximal frictional two-layer exchange flow. Journal of Fluid Mechanics 543, 1–17.

Harzhauser, M. and W. E. Piller (2007), Benchmark data of a changing seapalaeogeography, palaeobiogeography and events in the Central Paratethys during the Miocene. Palaeogeography, Palaeoclimatology, Palaeoecology 253, 8–31.

Hecht, M., W. Holland, V. Artale and N. Pinardi (1997), North Atlantic model sensitivity to Mediterranean waters. Assessing Climate Change: Results from the Model Evaluation Consortium for Climate Assessment 169–191.

Hennekam, R. (2015), High-frequency climate variability in the late Quaternary eastern Mediterranean: Associations of Nile discharge and basin overturning circulation dynamics, vol. 078. Utrecht Studies in Earth Sciences, Utrecht Univeristy.

Hernández-Molina, F. J., D. A. Stow, C. A. Alvarez-Zarikian, G. Acton, A. Bahr, B. Balestra, E. Ducassou, R. Flood, J.-A. Flores, S. Furota et al. (2014), Onset of Mediterranean outflow into the North Atlantic. Science 344, 1244–1250.

Herrmann, M., J. Bouffard and K. Béranger (2009), Monitoring open-ocean deep convection from space. Geophysical Research Letters 36, doi:10.1029/2008GL036422.

Hilgen, F. (1991), Extension of the astronomically calibrated (polarity) time scale to the Miocene/Pliocene boundary. Earth and planetary science letters 107, 349–368.

Hilgen, F., K. Kuiper, W. Krijgsman, E. Snel and E. van der Laan (2007), Astronomical tuning as the basis for high resolution chronostratigraphy: the intricate history of the Messinian Salinity Crisis. Stratigraphy 4, 231–238.

Hilgen, F. J. and W. Krijgsman (1999), Cyclostratigraphy and astrochronology of the Tripoli diatomite formation (pre-evaporite Messinian, Sicily, Italy). Terra Nova-Oxford 11, 16–22.

Hinsbergen, D. J., R. L. Vissers and W. Spakman (2014), Origin and consequences of western Mediterranean subduction, rollback, and slab segmentation. Tectonics 33, 393–419.

Hodell, D. A., J. H. Curtis, F. J. Sierro and M. E. Raymo (2001), Correlation of late Miocene to early Pliocene sequences between the Mediterranean and North Atlantic. Paleoceanography 16, 164–178.

Hoffmann, D. L., M. Rogerson, C. Spötl, M. Luetscher, D. Vance, A. H. Osborne, N. M. Fello and G. E. Moseley (2016), Timing and causes of North African wet phases during the last glacial period and implications for modern human migration. Scientific reports 6, doi:10.1038/srep36367.

Hsü, K., W. Ryan, M. Cita et al. (1973), Late Miocene desiccation of the Mediterranean. Nature 242, 240–244.

Hughes, J., P. Valdes and R. Betts (2004), Dynamical properties of the TRIFFID dynamic global vegetation model. Met office, Hadley Centre Tech. Note 56, 23.

Hüsing, S., O. Oms, J. Agustí, M. Garcés, T. Kouwenhoven, W. Krijgsman and W.-J. Zachariasse (2010), On the late Miocene closure of the Mediterranean–Atlantic gateway through the Guadix basin (southern Spain). Palaeogeography, Palaeoclimatology, Palaeoecology 291, 167–179.

Ivanovic, R. F., R. Flecker, M. Gutjahr and P. J. Valdes (2013), First Nd isotope record of Mediterranean–Atlantic water exchange through the Moroccan Rifian Corridor during the Messinian Salinity Crisis. Earth and Planetary Science Letters 368, 163–174.

Ivanovic, R. F., P. J. Valdes, R. Flecker and M. Gutjahr (2014), Modelling global-scale climate impacts of the late Miocene Messinian Salinity Crisis. Climate of the Past 10, 607–622.

Ivey, G. (2002), Stratification and mixing in exchange flows in sea straits. In: 2nd meeting on the Physical Oceanography of Sea Straits, Villefranche. American Geophysical Union, Citeseer.

Jayne, S. R. (2005), Ocean Topography, Tides, Mixing, and the Earths Climate. In: OCEANS, 2005. Proceedings of MTS/IEEE, IEEE, 1–4.

Johns, W., F. Yao, D. Olson, S. Josey, J. Grist and D. Smeed (2003), Observations of seasonal exchange through the Straits of Hormuz and the inferred heat and freshwater budgets of the Persian Gulf. Journal of Geophysical Research: Oceans (1978–2012) 108, doi:10.1029/2003JC001881.

Johnson, H. L., D. P. Marshall and D. A. Sproson (2007), Reconciling theories of a mechanically driven meridional overturning circulation with thermohaline forcing and multiple equilibria. Climate Dynamics 29, 821–836.

Jolivet, L. and C. Faccenna (2000), Mediterranean extension and the Africa-Eurasia collision. Tectonics 19, 1095–1106.

Jolivet, L., R. Augier, C. Robin, J.-P. Suc and J. M. Rouchy (2006), Lithospheric-scale geodynamic context of the Messinian salinity crisis. Sedimentary geology 188, 9–33.

Kidd, R. B., M. B. Cita and W. B. Ryan (1978), Stratigraphy of eastern Mediterranean sapropel sequences recovered during DSDP Leg 42A and their paleoenvironmental significance. Initial Reports of the Deep Sea Drilling Project 42, 421–443.

Knudsen, M. (1900), Ein hydrographischer Lehrsatz. Annalen der Hydrographie und Maritimen Meteorologie 28, 316–320.

Kostaschuk, R. and P. Villard (1996), Flow and sediment transport over large subaqueous dunes: Fraser River, Canada. Sedimentology 43, 849–863.

Kouwenhoven, T., F. Hilgen and G. Van der Zwaan (2003), Late Tortonian–early Messinian stepwise disruption of the Mediterranean–Atlantic connections: constraints from benthic foraminiferal and geochemical data. Palaeogeography, Palaeoclimatology, Palaeoecology 198, 303–319.

Krijgsman, W. and P. T. Meijer (2008), Depositional environments of the Mediterranean Lower Evaporites of the Messinian salinity crisis: constraints from quantitative analyses. Marine Geology 253, 73–81.

Krijgsman, W., F. Hilgen, I. Raffi, F. Sierro and D. Wilsonk (1999a), Chronology, causes and progression of the Messinian salinity crisis. Nature 400, 652–655.

Krijgsman, W., C. Langereis, W. Zachariasse, M. Boccaletti, G. Moratti, R. Gelati, S. Iaccarino, G. Papani and G. Villa (1999b), Late Neogene evolution of the Taza–Guercif Basin (Rifian Corridor, Morocco) and implications for the Messinian salinity crisis. Marine Geology 153, 147–160.

Krijgsman, W., A. Fortuin, F. Hilgen and F. Sierro (2001), Astrochronology for the Messinian Sorbas basin (SE Spain) and orbital (precessional) forcing for evaporite cyclicity. Sedimentary Geology 140, 43–60.

Kuhlbrodt, T., A. Griesel, M. Montoya, A. Levermann, M. Hofmann and S. Rahmstorf (2007), On the driving processes of the Atlantic meridional overturning circulation. Reviews of Geophysics 45, doi:10.1029/2004RG000166.

Kuroda, J., F. J. Jiménez-Espejo, T. Nozaki, R. Gennari, S. Lugli, V. Manzi, M. Roveri, R. Flecker, F. J. Sierro, T. Yoshimura et al. (2016), Miocene to Pleistocene osmium isotopic records of the Mediterranean sediments. Paleoceanography 31, 148–166.

Kutzbach, J., G. Chen, H. Cheng, R. Edwards and Z. Liu (2014), Potential role of winter rainfall in explaining increased moisture in the Mediterranean and Middle East during periods of maximum orbitally-forced insolation seasonality. Climate dynamics 42, 1079–1095.

Laskar, J., P. Robutel, F. Joutel, M. Gastineau, A. Correia and B. Levrard (2004), A long-term numerical solution for the insolation quantities of the earth. Astronomy & Astrophysics 428, 261–285.

Lawrence, G. A. (1993), The hydraulics of steady two-layer flow over a fixed obstacle. Journal of Fluid Mechanics 254, 605–633.

Leeder, M. (1999), Sedimentology and sedimentary basins: from turbulence to tectonics. Wiley-Blackwell.

Li, L. Z. (2006), Atmospheric GCM response to an idealized anomaly of the Mediterranean sea surface temperature. Climate dynamics 27, 543–552.

Lofi, J., J. Déverchère, V. Gaullier, H. Gillet, C. Gorini, P. Guennoc, L. Loncke, A. Maillard, F. Sage, I. Thinon et al. (2011), Seismic atlas of the Messinian Salinity Crisis markers in the Mediterranean and Black Seas. Mémoire de la Société Géologique ns 179, 1–72.

Lofi, J., A. Maillard and A. Camerlenghi (2016), The MSC central Balearic depression: an undeformed analog for the MSC sicilian basin? In: COST-ANR MEDSALT SYMPOSIUM, 44.

Lolis, C., A. Bartzokas and B. Katsoulis (2002), Spatial and temporal 850 hPa air temperature and sea-surface temperature covariances in the Mediterranean region and their connection to atmospheric

circulation. International Journal of Climatology 22, 663–676.
Lourens, L. J., A. Antonarakou, F. Hilgen, A. Van Hoof, C. Vergnaud-Grazzini and W. Zachariasse (1996), Evaluation of the Plio-Pleistocene astronomical timescale. Paleoceanography 11, 391–413.
Lugli, S., V. Manzi and M. Roveri (2008), New facies interpretation of the Messinian evaporites in the Mediterranean. In: CIESM Workshop Monogr, vol. 33, 67–72.
Lugli, S., V. Manzi, M. Roveri and C. Schreiber (2010), The Primary Lower Gypsum in the Mediterranean: a new facies interpretation for the first stage of the Messinian salinity crisis. Palaeogeography, Palaeoclimatology, Palaeoecology 297, 83–99.
Madof, A. and S. Connell (2016), Connell, Seismic stratigraphy of eastern Mediterranean Messinian evaporites. In: COST-ANR MEDSALT SYMPOSIUM, 57–58.
Maheras, P., E. Xoplaki, T. Davies, J. Martin-Vide, M. Bariendos and M. J. Alcoforado (1999), Warm and cold monthly anomalies across the Mediterranean basin and their relationship with circulation; 1860–1990. International Journal of Climatology 19, 1697–1715.
Maillard, A., O. Driussi, J. Lofi, A. Briais, F. Chanier, C. Huebscher and V. Gaullier (2014), Record of the Messinian Salinity Crisis in the SW Mallorca area (Balearic Promontory, Spain). Marine Geology 357, 304–320.
Malanotte-Rizzoli, P., B. B. Manca, M. R. d'Alcalà, A. Theocharis, A. Bergamasco, D. Bregant, G. Budillon, G. Civitarese, D. Georgopoulos, A. Michelato et al. (1997), A synthesis of the Ionian Sea hydrography, circulation and water mass pathways during POEM-Phase I. Progress in Oceanography 39, 153–204.
Manzi, V., R. Gennari, F. Hilgen, W. Krijgsman, S. Lugli, M. Roveri and F. J. Sierro (2013), Age refinement of the Messinian salinity crisis onset in the Mediterranean. Terra Nova 25, 315–322.
Mariotti, A., M. V. Struglia, N. Zeng and K. Lau (2002), The hydrological cycle in the Mediterranean region and implications for the water budget of the Mediterranean Sea. Journal of climate 15, 1674–1690.
Markwick, P. (2007), Deep-time perspectives on climate change: marrying the signal from computer models and biological proxies, chap. The palaeogeographic and palaeoclimatic significance of climate proxies for data-model comparisons. Micropalaeontol. Soc. Spec. Publ. London, 51–58.
Martín, J., M. Ortega-Huertas and J. Torres-Ruiz (1984), Genesis and evolution of strontium deposits of the Granada Basin (southeastern Spain): evidence of diagenetic replacement of a stromatolite belt. Sedimentary geology 39, 281–298.
Martín, J. M., J. C. Braga and C. Betzler (2001), The Messinian Guadalhorce corridor: the last northern, Atlantic–Mediterranean gateway. Terra Nova 13, 418–424.
Martín, J. M., J. C. Braga, J. Aguirre and Á. Puga-Bernabéu (2009), History and evolution of the North-Betic Strait (Prebetic Zone, Betic Cordillera): a narrow, early Tortonian, tidal-dominated, Atlantic–Mediterranean marine passage. Sedimentary Geology 216, 80–90.
Martín, J. M., Á. Puga-Bernabéu, J. Aguirre and J. C. Braga (2014), Miocene Atlantic-Mediterranean seaways in the Betic Cordillera (Southern Spain) 27, 175–186.
Marzeion, B. and A. Levermann (2009), Stratification-dependent mixing may increase sensitivity of a wind-driven atlantic overturning to surface freshwater flux. Geophysical Research Letters 36, doi:10.1029/2009GL039947.
Marzocchi, A., D. Lunt, R. Flecker, C. Bradshaw, A. Farnsworth and F. Hilgen (2015), Orbital control on late Miocene climate and the North African monsoon: insight from an ensemble of sub-precessional simulations. Climate of the Past 11, 1271.
Marzocchi, A., R. Flecker, C. G. van Baak, D. J. Lunt and W. Krijgsman (2016), Mediterranean outflow pump: An alternative mechanism for the Lago-mare and the end of the Messinian Salinity Crisis. Geology 44, 523–526.
Matthiesen, S. and K. Haines (2003), A hydraulic box model study of the Mediterranean response to postglacial sea-level rise. Paleoceanography 18, doi:10.1029/2003PA000880.
Mayser, J. P., R. Flecker, A. Marzocchi, T. J. Kouwenhoven, D. J. Lunt and R. D. Pancost (2017), Precession driven changes in terrestrial organic matter input to the Eastern Mediterranean leading up to the Messinian Salinity Crisis. Earth and Planetary Science Letters 462, 199–211.
Meijer, P. (2006), A box model of the blocked-outflow scenario for the Messinian Salinity Crisis. Earth and Planetary Science Letters 248, 486–494.
Meijer, P. and W. Krijgsman (2005), A quantitative analysis of the desiccation and re-filling of the Mediterranean during the Messinian Salinity Crisis. Earth and Planetary Science Letters 240, 510–520.
Meijer, P. T. (2012), Hydraulic theory of sea straits applied to the onset of the messinian salinity crisis. Marine Geology 326, 131–139.
Meilijson, A., J. Steinberg, O. Bialik, P. Illner, F. Hilgen and Y. Makovsky (2016), Integrated stratigraphy and chronology of Messinian evaporites from the Levant basin in the deep eastern Mediterranea. In: EGU General Assembly Conference Abstracts, vol. 18, 9788.
Mikolajewicz, U., E. Maier-Reimer, T. J. Crowley and K.-Y. Kim (1993), Effect of Drake and Panamanian gateways on the circulation of an ocean model. Paleoceanography 8, 409–426.
Modestou, S., D. Simon, M. Gutjahr, A. Marzocchi, T. J. Kouwenhoven, R. M. Ellam and R. Flecker (2017), Precessional variability of 87Sr/86Sr in the late Miocene Sorbas Basin: an interdisciplinary study of drivers of inter-basin exchange. Paleoceanography, doi:10.1002/2016PA003061 .
Montadert, L., J. Sancho, J. Fail, J. Debyser and E. Winnock (1970), De l'âge tertiaire de la série salifère responsable des structures diapiriques en Méditerranée Occidentale (Nord-Est des Baléares). CR Acad.

Sci. Paris 271, 812–815.
Munk, W. H. (1966), Abyssal recipes. In: Deep Sea Research and Oceanographic Abstracts, vol. 13, Elsevier, 707–730.
Murphy, L., D. Kirk-Davidoff, N. Mahowald and B. Otto-Bliesner (2009), A numerical study of the climate response to lowered Mediterranean Sea level during the Messinian Salinity Crisis. Palaeogeography, Palaeoclimatology, Palaeoecology 279, 41–59.
Myers, D. and C. Bonython (1958), The theory of recovering salt from sea-water by solar evaporation. Journal of Chemical Technology and Biotechnology 8, 207–219.
Natalicchio, M., F. D. Pierre, S. Lugli, T. K. Lowenstein, S. J. Feiner, S. Ferrando, V. Manzi, M. Roveri and P. Clari (2014), Did Late Miocene (Messinian) gypsum precipitate from evaporated marine brines? Insights from the Piedmont Basin (Italy). Geology 42, 179–182.
Nielsen, J. N. (1912), Report on the Danish Oceanographical Expeditions 1908-1910 to the Mediterranean and Adjacent Seas, chap. Hydrography of the Mediterranean and adjacent waters. 77–192, J. Schmidt (Ed).
Nihoul, J. C. (1982), Hydrodynamics of Semi-Enclosed Seas., chap. Oceanography of semi-enclosed seas. Elsevier, 1–12.
Ochoa, D., F. J. Sierro, J. Lofi, A. Maillard, J.-A. Flores and M. Suárez (2015), Synchronous onset of the Messinian evaporite precipitation: First Mediterranean offshore evidence. Earth and Planetary Science Letters 427, 112–124.
Officer, C. et al. (1976), Physical oceanography of estuaries (and associated coastal waters). John Wiley & Sons, Inc.
Ohneiser, C., F. Florindo, P. Stocchi, A. P. Roberts, R. M. DeConto and D. Pollard (2015), Antarctic glacio-eustatic contributions to late Miocene Mediterranean desiccation and reflooding. Nature communications 6, doi:10.1038/ncomms9765.
Özsoy, E., D. Di Iorio, M. C. Gregg and J. O. Backhaus (2001), Mixing in the bosphorus strait and the black sea continental shelf: observations and a model of the dense water outflow. Journal of Marine Systems 31, 99–135.
Paillou, P., S. Tooth and S. Lopez (2012), The Kufrah paleodrainage system in Libya: A past connection to the Mediterranean Sea? Comptes Rendus Geoscience 344, 406–414.
Pausata, F. S., G. Messori and Q. Zhang (2016), Impacts of dust reduction on the northward expansion of the African monsoon during the Green Sahara period. Earth and Planetary Science Letters 434, 298–307.
Pérez-Asensio, J., J. Aguirre, G. Schmiedl and J. Civis (2012), Impact of restriction of the Atlantic-Mediterranean gateway on the Mediterranean Outflow Water and eastern Atlantic circulation during the Messinian. Paleoceanography 27, doi:10.1029/2012PA002309.
Pinardi, N. and E. Masetti (2000), Variability of the large scale general circulation of the Mediterranean Sea from observations and modelling: a review. Palaeogeography, Palaeoclimatology, Palaeoecology 158, 153–173.
Platt, J., W. M. Behr, K. Johanesen and J. R. Williams (2013), The Betic-Rif Arc and Its Orogenic Hinterland: A Review. Annual Review of Earth and Planetary Sciences 41, 313–357.
Pope, J. O., M. Collins, A. M. Haywood, H. J. Dowsett, S. J. Hunter, D. J. Lunt, S. J. Pickering and M. J. Pound (2011), Quantifying uncertainty in model predictions for the Pliocene (Plio-QUMP): initial results. Palaeogeography, Palaeoclimatology, Palaeoecology 309, 128–140.
Pratt, L. (1984), A time-dependent aspect of hydraulic control in straits. Journal of physical oceanography 14, 1414–1418.
Pratt, L. (1986), Hydraulic control of sill flow with bottom friction. J. Phys. Oceanogr 16, 1970–1980.
Pratt, L. and J. Whitehead (2007), Rotating hydraulics: Nonlinear topographic effects in the ocean and atmosphere, vol. 36. Springer.
Price, J. F. and M. O. Baringer (1994), Outflows and deep water production by marginal seas. Progress in Oceanography 33, 161–200.
Rahmstorf, S. (1998), Influence of Mediterranean outflow on climate. Eos, Transactions American Geophysical Union 79, 281–282.
Rahmstorf, S. (2002), Ocean circulation and climate during the past 120,000 years. Nature 419, 207–214.
Roether, W., B. B. Manca, B. Klein, D. Bregant et al. (1996), Recent changes in eastern Mediterranean deep waters. Science 271, 333.
Rogerson, M., E. Rohling, G. R. Bigg and J. Ramirez (2012), Paleoceanography of the Atlantic-Mediterranean exchange: Overview and first quantitative assessment of climatic forcing. Reviews of Geophysics 50, doi:10.1029/2011RG000376.
Rögl, F. (1999), Mediterranean and Paratethys. Facts and hypotheses of an Oligocene to Miocene paleogeography (short overview). Geologica carpathica 50, 339–349.
Rohling, E., R. Schiebel and M. Siddall (2008), Controls on Messinian lower evaporite cycles in the Mediterranean. Earth and Planetary Science Letters 275, 165–171.
Rohling, E., G. Marino and K. Grant (2015), Mediterranean climate and oceanography, and the periodic development of anoxic events (sapropels). Earth-Science Reviews 143, 62–97.
Rossignol-Strick, M. (1983), African monsoons, an immediate climate response to orbital insolation. Nature 304, 46–49.

Roveri, M., R. Flecker, W. Krijgsman, J. Lofi, S. Lugli, V. Manzi, F. J. Sierro, A. Bertini, A. Camerlenghi, G. De Lange et al. (2014a), The Messinian Salinity Crisis: Past and future of a great challenge for marine sciences. Marine Geology 352, 25–58.

Roveri, M., V. Manzi, A. Bergamasco, F. Falcieri, R. Gennari, S. Lugli and B. Schreiber (2014b), Dense shelf water cascading and Messinian canyons: a new scenario for the Mediterranean salinity crisis. American Journal of Science 314, 751–784.

Ruggieri, G. (1967), The Miocene and later evolution of the Mediterranean Sea. Aspects of Tethyan biogeography 7, 283–290.

Ryan, W., K. Hsü, M. Cita, P. Dumitrica, J. Lort, W. Maync, W. Nesteroff, G. Pautot, H. Stradner and F. Wezel (1973), Leg 13. Initial Reports of the Deep Sea Drilling Project 13, 1–1447.

Ryan, W. B. (2008), Modeling the magnitude and timing of evaporative drawdown during the Messinian salinity crisis. Stratigraphy 5, 227–243.

Salhotra, A. M., E. E. Adams and D. R. Harleman (1985), Effect of salinity and ionic composition on evaporation: Analysis of Dead Sea evaporation pans. Water Resources Research 21, 1336–1344.

Santisteban, C. and C. Taberner (1983), Shallow marine and continental conglomerates derived from coral reef complexes after desiccation of a deep marine basin: the Tortonian-Messinian deposits of the Fortuna Basin, SE Spain. Journal of the Geological Society 140, 401–411.

Schneck, R., A. Micheels and V. Mosbrugger (2010), Climate modelling sensitivity experiments for the Messinian Salinity Crisis. Palaeogeography, Palaeoclimatology, Palaeoecology 286, 149–163.

Schroeder, K., J. Garcìa-Lafuente, S. Josey, V. Artale, B. Buongiorno Nardelli, A. Carrillo, M. Gacic, G. P. Gasparini, M. Herrmann, P. Lionello et al. (2012), The climate of the mediterranean region : from the past to the future, chap. Circulation of the Mediterranean Sea and its variability. Elsevier, doi:10.1016/B978–0–12–416042–2.00003–3.

Selli, R. (1960), The Mayer-Eymar Messinian 1867. Proposal for a neostratotype. In: 16th International Geological Congress, Copenhagen, vol. 28, 311–333.

Sevault, F., S. Somot, A. Alias, C. Dubois, C. Lebeaupin-Brossier, P. Nabat, F. Adloff, M. Déqué and B. Decharme (2014), A fully coupled Mediterranean regional climate system model: design and evaluation of the ocean component for the 1980-2012 period. Tellus A 66.

Shackleton, N. and M. Hall (1997), Proceedings of the Ocean Drilling Program, Scientific Results, vol. 154, chap. The late Miocene stable isotope record, site 9261. 367–373.

Sierro, F., J. Flores, I. Zamarreno, A. Vazquez, R. Utrilla, G. Francés, F. Hilgen and W. Krijgsman (1999), Messinian pre-evaporite sapropels and precession-induced oscillations in western Mediterranean climate. Marine Geology 153, 137–146.

Sierro, F., F. Hilgen, W. Krijgsman and J. Flores (2001), The Abad composite (SE Spain): a Messinian reference section for the Mediterranean and the APTS. Palaeogeography, Palaeoclimatology, Palaeoecology 168, 141–169.

Simon, D. and P. Meijer (2015), Dimensions of the Atlantic–Mediterranean connection that caused the Messinian Salinity Crisis. Marine Geology 364, 53–64.

Simon, D., R. Topper and P. Meijer (2016), The Mediterranean circulation during extreme precessional climate change: a high resolution transient simulation. In: American Geophysical Union Fall Meeting Abstracts.

Simon, D., A. Marzocchi, R. Flecker, D. Lunt, F. Hilgen and P. Meijer (2017), Quantifying the Mediterranean freshwater budget throughout the late Miocene: New implications for sapropel formation and the Messinian Salinity Crisis. Earth and Planetary Science Letters, doi:10.1016/j.epsl.2017.05.013 .

Sirota, I., A. Arnon and N. G. Lensky (2016), Seasonal variations of halite saturation in the Dead Sea. Water Resources Research 52, 7151–7162.

Slingerland, R. and L. Kump (2011), Mathematical Modeling of Earth's Dynamical Systems: A Primer. Princeton University Press.

Sofianos, S., W. Johns and S. Murray (2002), Heat and freshwater budgets in the Red Sea from direct observations at Bab el Mandeb. Deep Sea Research Part II: Topical Studies in Oceanography 49, 1323–1340.

Sonnenfeld, P. and I. Finetti (1985), Messinian evaporites in the Mediterranean: a model of continuous inflow and outflow , 347–353.

Soto-Navarro, J., F. Criado-Aldeanueva, J. García-Lafuente and A. Sánchez-Román (2010), Estimation of the Atlantic inflow through the Strait of Gibraltar from climatological and in situ data. Journal of Geophysical Research: Oceans 115, doi:10.1029/2010JC006302.

Stoica, M., W. Krijgsman, A. Fortuin and E. Gliozzi (2016), Paratethyan ostracods in the Spanish Lago-Mare: More evidence for interbasinal exchange at high Mediterranean sea level. Palaeogeography, Palaeoclimatology, Palaeoecology 441, 854–870.

Stommel, H. (1972), Deep winter-time convection in the western Mediterranean Sea. Studies in physical oceanography 2, 207–218.

Stommel, H. and H. Farmer (1953), Control of salinity in an estuary by a transition. J. Mar. Res 12, 13–20.

Te Chow, V. (1959), Open channel hydraulics. McGraw-Hill Book Company, Inc; New York.

Thorpe, S. A. (2005), The turbulent ocean. Cambridge University Press.

Tindall, J., R. Flecker, P. Valdes, D. N. Schmidt, P. Markwick and J. Harris (2010), Modelling the oxygen isotope distribution of ancient seawater using a coupled ocean–atmosphere GCM: implications for reconstructing early Eocene climate. Earth and Planetary Science Letters 292, 265–273.

Topper, R. and P. T. Meijer (2013), A modeling perspective on spatial and temporal variations in Messinian evaporite deposits. Marine Geology 336, 44–60.

Topper, R. and P. T. Meijer (2015a), Changes in Mediterranean circulation and water characteristics due to restriction of the Atlantic connection: a high-resolution ocean model. Climate of the Past 11, 233–251.

Topper, R. and P. T. Meijer (2015b), The precessional phase lag of Messinian gypsum deposition in Mediterranean marginal basins. Palaeogeography, Palaeoclimatology, Palaeoecology 417, 6–16.

Topper, R., R. Flecker, P. T. Meijer and M. Wortel (2011), A box model of the Late Miocene Mediterranean Sea: Implications from combined 87Sr/86Sr and salinity data. Paleoceanography 26, doi:10.1029/2010PA002063.

Toucanne, S., C. M. A. Minto'o, C. Fontanier, M.-A. Bassetti, S. J. Jorry and G. Jouet (2015), Tracking rainfall in the northern Mediterranean borderlands during sapropel deposition. Quaternary Science Reviews 129, 178–195.

Tsimplis, M. N., V. Zervakis, S. A. Josey, E. L. Peneva, M. V. Struglia, E. V. Stanev, A. Theocharis, P. Lionello, P. Malanotte-Rizzoli, V. Artale et al. (2006), Changes in the oceanography of the Mediterranean Sea and their link to climate variability. Developments in Earth and Environmental Sciences 4, 227–282.

Tuenter, E., S. Weber, F. Hilgen, L. Lourens and A. Ganopolski (2005), Simulation of climate phase lags in response to precession and obliquity forcing and the role of vegetation. Climate Dynamics 24, 279–295.

Tziperman, E. and K. Speer (1994), A study of water mass transformation in the Mediterranean Sea: analysis of climatological data and a simple three-box model. Dynamics of Atmospheres and Oceans 21, 53–82.

Valdes, P. J., E. Armstrong, M. P. Badger, C. D. Bradshaw, F. Bragg, T. Davies-Barnard, J. J. Day, A. Farnsworth, P. O. Hopcroft, A. T. Kennedy et al. (2017), The BRIDGE HadCM3 family of climate models: HadCM3@ Bristol v1. 0. Geoscientific Model Development Discussions , doi:10.5194/gmd–2017–16.

van Baak, C. G., E. P. Radionova, L. A. Golovina, I. Raffi, K. F. Kuiper, I. Vasiliev and W. Krijgsman (2015), Messinian events in the Black Sea. Terra Nova 27, 433–441.

van den Berg, B., F. Sierro, F. Hilgen, R. Flecker, J. Larrasoaña, W. Krijgsman, J. Flores, M. Mata, E. B. Martín, J. Civis et al. (2015), Astronomical tuning for the upper Messinian Spanish Atlantic margin: Disentangling basin evolution, climate cyclicity and MOW. Global and Planetary Change 135, 89–103.

van den Berg, B. C., F. J. Sierro, F. J. Hilgen, R. Flecker, J. C. Larrasoaña, W. Krijgsman, J. A. Flores and M. P. Mata (2017), Imprint of Messinian Salinity Crisis events on the Spanish Atlantic margin. Newsletters on Stratigraphy , doi:10.1127/nos/2017/0337.

van der Schee, M., F. Sierro, F. Jiménez-Espejo, F. Hernández-Molina, R. Flecker, J. Flores, G. Acton, M. Gutjahr, P. Grunert, Á. García-Gallardo et al. (2016), Evidence of early bottom water current flow after the Messinian Salinity Crisis in the Gulf of Cadiz. Marine Geology 380, 315–329.

von der Heydt, A. and H. A. Dijkstra (2006), Effect of ocean gateways on the global ocean circulation in the late Oligocene and early Miocene. Paleoceanography 21, doi:10.1029/2005PA001149.

Wåhlin, A. and C. Cenedese (2006), How entraining density currents influence the stratification in a one-dimensional ocean basin. Deep Sea Research Part II: Topical Studies in Oceanography 53, 172–193.

Warren, J. K. (2006), Evaporites: sediments, resources and hydrocarbons. Springer.

Warren, J. K. (2016), Evaporites: A geological compendium. Springer.

Weber, S. and E. Tuenter (2011), The impact of varying ice sheets and greenhouse gases on the intensity and timing of boreal summer monsoons. Quaternary Science Reviews 30, 469–479.

Wernli, R. (1988), Micropalontologie du Nogne post-nappes du Maroc septentrional et description systmatique des foraminifres planctoniques., vol. 331. Notes et Mmoires du Service Gologique du Maroc.

Whitehead, J. (1998), Topographic control of oceanic flows in deep passages and straits. Reviews of Geophysics 36, 423.

Wortel, M. J. R. and W. Spakman (2000), Subduction and slab detachment in the Mediterranean-Carpathian region. Science 290, 1910–1917.

Yoshimura, T., J. Kuroda, S. Lugli, Y. Tamenori, N. O. Ogawa, F. J. Jiménez-Espejo, Y. Isaji, M. Roveri, V. Manzi, H. Kawahata et al. (2016), An X-ray spectroscopic perspective on Messinian evaporite from Sicily: Sedimentary fabrics, element distributions, and chemical environments of S and Mg. Geochemistry, Geophysics, Geosystems 17, 1383–1400.

Zaremba, L. J., G. Lawrence and R. Pieters (2003), Frictional two-layer exchange flow. Journal of Fluid Mechanics 474, 339–354.

Zhang, Z., G. Ramstein, M. Schuster, C. Li, C. Contoux and Q. Yan (2014), Aridification of the Sahara desert caused by Tethys Sea shrinkage during the Late Miocene. Nature 513, 401–404.

Zhu, D. Z. and G. A. Lawrence (2000), Hydraulics of exchange flows. Journal of Hydraulic Engineering 126, 921–928.

Ziegler, M., E. Tuenter and L. J. Lourens (2010), The precession phase of the boreal summer monsoon as viewed from the eastern Mediterranean (ODP Site 968). Quaternary Science Reviews 29, 1481–1490.

"*One never notices what has been done; one can only see what remains to be done*"

Marie Curie

Marie Curie has inspired, inspires and will continue to inspire generations of scientists. Her curiosity and hard work led to two Nobel Prizes, in physics and chemistry. She is, therefore, the only person who was awarded two Nobel Prizes in two separate sciences and she consequently stands for interdisciplinary research. It is an honour to have had the opportunity to do research in a framework that caries her name. This thesis summarises the core scientific investigations, which I undertook in the past four years. However, from a personal point of view, it is the people I met along the way, and the friendships resulting from it, which will continue to have an impact on my life. In the following I want to acknowledge the ones, who deserve special attention.

First and foremost, I would like to thank my supervisor **Paul Meijer**. His skill to isolate a (scientific) problem to its core is what I admire and what taught me a lot about how to approach arising questions. Being able to consult him at any time to discuss research, as well as getting to know him as a person, was and is very valuable to me. I thank my promotor **Rinus Wortel**, who formed the backbone of my PhD; I very much appreciated gaining from his knowledge and experience. Moreover, I want to thank **Rachel Flecker**, experiencing her passion for science and her drive to step on untouched ground was very motivating for me. She has been an important mentor and often guided me in unforeseen, albeit exciting, directions. I am grateful to **Frits Hilgen** and **Wout Krijgsman** for sharing their expertise in stratigraphy with me and for exemplifying how scientific teamwork is done. I will always remember the discussions about extreme geological scenarios and thank them for the opportunities they granted me.

I acknowledge **Angelo Camerlenghi**, **Gert de Lange**, **Mike Rogerson**, **Paco Sierro** and **Anna Wåhlin** for evaluating this thesis. I look forward to discussing my research with them.

Collaborators
I acknowledge the hospitality of the BRIDGE research group at the University of Bristol, which I visited in 2014. Many thanks to **Dan Lunt**, in particular: I learned from his analytical skills during our discussions. I thank **Alice Marzocchi** for introducing me to the complex world of modelling the climate (or was it the weather?). I want to thank **Sevasti Modestou** for our discussions about the Sorbas basin and strontium isotopes. I very much enjoyed the discussions with **Jan-Peter Mayser**, on the correlation between runoff and sedimentation. Moreover, I want to acknowledge **Dan Palcu**, **Arjen Grothe** and **Chris van Baak** for many discussions on the Mediterranean-Paratethys connectivity. I am grateful to **Robin Topper** for all his support, especially with the Princeton Ocean Model. **Bas van den Berg**, **Marlies van der Schee** and **Walter Capella** are thanked for the exciting discussions about the opening of the Strait of Gibraltar.

Lifesavers
I want to thank **Ton Markus** for his help and advice on many figures in this thesis, as well as the fun conservations about surfing. In addition, I am grateful to **Margot Stoete** for designing the thesis cover and giving me advice concerning the thesis layout. I acknowledge **Theo van Zessen**, for always being on top of things regarding the Utrecht servers and making me consistently lead the "pbsserver league table". Moreover, I want to thank my "ghost-reader" **Gene Strasbaugh** for reviewing most of my writing. I want to acknowledge **Ildikó**, **Jan-Willem**, **Marjolein** and **Maarten** for pulling the strings in the background, which often made my life a lot easier. Moreover, I thank my friends at Tricolore, **Piero**, **Mauro**, **Vincenzo**, **Antonio** and **Carlos**, for giving me an escape point and making sure that I eat enough tasty pizza.

The MEDGATE team
I thank **Ali**, **Bas**, **Diana**, **Eva**, **Maria**, **Marlies**, **JP**, **Sevi** and **Walter** for everything we did together; whether it was all-night work sessions, being stuck on a train in Morocco or in an elevator in Spain, it was always worthwhile and fun. Furthermore, I would like to extend my gratitude to all members of the MEDGATE network; I very much appreciate all the effort that went into the workshops, meetings and trips. A special "thanks" goes to **Carla Sands**, who provided the base for MEDGATE by making sure that the logistics always ran smoothly.

Partners in crime
I thank **Walter** for always being there to discuss and implement brilliant ideas and the adrenaline that came with it. Being able to defend our theses on the same day is a great achievement, and thus I want to thank our paranymph-team (Maria, Marlies, Bas and Ahmet). I thank **Maria** for her friendship and for being there to distract me when things started to become stressful. I would like to thank **Marlies** and **Ahmet** for adopting me during the final writing phase; they gave me a lot of ENERGY and consequently, I thank them for standing behind me during the defence. I want to thank **Bas** for taking me to field — our Ronda trips were my favourite ones; everything is possible in Andalusia: "Chopitos, chicas y corridors."

Day-to-day heroes
I am grateful to **Alba** for sharing an office with me for 3 years; I had great fun when we got excited about each other's research problems and tried to solve them together. Moreover a big "thank you" goes to my office mate **Candela** for being there to chat about life on a daily basis. I want to thank **Chloé** and **George** for countless extended coffee breaks and the *odd* beer after work. Not to be forgotten is **Rob** 'I want to be a sofa' Govers, whom I thank for a lot of good vibes, especially during the final phase of completing my thesis. "Thank you" to everybody else on the 8^{th} floor for my scientific experience as well as for the fun times in and outside the office; I would like to acknowledge everybody's patience for letting me stumble into their offices to draw on the whiteboards: **Alexis**, **Anne** G, **Cedric**, **Douwe**, **Eldert**, **Ivette**, **Lukas**, **Menno**, **Nicolai**, **Nienke**, **Pete**, **Pieter**, **Suzanne**, **Taco** and **Wimmi**. I want to thank all Forters for always treating me as a welcomed guest, with particular mention of **Anne-Christine**, **Nathan** and **Tom**. Moreover, I want to acknowledge and thank everybody else I met in Utrecht; especially for being awesome housemates, great colleagues and friends: **Yue** and **Ole**, **Özlem** and **Rasim**, **Claudia** and **Marco**, **Annemarie** and **Hans**, **Dragos**, **Alfredo**, **Alejandro**, **Katharina**, **Bob**, **Anne** K, **Melissa** and **Stefanie**. This list could go on and on, but I want to make sure this thesis does not exceed *100* pages.

I owe a lot to **Berny Torre**, "competing" with him during physics lessons at school, since it motivated me to choose my undergraduate in Natural Sciences. Moreover, I would like to thank **Nigel Woodcock**, who introduced me to geology and inspired me when we were rowing during my time in Cambridge. I also want to thank my advisers, **Keith Priestley** and **Neil Greenham** for their support during my masters.

I want to thank all my friends whom I met in Nuremberg, Scotland and Cambridge. Here, I especially want to thank my windsurfing buddies from Amrum for being my home base to which I could always return to recover. Moreover, I thank **Kai Britzke** for many windsurfing sessions in the Dutch North Sea, which often resulted in me returning to my desk with new ideas.

I want to extend my gratitude to my family, to whom I dedicate this book; their continuous support allowed me to develop my curiosity and openness to meet new people.

Last but not least I want to thank **Derya**, whom I met during this time, for all her love.

Dirk Simon

Publication list

Chapter 2

D. Simon and P.Th. Meijer. Dimensions of the Atlantic–Mediterranean connection that caused the Messinian Salinity Crisis. *Marine Geology*, 364, pp. 53–64, 2015.

Chapter 3

D. Simon, A. Marzocchi, R. Flecker, D.J. Lunt, F. Hilgen, and P.Th. Meijer. Quantifying the Mediterranean freshwater budget throughout the late Miocene: New implications for sapropel formation and the Messinian Salinity Crisis. *Earth and Planetary Science Letters*, doi:10.1016/j.epsl.2017.05.013.

Chapter 4

D. Simon and P.Th. Meijer. Salinity stratification of the Mediterranean Sea during the Messinian crisis: A first model analysis. Under review in *Earth and Planetary Science Letters*.

Collaborations within the MEDGATE group (not in this thesis):

with the University of Bristol

R. Flecker, W. Krijgsman, W. Capella, C. Martins, E. Dmitrieva, J.P. Mayser, A. Marzocchi, S. Modestu, D. Ochoa, D. Simon, M. Tulbure, B. van den Berg, M. van der Schee, G. de Lange, R. Ellam, R. Govers, M. Gutjahr, F. Hilgen, T. Kouwenhoven, J. Lofi, P.Th. Meijer, F.J. Sierro, N. Bachiri, N. Barhoun, A. Chakor Alami, B. Chacon, J.A. Flores, J. Gregory, J. Howard, D.J. Lunt, M. Ochoa, R. Pancost, S. Vincent, M.Z. Yousfi. Evolution of the late Miocene Mediterranean–Atlantic gateways and their impact on regional and global environmental change. *Earth-Science Reviews*, 150, pp. 365-392, 2015.

with the University of Glasgow

S. Modestou, D. Simon, M. Gutjahr, A. Marzocchi, T.J. Kouwenhoven, R.M. Ellam, and R. Flecker. Precessional variability of $^{87}Sr/^{86}Sr$ in the late Miocene Sorbas Basin: an interdisciplinary study of drivers of inter-basin exchange. *Paleoceanography*, doi:10.1002/2016PA003061.

with Salamanca University

B. van den Berg & M. van der Schee, W. Capella, D. Simon, W. Krijgsman, F.J. Sierro. New age constraints on the western Betic intramontane basins: a late Tortonian closure of the Guadalhorce Corridor? In preparation to be submitted to *Terra Nova*.

within Utrecht University

W. Capella, R. Flecker, F.J. Hernández-Molina, D. Simon, P.Th. Meijer, F.J. Sierro, W. Krijgsman. Mediterranean isolation as a trigger for global late Miocene cooling. In preparation to be submitted to *Geology*.

About the author

Dirk studying the Messâdit section (Melilla Basin, Morocco) near the Mediterranean coast.

Dirk Simon was born on October 13^{th} 1989 in Nuremberg (Germany), as the youngest of three brothers. From his earliest years, the entire family loved to escape to the small island of Amrum, amid the mud flats of the German North Sea. Not only did these trips trigger his passion for windsurfing, but it also prompted his deep curiosity about the ocean. To this day, Amrum is where Dirk's heart lies, where he can live out his longing for strong winds and rough seas. At 16, a student exchange to Scotland provided new adventures, particularly hiking the Highlands and sailing in the northern Atlantic, and the exchange culminated in A-Levels at Gordonstoun School (Moray). In 2008, Dirk began his undergraduate degree in Natural Sciences at Clare College, Cambridge. Here he dived into the depth of physics, being impressed and inspired to be taught in lecture rooms in which none other than Sir Isaac Newton had questioned how the world works. During this period, Dirk learned how to row and was an avid member of his colleges boat club. Equipped with his thirst to learn more about our Earth and his background in physics, he was fortunate to be selected for a postgraduate position in Earth Sciences at Utrecht University in 2012. His research focused on the ancient ocean circulation of the Mediterranean Sea and led to this doctoral thesis. Although Dirk's investigations were predominantly of theoretical nature, being a member of the European-funded training network MEDGATE allowed him to join his colleagues in the field to explore and learn about the geology of the Mediterranean region.